

Wilfrid Laurier University

Scholars Commons @ Laurier

Theses and Dissertations (Comprehensive)


2014

SURFACE COMPLEXATION OF MONOSUBSTITUTED ORGANOARSENICALS ON HEMATITE: ATR-FTIR INVESTIGATIONS

Md Abdus Sabur

Wilfrid Laurier University, sabu0830@mylaurier.ca

Follow this and additional works at: <https://scholars.wlu.ca/etd>

 Part of the [Analytical Chemistry Commons](#), [Environmental Chemistry Commons](#), [Geochemistry Commons](#), and the [Physical Chemistry Commons](#)

Recommended Citation

Sabur, Md Abdus, "SURFACE COMPLEXATION OF MONOSUBSTITUTED ORGANOARSENICALS ON HEMATITE: ATR-FTIR INVESTIGATIONS" (2014). *Theses and Dissertations (Comprehensive)*. 1638. <https://scholars.wlu.ca/etd/1638>

This Thesis is brought to you for free and open access by Scholars Commons @ Laurier. It has been accepted for inclusion in Theses and Dissertations (Comprehensive) by an authorized administrator of Scholars Commons @ Laurier. For more information, please contact scholarscommons@wlu.ca.

**SURFACE COMPLEXATION OF MONOSUBSTITUTED
ORGANOARSENICALS ON HEMATITE: ATR-FTIR
INVESTIGATIONS**

By

Md Abdus Sabur

Bachelor of Science (Honours), Jahangirnagar University, 2001

THESIS

Submitted to the Department of Chemistry
Faculty of Science
in partial fulfillment of the requirements for the
Master of Science in Chemistry
Wilfrid Laurier University

2014

©Md Abdus Sabur 2014

Table of Contents

Acknowledgements.....	iii
Dedication.....	v
List of Publications.....	vi
Abstract.....	vii
List of Tables.....	ix
List of Figures.....	x
1 Introduction.....	1
1.1 Sources of arsenic compounds in the environment.....	1
1.1.1 Inorganic and organic arsenic.....	3
1.1.2 Arsenic cycling pathways: redox and methylation chemistry.....	5
1.1.3 Environmental fate of arsenic compounds.....	7
1.1.4 Toxicity of arsenicals.....	9
1.1.5 Environmental regulations of arsenic in soils and drinking water.....	10
1.2 Previous research on the geochemistry of arsenic.....	11
1.2.1 Field measurements of monosubstituted organoarsenicals.....	11
1.2.2 Surface chemistry of arsenic compounds with metal (oxyhydr)oxides.....	12
1.2.3 Bulk/batch studies on the adsorption/desorption behavior of monosubstituted organoarsenicals on soils and metal oxides.....	17
1.3 Research objectives and goals.....	20
2 Experimental.....	21
2.1 Description of the ATR-FTIR setup.....	21
2.2 Reagents.....	22
2.3 Film preparations on the ATR-FTIR crystal.....	23
2.4 Experimental procedure.....	23
2.4.1 Preparation of calibration curve using ATR-FTIR.....	23
2.4.2 Adsorption kinetics using ATR-FTIR.....	24
2.4.3 Desorption kinetics using ATR-FTIR.....	25
2.4.4 Adsorption isotherm using ATR-FTIR.....	25
2.4.5 Adsorption pH(D) edge using ATR-FTIR.....	26

3 Results and Discussion	28
3.1.1 ATR-FTIR spectra for inorganic and organic arsenicals in the aqueous phase	28
3.2 Adsorption kinetics	31
3.2.1 Spectra for the adsorption of arsenicals on hematite	31
3.2.2 Mathematical models used in describing adsorption kinetics.....	33
3.2.3 Adsorption kinetic curves	34
3.3 Desorption kinetics of monosubstituted orboarsenicals.....	39
3.3.1 Spectra for the desorption of surface arsenicals	39
3.3.2 Mathematical models used in describing desorption.....	41
3.3.3 Desorption kinetic curves	41
3.3.4 Adsorption kinetics of phosphate concurrent with arsenicals desorption....	46
3.4 Temperature-dependent adsorption isotherm of arsenicals	50
3.4.1 Spectra for the adsorption isotherm as a function of temperature and concentration.....	50
3.4.2 Mathematical models used in describing adsorption isotherm	52
3.4.3 Results from the temperature-dependent adsorption isotherm experiments	54
3.4.4 Discussion on the results obtained from the temperature-dependent isotherm experiments	58
3.4.5 Discussion on the results obtained from the temperature-dependent isotherm experiments considering integrated peak area as analysis method.....	59
3.5 Adsorption of monosubstituted arsenicals as a function of pH(D).....	62
4 Conclusions and future work	69
Appendix A.....	72
Appendix B	85
5 References.....	88

Acknowledgements

I feel fortunate to have Dr. Hind A. Al-Abadleh as my research supervisor at Wilfrid Laurier University. From Bangladesh, I contacted Dr. Al-Abadleh expressing my research interest in arsenic geochemistry and finally she responded to me by offering a graduate position. Thank you Dr. Al-Abadleh for giving me the opportunity to work in your group. You are always very keen on teaching your students and I learned a lot from you in this short time. I am sure it would have never been possible bringing this thesis to this level without your close guidance and cordial cooperation.

I would also like to offer my thanks to my committee members, Professor Ian Hamilton and Professor Carol Ptacek for their valuable comments about this thesis. I acknowledge Professor Philippe Van Cappellen for agreeing to be present in my thesis defence as an external examiner. I went to Dr. Scott Smith several times and he introduced me with MATLAB in predicting basic geochemical interactions, thanks goes to him too.

I always would like to take the opportunity to acknowledge the company of Adrian Adamescu, Julia Tofan-Lazar, Derek Arts, Arthur Situm, Jonathan Ruffolo, Kevin Jakiela, Samantha Slikboer and Willie Buck in lab. They are really very great as co-workers as well as in exchanging research ideas!!! Thank you all very much. Special gratitude to Adrian for going through this dissertation with some considerable notes.

In the past two years in Waterloo, I spent a very good time with some excellent friends and most of them were not familiar with me prior to coming here. I don't want to miss this chance to mention their names in this tiny space. They are: Ilias Mahmud, Afroza Begum, Syed Ismail Hussain, Farzana Sultana, Tulip Shaheen, Abdulla Al-

Manum, Tapan Dhar and Rubayet R. Khan. They are really great!!! I am also grateful to Kamrul Hasan, Mainul Hossain and Nasir Uddin who especially encouraged my study here in Canada. Since my arrival, I have been receiving constant mental support from them. Besides them, I like to add my friends: Rahat, Kausar and Idrish in this list, thank you all.

All of my colleagues, most of them are my teachers, in the Department of Chemistry at Jahangirnar University are always very encouraging. I definitely would mention here the name of Professor Syed Safiullah, my teacher and research guru.

I understand, my family members, especially my parents are missing me a lot from Bangladesh. I am grateful to them for their constant support and encouragement throughout my life. I sometimes feel sad to be here, for my study, like a selfish person leaving them several thousand miles away back in Bangladesh.

Last of all, my life partner, Sharmin Jahan. You are always deprived from my time and the company you deserve. In spite of these, I see you accepting everything with a smiling face. Your silent inspiration has been pushing me towards my stepwise achievements.

Dedication

This thesis is dedicated to Professor Syed Safiullah who is one of the leading environmental scientists in Bangladesh.

List of Publications

- (1) Derek Arts, **Md Abdus Sabur** and Hind A. Al-Abadleh, Surface Interactions of Aromatic Organoarsenical Compounds with Hematite Nanoparticles Using ATR-FTIR: Kinetic Studies, *Journal of Physical Chemistry A*, 117, 2195-2204, 2013

- (2) **Md Abdus Sabur**, Sabine Goldberg and Hind A. Al-Abadleh, Temperature-dependent Adsorption Isotherm Studies on Methylated Arsenicals and Arsenate Interactions with Hematite Nanoparticles Using ATR-FTIR (Manuscript in preparation)

- (3) **Md Abdus Sabur** and Hind A. Al-Abadleh, Thermodynamics and Kinetics of Surface Interactions of Monomethylarsonic Acid with Hematite Nanoparticles Using ATR-FTIR (Manuscript in preparation)

Abstract

Little is known about the surface chemistry of organoarsenic compounds with iron-containing materials commonly found in geosorbents and arsenic removal technologies. In this thesis, these organoarsenicals include aliphatic and aromatic arsenicals that historically have been used as herbicides, pesticides and in the poultry feed industry, respectively. Attenuated total internal reflectance Fourier transform infrared spectroscopy has been used to study the surface interactions of organoarsenicals at the molecular level under various environmentally-relevant conditions. Kinetic and thermodynamic parameters extracted from these molecular level experiments provide trends that are not observed in any published bulk experiments. Apparent initial rates of adsorption and desorption for these arsenicals were extracted from experimental data as a function of spectral components. Initial first order pseudo-adsorption rate constants (k_{ads}) for arsenate (iAs), monomethylarsonic acid (MMA), p-arsanilic acid (pAsA) and phenylarsonic acid (PhAs) were quantified and show that arsenate and monosubstituted organoarsenicals adsorb with similar rate on Fe-(oxyhydr)oxide. Hydrogen phosphate was used as a desorbing agent due to its ubiquitous presence in arsenic contaminated aquatic environments. The desorption of monosubstituted organoarsenicals from hematite surfaces takes place faster than iAs(ads). The initial desorption of these organoarsenicals with an overall non-unity order suggests the existence of more than one type of surface complex. Adsorption kinetics for aqueous hydrogen phosphate was also investigated on surfaces in the presence and absence of surface arsenic, and the values of k_{ads} follow the order: Fresh hematite > pAsA/hematite \geq PhAs/hematite > MMA(V)/hematite \geq iAs(V)/hematite. From this study, it is observed that the amount of weakly bonded

pAsA(ads) and PhAs(ads) surface species are larger than those for MMA(ads) and iAs(ads) at neutral pH.

Moreover, thermodynamic parameters were obtained for the adsorption of iAs(V), MMA(V) and DMA(V) on iron (oxyhydr)oxide surfaces as a function of concentration (0.001 to 2 mM) and temperature (5 to 50 °C). Values of the free energy of adsorption (ΔG_{ads}^0) were extracted from fits using the Langmuir adsorption model and found to be negative within the experimental temperatures range. The entropy (ΔS_{ads}^0) and enthalpy (ΔH_{ads}^0) of adsorption were also extracted from the linear least-squares regression analysis of van't Hoff plots constructed from the experimental data. The values of ΔS_{ads}^0 are positive for all the arsenicals undertaken in this study. The values of ΔH_{ads}^0 suggest that adsorption of iAs(ads) and MMA(ads) are endothermic processes whereas those for DMA(ads) are exothermic. The positive ΔS_{ads}^0 along with the positive ΔH_{ads}^0 suggest that the ligand exchange reactions are entropy driven.

In order to gain further insight into the mechanism of binding, pH(D) edge experiments were carried out for the adsorption of iAs(V) and the monosubstituted organoarsenicals, MMA(V) and PhAs, on hematite nanoparticles at room temperature. The arsenicals show stronger adsorption on iron (oxyhydr)oxide with slight shifting of the spectral features to higher wavenumbers in relatively acidic pH(D). The infrared signatures obtained from the pD edge experiments provide clear spectral information for the surface species. Spectra show that the extent of adsorption increases with decreasing pH(D). Arsenate forms mainly bidentate surface complex. In the case of MMA(ads) and PhAs(ads), surface complexes are most likely to be inner-sphere monodentate in acidic pD with longer adsorption time.

List of Tables

Table 1. Major arsenicals in the environment	4
Table 2. Recommended maximum contaminant levels of arsenic concentrations	11
Table 3. List of ϵ values for each arsenical at pH 7	30
Table 4. Least-squares estimates of the linear regression parameters fitted to the experimental data of r_{obs} versus $[\text{As}(\text{aq})]$ shown in Figures 3.5a-d	38
Table 5. Least-squares estimates of the linear regression parameters fitted to the experimental data of $\ln k'_{\text{des}}$ vs $\ln[\text{Phosphate}_{\text{aq}}]$ shown in Figure 3.11	45
Table 6. Least-squares estimates of the linear regression parameters fitted to the experimental data of r_{obs} versus $[\text{HPO}_4^{2-}(\text{aq})]$ (date and figures are not shown here) for the adsorption of phosphate as a function of spectral components 1003 cm^{-1} in the presence and absence of surface arsenic	48
Table 7. Least-squares estimates of the linear regression parameters fitted to the experimental data of $\ln(55.5K_{\text{eq}})$ versus $1/T (\text{K}^{-1})$ shown in Figure 3.19 from the peak height measurements	58
Table 8. Least-squares estimates of the linear regression parameters fitted to the experimental data of $\ln(55.5K_{\text{eq}})$ versus $1/T (\text{K}^{-1})$ shown in Figure 3.21 based on the integrated peak area	61

List of Figures

Figure 1.1. Reactions involved in the Challenger mechanism (a) top reaction involves the reduction of As(V) to As(III); and (b) the bottom reaction corresponds to the oxidative methylation. Note that R_1 and R_2 represent OH, CH_3 or both depending on the arsenic compounds (Bentley and Chasteen, 2002).....	6
Figure 1.2. Challenger mechanism for the biological methylation of arsenic. The vertical arrows indicate the reduction of pentavalent arsenic to its trivalent form and diagonal arrows indicate the oxidative methylation.....	7
Figure 1.3. Distribution of positive, negative and neutral surface hydroxyl groups on iron (oxyhydr)oxides as a function of pH.....	15
Figure 1.4. Distribution diagram for the species formed by (a) iAs(V); (b) MMA(V); (c) PhAs; and (d) DMA(V) species as a function of pH.....	16
Figure 2.1. ATR-flow cell (100 μ L), Film thickness $\sim 5 \times 10^{-4}$ cm.....	21
Figure 3.1. Bulk phase ATR-FTIR spectra collected for (a) iAs (1, 2, 3, 4, 5, 7, 8 and 10 mM), (c) MMA (10, 50 and 100 mM), (e) PhAs (8, 15, 20, 40, 60 and 100 mM), and (g) DMA (8, 15, 20, 40, 60 and 100 mM) as a function of concentration at room temperature pH=7, $I=0.01$ M NaCl at room temperature. The right panels show the corresponding calibration curves. Two trials were averaged for the preparation of each calibration curve.....	29
Figure 3.2. ATR-FTIR adsorption spectra collected during the adsorption of (a) iAs; (b) MMA; (c) pAsA; and (d) PhAs on hematite at pH=7, $I=0.01$ M NaCl, and 2 mL/min flow rate at room temperature as a function of time.....	32
Figure 3.3. Kinetic curve generated for the adsorption of (a) iAs(aq), (b) MMA(aq), (c) pAsA(aq) and (d) PhAs(aq) on hematite at pH=7, $I=0.01$ M NaCl, and 2 mL/min flow rate at room temperature as a function of time. Not all the concentrations are shown in the kinetic curves. Data points represent the average of two to four experiments and error bars were removed for clarity. The uncertainty in the measurements is 5% ($\pm\sigma$).....	35
Figure 3.4. Linearized absorbances for the adsorption of (a) iAs(aq), (b) MMA(aq), (c) pAsA(aq) and (d) PhAs(aq) on hematite at pH=7, $I=0.01$ M NaCl, and 2 mL/min flow rate at room temperature as a function of time. Data for each concentration represent the average of two experiments.....	36
Figure 3.5. Dependency of r_{obs} with the bulk concentration of arsenicals at pH=7, $I=0.01$ M NaCl/KCl, and 2 mL/min flow rate at room temperature, 6 mg hematite.....	37
Figure 3.6. Schematic representation of probable surface species that may form by MMA(V) on the hematite surface.....	39

Figure 3.7. Spectra for the desorption of surface- (a) MMA; (b) pAsA; and (c) PhAs by aqueous hydrogen phosphate (not shown here for iAs(ads)). The experiment carried out at pH 7, $I=0.01$ M NaCl and 2 mL/min flow rate at room temperature.....	40
Figure 3.8. Desorption kinetics of (a) iAs(V), (b) MMA, (c) pAsA and (d) PhAs from hematite surface by various concentrations of phosphate (at pH=7) with 2 mL/min flow rate and at room temperature. Data points represent the average of two to four experiments and error bars were removed for clarity. The uncertainty in the measurements is 5% ($\pm\sigma$).....	42
Figure 3.9. Linearized absorbances for the desorption of (a) iAs(ads), (b) MMA(ads), (c) pAsA(ads) and (d) PhAs(ads) from the hematite surface by using different concentrations of aqueous phosphate (pH=7) at flow rate 2 mL/min and room temperature.....	43
Figure 3.10. Dependency of the initial desorption rate constants, k'_{des} , on the concentration of $[\text{HPO}_4^{2-}(\text{aq})]$ from studies conducted using hematite films (6 mg) at pH 7 and 2 mL/min flow rate. Adsorbed arsenicals were introduced by flowing 0.5 mM of aqueous solutions at pH 7 and $I = 0.01$ M KCl/NaCl. Solid lines through the data represent least-squares linear fits. Dashed lines represent the non-unity overall order ($n \neq 1$).....	44
Figure 3.11. Dependency of the initial desorption rate constants, k'_{des} , obtained from the linear least-squares fitting to the experimental data shown in Figures 3.9a-d for the desorption of arsenicals as a function of $[\text{HPO}_4^{2-}(\text{aq})]$ at pH 7 and 2 mL/min flow rate.....	44
Figure 3.12. The rate of phosphate adsorption in presence and absence of surface arsenic from analyzing the spectral component 1003 cm^{-1} . Lines through the data represent linear least-squares fits and slopes of linear fits represent pseudo k_{ads}	47
Figure 3.13. Ligand exchange process between incoming phosphate and surface MMA.....	49
Figure 3.14. Representative ATR-FTIR absorbance spectra of iAs(ads) on hematite nanoparticles as a function of increasing temperature and concentration (from bottom): 0.005, 0.01, 0.03, 0.05, 0.25, 0.5 and 1 mM at pH 7, $I = 0.01$ M NaCl and 1 mL/min flow rate.....	50
Figure 3.15. Representative ATR-FTIR absorbance spectra of MMA(ads) on hematite nanoparticles as a function of increasing temperature and concentration (from bottom): 0.005, 0.01, 0.03, 0.05, 0.25, 0.5 and 1 mM at pH 7, $I = 0.01$ M NaCl and 1 mL/min flow rate.....	51
Figure 3.16. Representative ATR-FTIR absorbance spectra of DMA(ads) on hematite nanoparticles as a function of increasing temperature and concentration (from bottom): 0.005, 0.01, 0.03, 0.05, 0.25, 0.5 and 1 mM at pH 7, $I = 0.01$ M NaCl and 1 mL/min flow rate.....	52

Figure 3.17. Adsorption isotherms of iAs (upper left), MMA (upper right) and DMA (bottom) on hematite nanoparticles as a function of temperature (filled markers) at pH 7 and 0.01 M NaCl. The solid line represents the least-squares fitting of the 1-site Langmuir adsorption model. Data points represent the average of two to four experiments and error bars were removed for clarity. The uncertainty in the measurements is 5% ($\pm\sigma$).....54

Figure 3.18. Linearized absorbances for the adsorption of iAs (upper left), MMA (upper right) and DMA (bottom) on hematite nanoparticles as a function of temperature and concentration at pH 7 and 0.01 M NaCl. Data points represent the average of two to four experiments and error bars were removed for clarity.....55

Figure 3.19. Temperature-dependence of the Langmuir equilibrium constants, K_{eq} , plotted according to van't Hoff equation (filled markers). Values of K_{eq} were extracted from least-squares Langmuir fits to adsorption isotherms obtained from the baseline-corrected absorbance at 875 and 795 cm^{-1} for iAs(ads); 872, 840 and 795 cm^{-1} for MMA(ads); and 837 and 798 cm^{-1} for DMA(ads). The solid line is the linear least-squares fitting with a slope corresponding to $-\Delta H_{ads}^0/R$56

Figure 3.20. Temperature-dependence of the Gibbs free energy, ΔG_{ads}^0 , for the adsorption of (a) iAs(ads), (b) MMA(ads) and (c) DMA(ads) which were obtained using: $\Delta G_{ads}^0 = -RT \ln(55.5K_{eq})$ (filled markers). The solid line represents the linear least-squares fitting and the slope, which corresponds to $-\Delta S_{ads}^0$57

Figure 3.21. Temperature-dependence of the Langmuir equilibrium constants, K_{eq} , plotted according to van't Hoff equation (filled markers). Values of K_{eq} were extracted from least-squares Langmuir fits to adsorption isotherms obtained from the integrated peak area for iAs(ads), MMA(ads) and DMA(ads). The solid line is the linear least squares fitting and the slope, which corresponds to $-\Delta H_{ads}^0/R$. The right panel shows the temperature-dependence of the Gibbs free energy of adsorption, ΔG_{ads}^0 , which were obtained using: $\Delta G_{ads}^0 = -RT \ln(55.5K_{eq})$ (filled markers). The solid line represents the linear least-square fitting and the slope, which corresponds to $-\Delta S_{ads}^0$60

Figure 3.22. pH edges of iAs(V), MMA(V) and PhAs on (a) effect of pH on the wavenumber of the most intense spectral feature; and (b) pH edge at room temperature, $I=0.01$ M NaCl and 1 mL/min flow rate. Data points represent the average of two to four experiments and error bars were removed for clarity.....63

Figure 3.23. Spectra recorded as a function of pD and at $I=0.01$ M KCl for (a) aqueous iAs(V) on Ge crystal, and (b) aqueous MMA(V) on ZnSe crystal.....64

Figure 3.24. ATR-FTIR adsorption spectra for 0.5 mM iAs(ads) on hematite (6.0 mg) as a function of pH(D) at equilibrium with 1 mL/min flow rate and $I=0.01$ M KCl (Left panel). The right panel shows the differences between normalized absorbance spectra shown in the left panel. Spectra are offset for clarity.....66

Figure 3.25. ATR-FTIR adsorption spectra for MMA(ads) on hematite (6.0 mg) as a function of pH(D) at equilibrium with 1 mL/min flow rate and $I=0.01$ M KCl (left panel). The right panel shows the differences between normalized absorbance spectra shown in the left panel. Spectra are offset for clarity.....67

Figure 3.26. ATR-FTIR adsorption spectra for PhAs(ads) on hematite (6.0 mg) as a function of pH(D) at equilibrium with 1 mL/min flow rate and $I=0.01$ M KCl (left panel). The right panel shows the differences between normalized absorbance spectra shown in the left panel. Spectra are offset for clarity.....68

1 Introduction

1.1 Sources of arsenic compounds in the environment

For the last few decades, the presence of arsenic mainly in ground water has received much attention as a public health problem in many parts of the world (Clarke, 2001; Nickson et al., 2005; Smedley and Kinniburgh, 2002). Arsenic is the 20th most abundant element in earth's crust and occurs naturally in more than 200 different minerals as elemental arsenic, arsenates, arsenides, arsenites, sulphides and sulfosalts, silicates and oxides (Mandal and Suzuki, 2002). Arsenic is released to the environment mainly from natural sources and its release is intensified by anthropogenic activities. Natural sources include the weathering of arsenic rich rocks and minerals, volcanic activity, and biogeochemical transformations of arsenicals. Mining, combustion of fossil fuels, use of organoarsenicals as herbicides, in the poultry feed industries and in wood preservatives are the most common anthropogenic sources (Smedley and Kinniburgh, 2002).

The average arsenic level in soils varies considerably among geographic regions ranging from 5 to 6 mg/kg (Mandal and Suzuki, 2002). For freshwater systems, higher arsenic concentrations occur in groundwaters due to water-rock interactions in favourable geochemical conditions. The worldwide reported arsenic concentration in natural water varies from as low as 2×10^{-5} to >5 mg/kg (Wang and Mulligan, 2006). In the sea and estuarine waters, arsenic is present mostly as As(V) in the upper surface oxic environment, while in the lower anoxic bottom layer, the relative concentrations of As(III) increase. In lakes and rivers As(V) dominates over As(III), though their concentrations vary depending on the incoming sources and other environmental factors.

Most of the arsenic compounds in the environment are present as ore minerals and

their various products. The concentrations of these compounds are higher in mineralized areas in close association with transition metals and also with Cd, Pb, Ag, Au, Sb, P, W and Mo. Among the ore minerals, arsenopyrites (FeAsS) are the most abundant in the earth's crust and they are formed under high temperature conditions along with other minerals. The presence of arsenic has also been reported in sediments and the mineral arsenian pyrite, $\text{Fe}(\text{As}, \text{S})_2$, is believed to be the most important source of arsenic in ore zones (Smedley and Kinniburgh, 2002).

Both monomethylarsonic acid (MMA) and dimethylarsinic acid (DMA) are introduced to the environment through agricultural and industrial activities (Xu et al., 2007). The worldwide use of alkylarsenicals started in agriculture to replace the more toxic inorganic arsenic after World War II where MMA(V), DMA(V) and their sodium salts were the most common ingredients used in pesticides and herbicides (Cullen, 2008). Around 1500 metric tons of monosodium methylarsonate (MSMA) were applied annually to US roadsides as herbicides. Their application started increasing over time and reached ~2700 metric tons for cotton fields alone in the US in 1990. In the meantime, with the availability of organic pesticides on the market, the use of MSMA decreased rapidly. Although the industrial representatives were claiming that MSMA could not be released easily because of its rapid binding to soil components, later on, it became clear that MSMA can enter the ground water and the food chain through its conversion to inorganic arsenic (Cullen, 2008). With this news, the US and Canada re-evaluated the registration for MSMA. Finally, in 2006, all the products containing MSMA, disodium methylarsonate (DMSA), DMA, calcium acid methanearsonate (CAMA) were banned from further registration in USA. As of 2011, MSMA in USA has been used only on

cotton fields located away from drinking water sources (Environment Canada, 2013).

In Canada, the use of alkyl arsenicals such as MSMA started in 1980 to prevent the devastation of forests in British Columbia (BC) from the attack of the mountain pine beetle and that expanded in the 1990s. Considering the potentially harmful effects of this arsenical, the application of MSMA was no longer used in this province after 2005. In 2007, the BC government employed a policy for the restricted use of arsenical pesticides for its application on the mountain pine beetle. Now, organic arsenicals including MSMA have been banned in Canada (Environment Canada, 2013). Besides these, methylated forms of arsenic were reported in the leachates from arsenic rich landfills and biologically pretreated municipal solid waste (Li et al., 2011; Li et al., 2010).

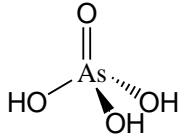
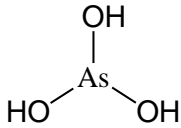
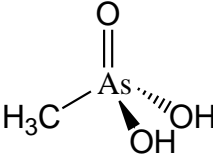
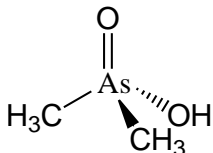
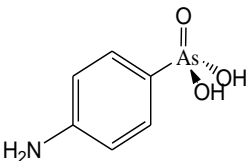
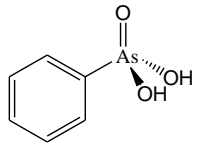
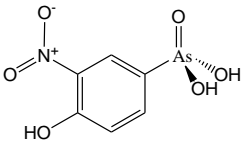
Another important class of arsenicals are man-made aromatic organoarsenicals; *p*-arsanilic acid (pAsA) and 3-nitro-4-hydroxyphenylarsonic acid (roxarsone) which are commonly used as poultry feed additives to improve feed efficiency, mainly to increase the weight gain of poultry. The majority of these compounds are not metabolized in the poultry and they enter the environment through the poultry litter (Garbarino et al., 2003). This litter is extensively used as fertilizer on some agricultural lands (Brown et al., 2005; Jackson et al., 2006). Most of these arsenicals become mobile in wet conditions through ligand exchange reactions with soil phosphate and the rest of them are released slowly. Table 1 shows some common arsenic compounds and their corresponding pK_a values.

1.1.1 Inorganic and organic arsenic

When arsenic is combined with elements other than carbon, it is called inorganic arsenic. Arsenopyrite ($FeAsS$), realgar (AsS), and orpiment (As_2S_3) are the most common inorganic forms of arsenic present in ore. Inorganic arsenicals are introduced to the

environment mainly from mining and smelting activities. Another inorganic form of arsenic, chromated copper sulfate (CCA), is introduced to the environment through its application in wood preservations (Wang and Mulligan, 2006). In organoarsenicals, the

Table 1. Major arsenicals in the environment

Arsenicals	Name	Structure	pK _a	References
Inorganic arsenic	Arsenic acid		2.22 6.98 11.53	Dzombak and Morel, 1990
	Arsenous acid		9.23 12.1 12.7	Dzombak and Morel, 1990
	Monomethylarsonic acid (MMA)		3.6 8.2	Wu and Ho, 2004
Some organic arsenicals of environmental importance	Dimethylarsinic acid (DMA)		6.14	Wu and Ho, 2004
	p-arsanilic acid (pAsA)		(-NH ₃ ⁺)1.9 4.1 9.2	Nuallain and Cinneide, 1973
	Phenylarsonic acid (PhAs)		3.6 8.7	Nuallain and Cinneide, 1973
	4-hydroxy-3-nitrobenzene-arsenic acid (Roxarzone)		3.5 (-OH)5.7 9.1	Qiang and Adams, 2004

arsenic is covalently bonded to at least one carbon atom and they are introduced to the environment by microbes that methylate inorganic arsenic and various anthropogenic activities.

1.1.2 Arsenic cycling pathways: redox and methylation chemistry

In the environment, arsenic exists in both organic and inorganic forms with various oxidation states (-3, 0, +3, +5) depending on the redox potential, pH and the microbial activity of the system. In an oxidizing environment, at a pH less than 6.9, H_2AsO_4^- is the dominant species, while at higher pH values, HAsO_4^{2-} becomes dominant. Under reducing conditions, at a pH less than 9.2, the species H_3AsO_3 will dominate. Oxidation of As(III) and reduction of As(V) may occur during their storage also and, so arsenic solutions are sometimes preserved by the addition of small amounts of HCl and ascorbic acid. Though this method has been successful for keeping the oxidation state of arsenic unchanged, it can destroy MMA if present in the sample and hence cause problems in arsenic speciation (Smedley and Kinniburgh, 2002).

The term bioalkylation of arsenicals refers to the process that causes attachments of alkyl groups to arsenic in living cells. Though the involvement of ethyl and propyl groups in the bioalkylation of arsenic is rare, the existence of the compounds, $\text{As}(\text{C}_2\text{H}_5)(\text{CH}_3)_2$, $\text{As}(\text{C}_2\text{H}_5)_2(\text{CH}_3)$ and $\text{As}(\text{C}_2\text{H}_5)_3$ in the environment has been reported (Bentley and Chasteen, 2002).

Biomethylation is a common route through which inorganic arsenic can be methylated by intracellular metabolism in various organisms living in the soil and sediments and they include algae, bacteria and fungi. This leads to the production of a variety of methylated arsenicals such as MMA, DMA and trimethylarsine (TMA). This

biomethylation process was proposed by Challenger (1945) which involves stepwise reduction and oxidative methylation. The reduction steps involve the formation of arsenicals with a lone pair of electrons on the arsenic atom which then undergo subsequent methylation by S-adenosylmethionine (SAM). The basic mechanism of this reduction and oxidative methylation is shown in the following reaction scheme (Bentley and Chasteen, 2002).

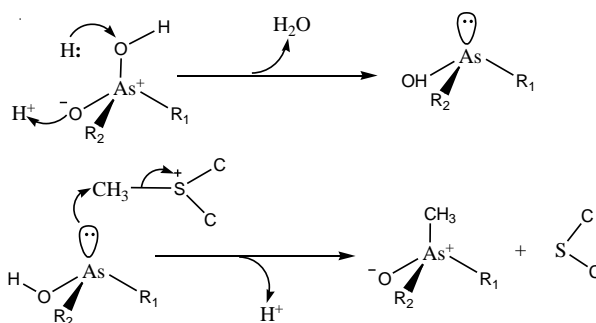


Figure 1.1. Reactions involved in the Challenger mechanism (a) top reaction involves the reduction of As(V) to As(III); and (b) the bottom reaction corresponds to the oxidative methylation. Note that R_1 and R_2 represent OH, CH_3 or both depending on the arsenic compounds (Bentley and Chasteen, 2002).

Figure 1.2 shows a reaction scheme which describes the Challenger mechanism for the biomethylation of arsenate where TMA is the ultimate product. Another pathway has been proposed for the biomethylation of inorganic arsenic where As(III) species persists during methylation and its oxidation to As(V) takes place after methylation (Hayakawa et al., 2005). The methylation pathway proposed by Hayakawa and co-workers (2005) ends with the formation of DMA(V) rather than via repetitive reduction and oxidative methylation.

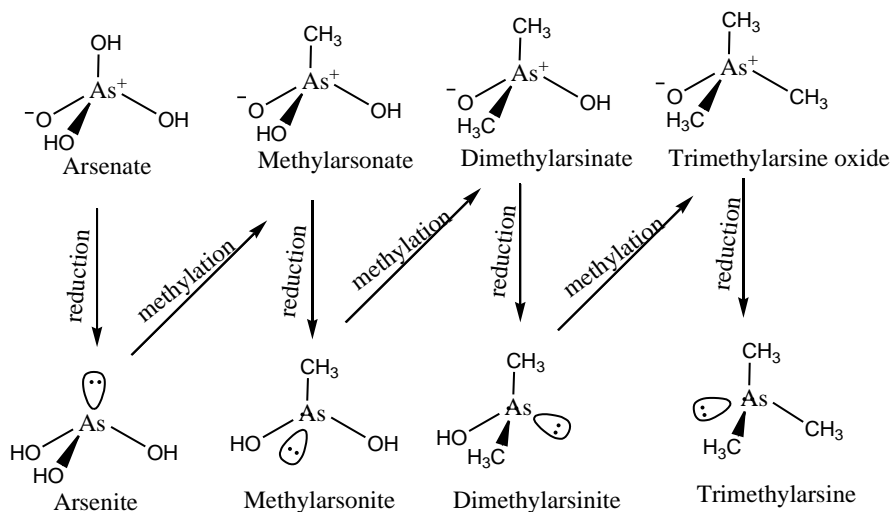


Figure 1.2. Challenger mechanism for the biological methylation of arsenic. The vertical arrows indicate the reduction of pentavalent arsenic to its trivalent form and diagonal arrows indicate the oxidative methylation.

1.1.3 Environmental fate of arsenic compounds

When arsenic is released into the environment, it may interact with various environmental surfaces. The nature of the interaction varies widely with the oxidation state of arsenic, whether it is in the organic or inorganic form, the types of environmental surfaces, environmental conditions such as temperature and pH, and the concentrations of other species present in the water sediment interface. Major sinks of arsenic in aquatic environments are iron rich sediments, though adsorption on Mn and Al-oxides has also been reported (Smedley and Kinniburgh, 2002). Arsenic is present in aquatic environments mainly as oxyanions and, because of this, other oxyanions such as phosphate, sulfate, carbonate, molybdate, and others may compete with arsenic for the same binding sites on clay and oxide minerals (Wang and Mulligan, 2006).

Degradation of soil arsenic contaminated by MSMA containing pesticides was investigated where both arsenate (iAs) and DMA are the final degradation products under flooded condition in finer textured soils (Akkari et al., 1986). Biotransformation of

MMA(V) and DMA(V) under methanogenic and sulfate reducing conditions leads to the formation of MMA(III) and MMA(V), respectively. These metabolites indicate that reduction and demethylation are important steps in the anaerobic bioconversion of methylated arsenicals (Sierra-Alvarez et al., 2006). Recent experiments by Shimizu et al. (2011a) demonstrate that MMA(V) and DMA(V) are demethylated to arsenate in soil over one year of aerobic incubation. In anaerobic conditions, methylation of MMA(V) to DMA(V) takes place, while DMA(V) remains unchanged over three months of incubation.

Both pAsA, roxarsone, and their mineralization products have been identified in the environment. It has been reported that the degradation of roxarsone leads to the formation of inorganic arsenic in the presence of water and that this process is facilitated by increasing temperature (Garbarino et al., 2003). The stability of roxarsone in the presence of light in heat-sterilized poultry-litter slurry suggests that there is a key involvement of microorganisms in the degradation process (Garbarino et al., 2003).

A study in the southern United States was carried out to observe the changes in arsenic level in a soil that had been previously exposed to arsenical herbicides. It was found that a significant amount of arsenic was present in the soil after several decades even after one time sacrificial application (Qi and Donahoe, 2008). Leaching tests on arsenic contaminated soils in the same study indicate that arsenic is bound to soil in two distinct ways. In the one case, surface species can be released rapidly while in the other they are relatively stable to removal. Almost similar findings have been observed by Tofan-Lazar and Al-Abadleh (2012a), during kinetic dependent studies for the adsorption of DMA on an iron (oxyhydr)oxide surface. There are two types of adsorption rates. Fast

and slow adsorption is the reason for the formation of these two types of surface species.

CCA is a commonly used wood preservative and arsenic leaches slowly from CCA-treated wood products over time and causes arsenic pollution in the nearby environment (Wang and Mulligan, 2006). Due to its adverse environmental impact, arsenic containing wood preservatives are no longer used to treat nonindustrial wood (Health Canada, 2005). Whatever the sources, arsenic in contaminated soil accumulates in various types of plants and enters into the food chain (Chen et al., 2008; Khan et al., 2010; Mudhoo et al., 2011; Safiullah et al., 2013; Zheng et al., 2011). Jones (2007) reported that, with equivalent soil arsenic concentrations, plants grown on sandy soil usually have higher total arsenic contents than those grown on heavier-textured soils.

1.1.4 Toxicity of arsenicals

The toxicity of arsenic compounds depends on the type of arsenical, organisms to which they are exposed, the dose, time and route of exposure. The LD₅₀ is a frequently used measure of toxicity and can be defined as the dose at which half of the target population will exhibit a specific response in a given experimental condition. Among the arsenic compounds, inorganic forms with +3 and +5 oxidation states are readily absorbed by blood and taken up by cell tissues. The more toxic inorganic forms of arsenic are considered to be detoxified primarily in liver cells of human and other living organisms (Bentley and Chasteen, 2002; Cohen et al., 2006; Tchounwou et al., 2002). In general, once adsorbed, As(V) is reduced to As(III) in presence of reducing agents; glutathione (GSH) and thioredoxin. As(III) is then taken up by cells and methylated to MMA(V) and DMA(V) through the intracellular metabolism and the main source of methyl groups for the biomethylation is SAM (Cohen et al., 2006). This metabolic process in human usually

leads to the formation of MMA(V) and DMA(V) (mostly) which are readily excreted in the urine (Fillol et al., 2010). The presence of trivalent intermediates, MMA(III) and DMA(III), have also been detected in the urine of peoples who are exposed to high level of arsenic (Vahter, 2002).

In the cell, As(III) can bind to body enzymes containing -SH groups and disrupts their functioning. Again, arsenate having the same chemical structure to phosphate can interfere with adenosine triphosphate (ATP) production, thereby hampering the energy storage system in the body (Bentley and Chasteen, 2002). The LD₅₀ values of various arsenic compounds were tested on mice where gaseous arsine (AsH₃) was found to be the most toxic and the methylated organoarsenicals were found to be the least toxic in following order: AsH₃ > methylated arsenic (III) > inorganic arsenic (III) > inorganic arsenic (V) > methylated arsenic (V) (Cullen, 2008). Among the methylated arsenic compounds, MMA(III) is the most toxic and DMA(III) is almost equal or more toxic than iAs(III) in all cells (Styblo et. al., 2000).

1.1.5 Environmental regulations of arsenic in soils and drinking water

Different environmental components contain different levels of arsenic and their exposures to human and animals are not always the same. Considering their uses, various national and international organizations have set maximum permissible limits of arsenic for different types of water and soils. In some cases socioeconomic conditions are also taken into account for establishing the maximum limit. For example, in Bangladesh the allowable level of arsenic in drinking water is 0.05 mg/L. This is five times higher than the standard set by WHO and US EPA. Table 2 shows the guideline values (the maximum concentration limit, MCL) of arsenic for a variety of uses.

Table 2. Recommended maximum contaminant levels of arsenic concentrations

Water type	MCL	References
Drinking water	0.01 mg/L	Health Canada, 2012; US EPA, 2012; WHO, 2004
	0.05 mg/L	The Environmental Conservation Rules, 1997
Irrigation water	100 µg/L	CCME, 1997
Livestock water	25 µg/L	CCME, 1997
Agricultural land	20 mg/kg	CCME, 1991
Residential and parkland	30 mg/kg	CCME, 1991
Commercial soil	50 mg/kg	CCME, 1991
Industrial use	50 mg/kg	CCME, 1991

*CCME Canadian Council of Ministers of the Environment

1.2 Previous research on the geochemistry of arsenic

1.2.1 Field measurements of monosubstituted organoarsenicals

In natural waters, inorganic arsenic in the form of arsenate and arsenite are the predominant species, but the presence of methylated organoarsenicals cannot be ignored. A variety of methylated arsenicals has been reported (<10% of the total dissolved arsenic) in some sub-arctic lakes near Yellowknife area in the Northwest Territories of Canada (Bright et al., 1996). Methylated form of arsenic compounds have also been detected, up to ~60% of total dissolved arsenic, in a number of lakes and estuaries in California (Anderson and Bruland, 1991) and in the Tinto and Odiel rivers and their respective estuary in southwest Spain (Sanchez-Rodas et al., 2005). In some cotton producing areas of the southern US where organoarsenical pesticides were used, MMA(V) and DMA (V) were detected (>10 µ/L) along with arsenate and arsenite in the respective surface and ground water (Bednar et al., 2002). Mcknight-Whitford et al.,

(2010) designed an HPLC-ESI-MS/MS method which is capable in quantifying As(III), As(V), DMA(III), MMA(V), DMA (III) and DMA (V) at environmentally relevant levels (μL). Field measurements for MMA(III) and DMA(III) in the environmental samples are very limited and their concentrations were reported <15 ng/L in Lake Biwa, Japan (Hasegawa, 1997). The trivalent methylarsenical is usually unstable and can easily be converted to its pentavalent form (Gong et al., 2001). This may be the reason for its unavailability or its extremely low levels in the environment.

The arsenicals pAsA and roxarsone are used as feed additives in the poultry industry, where roxarsone concentrations in feed formulations range from 22.7 to 45.4 g/ton. Roxarsone is the primary arsenic species used in this case and it has been found to be stable for at least 7 days in fresh dried litter. In presence of water, roxarsone in litter slurry is gradually converted to arsenate and the rate of degradation increases with increasing the amount of water (Garbarino et al., 2003). The degradation of roxarsone takes place over time when the poultry litter is applied to agricultural lands as fertilizer. At high temperature in wet condition, microbial activity accelerates the process and leads to the formation of arsenate (Brown et al., 2005; Garbarino et al., 2003).

1.2.2 Surface chemistry of arsenic compounds with metal (oxyhydr)oxides

Effective surface interactions depend on the surface charge of adsorbents and the speciation of adsorbates present in the system at a specific pH. The concept, point of zero charge (PZC), describes the condition of a surface when the net electrical charge density on a surface is zero. It is usually expressed in terms of pH at which a solid submerged in an electrolyte exhibits zero net electrical charge on the surface. The PZC is typically determined by acid-base titrations of colloidal dispersions by monitoring the

electrophoretic mobility of the particles and the pH of the suspension. The term isoelectric point (IEP) also describes the surface charge condition and it is a pH at which the colloidal particle remains stationary in an electrical field. The IEP is expected to be somewhat different than the PZC at the particle surface, but this difference is often ignored for so-called pristine surfaces, i.e., surfaces with no specifically adsorbed positive or negative species. Thus, a PZC on a surface is considered equal to the IEP in the absence of specific adsorption on that surface. The PZC is an important factor for the stability of surface particles and hence its sorption capacity. At PZC, hydrous ferric oxide (HFO) has zero surface charge because of the equal concentration of ($\equiv\text{FeOH}_2^+$) and ($\equiv\text{FeO}^-$) on the surface. The PZC of HFO usually falls in the range 7.0 to 9.5 which varies depending on the type and sources of minerals and also on the methods of determination (Kosmulski, 2009). The iron-mineral used in this thesis was hematite nanoparticles and its zero net surface charge was measured in terms of IEP, and found to be 8.6.

The values of the PZC/IEP of iron oxides are influenced by several factors such as temperature, presence of foreign ions, impurities, etc. The PZC of iron oxide usually drops as the temperature increases. With increasing temperature, ionization constant of water rises and hence the relative affinity of proton for the surface increases. Dehydroxylation of the oxide surface is caused at high temperature and results in an acid shift in the PZC. Specific adsorption of cations causes the PZC at the surface to lower to pH values whereas anions change the PZC in opposite direction. The shift of IEP usually goes up, unlike PZC, when adsorption of cations takes place on the specific sites of the surface. The adsorption of anion leads to the IEP to a lower pH. The PZC/IEP is sensitive

to the presence of traces of impurities, i.g., CO₂ and the adsorption of CO₂ species on iron oxide surface shifts to the PZC/IEP to low pH (Cornell and Schwertmann, 2003).

Metal ion in dry iron oxides is not fully coordinated with water molecules. But on exposure to water or water vapor, the dissociative sorption of water molecules through proton transfer reactions results in the formation of hydroxyl groups on the oxide surface. Hydroxylation of many metal oxides is possible even at 1 percent humidity or below (James and Parks, 1982). Water sorbs on the hydroxylated water surface and forms a layer of saturated water at the oxide/water interface. The process can be supported by variety of experimental evidence, especially by infrared (IR) spectroscopy due to the distinct absorption band for O-H stretching. There are two types of surface hydroxyl groups on iron (oxyhydr)oxides, singly coordinated (bound to one metal ion) and doubly coordinated (bound to two metal ions). The second type (doubly coordinated) is strongly polarized by metal ion and hence acidic in nature. In the singly coordinated OH groups, the polarization by the metal cation is weaker and these groups usually show basic characteristics and can possibly be exchangeable by another anion. Acidic and basic surface hydroxyl groups can be detected in IR spectra and can be quantified by the reaction with specific reagents (Dzombak and Morel, 1990).

Iron (oxyhydr)oxide surfaces are usually amphoteric in nature and can be presented by the following chemical reaction where the hydroxyl groups may be present as positively, neutral and negatively charged.



Energy is required to move the sorbing ions to the surface through the potential gradients near the charged surface. Charge on oxide surfaces affects the tendency of surface hydroxyl groups to coordinate or to dissociate protons and, depending on that, different types of surface complexes is formed. Two types of energies contribute to the total sorption energy; chemical and electrical. It is not possible to separate them experimentally but they can be separated theoretically. The contribution of chemical energy does not vary with the surface charge and the electric contribution term may be considered as variable (Dzombak and Morel, 1990).

Using the surface reactions (a) and (b), and with help of the MATLAB equilibrium solver (Smith, 2007) a distribution diagram for an iron (oxyhydr)oxide species in pristine condition can be obtained (Figure 1.3). At neutral pH, $\equiv\text{FeOH}_2^+$ and $\equiv\text{FeOH}$ are the dominant iron (oxyhydr)oxide species.

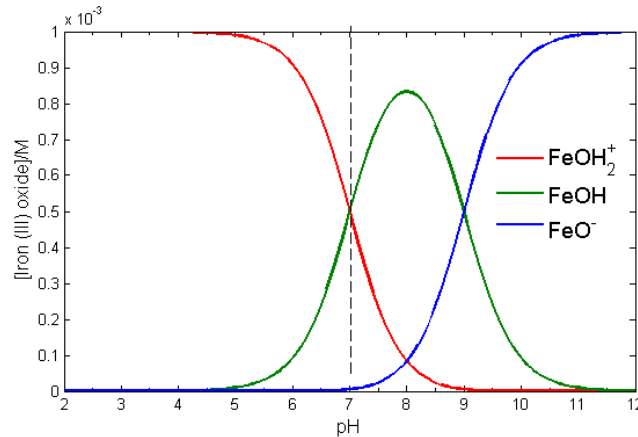


Figure 1.3. Distribution of positive, negative and neutral surface hydroxyl groups on iron (oxyhydr)oxides as a function of pH.

The distribution diagrams obtained for aqueous species of iAs(V), MMA(V), PhAs and DMA(V) as a function of pH are shown in Figure 1.4. For arsenate, H_2AsO_4^- and HAsO_4^{2-} are the predominant species at pH 7, whereas, MeHAsO_3^- and PhHAsO_3^- are

the major species of MMA(V) and PhAs, respectively. That is, the aqueous arsenicals undertaken in this study present in anionic forms for the interaction with iron (oxyhydr)oxide surfaces within environmental pH \sim 7.

There are two general proposed mechanisms for the adsorption of arsenicals on mineral oxide surface; nonspecific adsorption and specific adsorption. Nonspecific adsorption involves electrostatic attraction between the oppositely charged adsorbing species and adsorbent surface which usually leads to the formation of outer-sphere complexes; no specific sites of the adsorbent molecules contribute in such interactions. But in case of inner-sphere complexes, the hydroxyl groups of the iron oxides interact strongly with the adsorbing species and such adsorption is strongly pH dependent (Cheng et al., 2009).

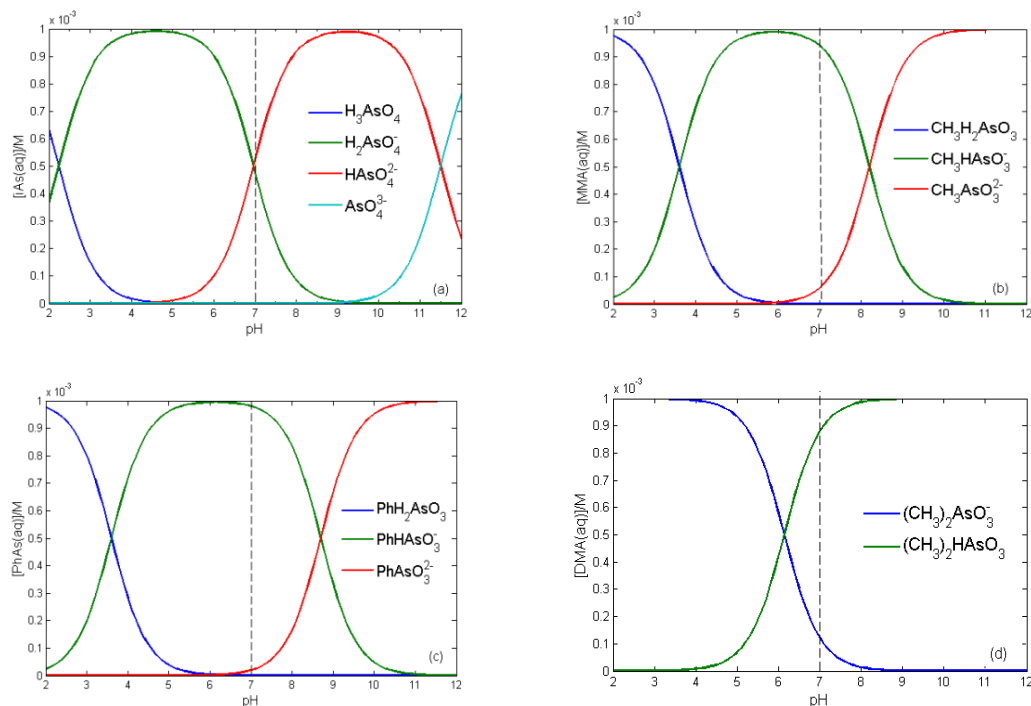


Figure 1.4. Distribution diagram for the species formed by (a) iAs(V); (b) MMA(V); (c) PhAs; and (d) DMA(V) species as a function of pH.

At acidic pH, the hydroxyl groups of iron oxides are doubly protonated ($\equiv\text{FeOH}_2^+$) and hence the surface charge becomes positive. At a PZC, the surface charge becomes neutral and can be presented as $\equiv\text{Fe-OH}$. In alkaline conditions, above the PZC, surface becomes deprotonated, and gains negative charge. Maximum adsorption occurs at acidic pH because of the interaction of anionic arsenical species with positively charged iron oxide surface. But in a very strongly acidic condition, electrostatic attraction between the fully protonated arsenicals and the positively charged oxide surface ($\equiv\text{FeOH}_2^+$) will no longer be possible. In strongly alkaline condition, adsorption does not occur or is very poor due the repulsion of negatively charged arsenic oxyanion with the negatively charged iron oxide surface (Carabante et al., 2009). Ionic strength also affects the electrostatic forces near the oxide surfaces and hence influences the formation and stability of the weakly bounded outer-sphere complexes. The directly coordinated inner-sphere complexes are usually strong and are relatively independent of the ionic strength (Cheng et al., 2009). Sorption of anionic arsenicals on iron (oxyhydr)oxides takes place by the ligand exchange reaction where basic hydroxides from the surface are replaced by the sorbing anions.

1.2.3 Bulk/batch studies on the adsorption/desorption behavior of monosubstituted organoarsenicals on soils and metal oxides

Ligand exchange reactions between charged arsenic compounds and surface sites on metal oxides drive the adsorption reactions of arsenicals. Surface complexation of arsenic in oxidation state of +5 occur over a wide pH range because these arsenic species are negatively charged and metal oxides are mostly positively charged due to their high PZC.

Methylated forms of arsenic are of special interest because of their widespread distribution, their acute toxicity and their adsorption/desorption behavior to/from soil components. Like inorganic arsenicals, surface interactions of MMA and DMA with iron oxides are greatly influenced by pH (Bowell, 1994; Cox and Ghosh, 1994; Lafferty and Loeppert, 2005; Xu et al., 1991). Competitive adsorption of methylated arsenicals with other inorganic arsenicals on alumina oxide surfaces (Xu et al., 1991) follows the order; $iAs(V) > DMA(V) = MMA(V) > iAs(III)$ at $pH < 6$ but at or above pH 6, it follows a different trend; $iAs(V) > iAs(III) > DMA = MMA$. Almost similar adsorption patterns have been observed for these arsenicals on iron oxide surfaces (Bowell, 1994).

Lafferty and Loeppert (2005) carried out a detailed experiment for the comparative adsorption/desorption of iAs , MMA and DMA in both the oxidation states, +3 and +5 on/from iron oxides. From this study, it reveals that MMA(III) and DMA(III) are negligibly adsorbed by both goethite and ferrihydrite where $iAs(III)$ binds strongly to these minerals within the experimental pH range (3 to 11). In the same study, MMA(V) and $iAs(V)$ show greater affinity to both iron oxides between pH 3 and 10, but adsorption of DMA(V) takes place at pH values below 8 for ferrihydrite and below 7 for goethite. The adsorption affinities of $iAs(V)$ and MMA(V) are also much greater than that of DMA(V). This may be due to the presence of the additional methyl group in DMA(V) and its molecular geometry (Adamescu et al., 2010). The fact can be explained by the rapid removal of MMA(V) during the desorption from a surface. The difference in the surface binding strengths of MMA(V) and $iAs(V)$ could be explained by the electron donating capabilities of the methyl group. Along with the inner-sphere complexes, the formation of outer-sphere complexes of $iAs(V)$ (Catalano et al., 2008) and DMA(V)

(Adamescu et al., 2010) with iron (oxyhydr)oxides have also been reported. Similarly to iAs and DMA, MMA having a similar molecular structure and sorption behavior towards hematite/goethite, can form outer-sphere complexes with goethite (Shimizu et al., 2011b).

The nature of the surface complexes formed by MMA and DMA varies depending on which surfaces they interact. On amorphous aluminum oxides (AAO), both MMA and DMA have been reported to form bidentate binuclear complexes when studied by FT-IR and EXAFS techniques (Shimizu et al., 2010). The same mechanism was put forward for the binding of MMA and DMA when the study was conducted with goethite using EXAFS (Shimizu et al., 2011b). However, a different picture was obtained for the surface complexation of MMA and DMA with titanium dioxide. The mechanism for the adsorption of methylated organoarsenicals (MMA/DMA) on nanocrystalline TiO₂ has been investigated by X-ray absorption spectroscopy (XAS). Both MMA and DMA form different types of inner-sphere complexes as explained by the different As-Ti bond distances. The experimental data suggests that MMA forms a bidentate surface complex on the metal oxide whereas formation of a monodentate complex is favored by DMA (Jing et al., 2005). There are very few studies on the surface chemistry of pAsA and roxarsone. A laboratory study shows that roxarsone is more easily extractable than As(V) by aqueous phosphate from soils previously exposed to the arsenicals (Jackson et al., 2006).

The majority of studies for the binding of arsenicals are batch experiments that explored the thermodynamics and kinetics of binding indirectly by quantifying the concentration before and after adsorption. Therefore, a surface sensitive technique is required for a more detailed understanding of the surface chemistry at the molecular

level. An ATR-FTIR study (part of this thesis) on the adsorption of pAsA and PhAs shows that these aromatic arsenicals form mostly inner-sphere monodentate complexes on hematite nanoparticles (Arts et al., 2013).

1.3 Research objectives and goals

The objective of this research is to utilize a surface sensitive technique to study the structure, kinetics, and thermodynamics of the interactions of monosubstituted organoarsenic compounds with hematite. This thesis comprises the experimental methodology; attenuated total internal reflectance Fourier transform infrared (ATR-FTIR) spectroscopy, which is useful to study surface interactions in situ at the molecular level at the liquid-solid interfaces. Another advantage of this technique is the relatively short path length (1-3 μm) of the IR beam which helps to isolate the signals for surface species after subtracting the signals for the solution.

Using this technique, adsorption kinetics of some monosubstituted organoarsenicals such as MMA, pAsA and PhAs on iron(oxyhydr)oxides were studied at environmentally relevant conditions, i.e. neutral pH, flow mode of aqueous phase and 0.01 M NaCl/KCl ionic strength. The desorption kinetics of these arsenicals from the surface using different concentrations of phosphate were also investigated. Because of the structural similarities, adsorption and desorption studies with iAs(V) were completed for comparison. In addition, pH(D) edge and adsorption isotherm experiments as a function of concentrations and temperature were carried out for iAs(V), MMA(V) and DMA(V) on iron(oxyhydr)oxides to study the binding thermodynamics.

2 Experimental

2.1 Description of the ATR-FTIR setup

ATR-FTIR spectra were collected as a function of time on a freshly prepared hematite film using a HATRPlus accessory (Pike Technologies) installed in a Nicolet 8700 FTIR spectrometer (Thermo Instruments) equipped with a thermo detector. The ATR flow cell (Figure 2.1) used in the experiments contains a 60° ZnSe crystal IRE (80×10×4 mm, 100 μL). The IR beam incidents at a 60° angle in the ZnSe crystal and passes through the crystal by propagative internal reflection. At each reflection point, an evanescent wave is produced that extends beyond the surface of the crystal into the sample held in contact with the crystal. The sample absorbs energy causing the attenuation of the evanescent wave and is passed back to the IR beam which finally goes to the detector.

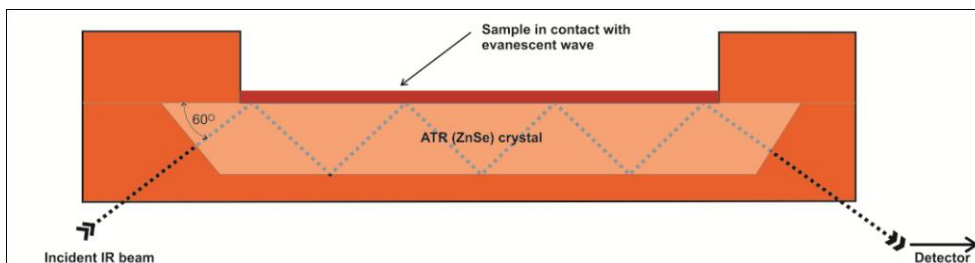


Figure 2.1. ATR-flow cell (100 μL), Film thickness $\sim 5 \times 10^{-4}$ cm.

The path length of the IR beam can be calculated as:

$$\text{Total path length, } \mathbf{b} = N \cdot d_p = N \cdot \frac{\lambda_{IR}}{2\pi n_1 \sqrt{\sin^2 \theta - \left(\frac{n_2}{n_1}\right)^2}}$$

Where, θ = angle of incidence, N = number of reflections inside the crystal, d_p = depth of penetration into the sample, n_1 and n_2 are the refractive index of the ATR crystal and sample, respectively, λ_{IR} = wavelength of IR.

2.2 Reagents

Arsenic solutions were made by dissolving respective compounds in 0.01 M NaCl (crystalline solid, 99.0%, ACS reagent, BDH) or KCl (GR ACS, 99.0%, EMD) solution prepared previously in 18 M Ω -cm Millipore water and finally adjusted to the desired pH by using dilute and concentrated HCl (6 N, Ricca Chemical Company) and NaOH (GR ACS, 99.0-100%, EMD) solutions. Arsenicals used herein include iAs(V) (Sodium hydrogen arsenate heptahydrate, Na₂AsO₄·7H₂O, ACS reagent, J. T. Baker), pAsA (p-arsanilic acid, C₆H₈AsNO₃, 99%, Sigma-Aldrich), PhAs (phenylarsonic acid, C₆H₇AsO₃, 97%, Acros Organics), MMA(V) (Disodium methyl arsonate hexahydrate, CH₃AsNa₂O₃·6H₂O, 97.5%, Chem Service Inc.), and DMA(V) (sodium cacodylate trihydrate, C₂H₆AsO₂Na·7H₂O, \geq 98.0%, Sigma-Aldrich) as received without further purification. ***Caution: The aforementioned arsenical compounds are highly toxic via inhalation and skin contact and are carcinogens.*** Some preventive measures were taken to minimize exposure to arsenicals: (i) using personal protective equipment and (ii) opening arsenic bottles inside a fume hood. Phosphate (monohydrogen phosphate, Na₂HPO₄, 99.99%, Sigma-Aldrich) solutions were used as the desorbing agent. The solutions of phosphate, HPO₄²⁻ (aq), were prepared only in 18 M Ω -cm Millipore water adjusted to the desired pH. All the solutions were prepared freshly before the start of each experiment and were kept covered with parafilm until used. The iron (oxyhydr)oxide used as adsorbent for the preparation of film on the ATR crystal was hematite nanoparticles (α -Fe₂O₃, Inc., >99.9%). This nanostructured and amorphous material was characterized previously (Depalma et al., 2008) with 19 m²/g surface area, 67 nm average diameter, and an IEP of 8.6. The IEP was determined via zeta potential titration. In

addition, the chemicals used for pD edge experiments were deuterium oxide (D_2O , 99.9 atom % D, Sigma-Aldrich), deuterium chloride solution (35 wt% in D_2O , 99 atom %D, Sigma-Aldrich), sodium deuterioxide (40 wt% in D_2O , 99.5 atom %D, Sigma-Aldrich) and pHydrion Tri-chek buffer capsule set (pH = 4.00 \pm 0.02, 7.00 \pm 0.02, 10.00 \pm 0.02, Micro Essential Laboratory, USA).

2.3 Film preparations on the ATR-FTIR crystal

A film was prepared using 6 mg of hematite nanoparticles in a 1.30 mL water-ethanol [0.91:0.39 (v/v)] mixture. The mixture was ultrasonicated (default power, Fisher Scientific Mechanical Ultrasonic Cleaner FS20) for one hour and the slurry obtained was deposited on a dry ZnSe ATR crystal. The deposited film was allowed to dry for 10-12 hours in air at room temperature under an Al-foil tent on the lab bench. The film was then ready for use for the adsorption/desorption experiments. The thickness of the dry film was estimated to be $\sim 5 \times 10^{-4}$ cm, which is larger than the effective penetration depth of the evanescent wave ($\sim 2 \times 10^{-4}$ cm/reflection at 840 and 880 cm^{-1} and 1.5×10^{-4} cm/reflection at 1003 cm^{-1} using the same method described in Depalma et. al., 2008).

2.4 Experimental procedure

2.4.1 Preparation of calibration curve using ATR-FTIR

For the preparation of calibration curves, standard solutions of 1 to 10 mM iAs(V), 10 to 100 mM MMA and 8 to 100 mM for each of PhAs and DMA(V) were prepared in 0.01 M NaCl/KCl background solutions at pH 7. Background solution was passed through the ATR cell over the ZnSe crystal for 30 minutes and then arsenical solutions were flowed for 10 minutes from lower to higher concentrations. ATR-FTIR spectra were collected in flow mode (2 mL/min) at 8 cm^{-1} resolution with 100 average

scans. The absorbance spectra for each of the arsenicals of a given concentration were obtained by referencing the respective single beam spectra against the last spectrum collected for the background solution. To obtain the absorbance values, the spectral math tool in the OMNIC software was used to obtain baseline-corrected heights.

2.4.2 Adsorption kinetics using ATR-FTIR

The solutions were flowed at a rate of 2 mL/min across the hematite film using Tygon tubes (0.8 mm I.D., Masterflex) and a compact pump (Masterflex L/S). Single beam ATR-FTIR spectra were collected at 8 cm^{-1} resolution all through the experiments. At the beginning of every adsorption experiment, 0.01 M NaCl/KCl at pH 7 was flowed first for 90 minutes over the film to record background spectra with 100 averaged scans. Then, arsenic solutions of known concentrations at pH 7 were flowed across the same film. Collection of adsorption spectra started as the solution entered the ATR flow cell and spectral averaging was 5 scans for up to 30 min. Collection of adsorption spectra was automated using a custom-written macro in OMNIC. This software was installed on a PC computer with these specifications: Dell Optiplex GX620, Intel, ACPI Multiprocessor, and Premium 4 CPU 3.20 GHz with 1 GB RAM. The collection acquisition times were calculated from the time saved by the computer in the file names. For collecting 5 and 100 averaged scans, the collection times were 6 and 50 s, respectively. Each single beam spectrum was referenced to the last one recorded for the background solution to obtain the absorbance spectra reported herein (Details for the collection of spectra and the referencing to absorbance spectra are described in Appendix A). To determine the uncertainty in the measurements, the experiments were repeated at least two times on freshly prepared films under identical conditions.

2.4.3 Desorption kinetics using ATR-FTIR

Aqueous hydrogen phosphate (Na_2HPO_4) at pH 7 was used as a desorbing agent for the desorption part of the experiments. Collection of desorption spectra started once the solution of the desorbing agent entered the ATR flow containing the same hematite film previously exposed to arsenic solution (0.50 mM) for 30 min. Single beam ATR spectra were collected and reprocessed against the last spectrum collected for the background solution for obtaining the absorbance spectra as described in the previous section for the adsorption experiments. Since desorption of surface arsenicals due to flowing aqueous hydrogen phosphate would occur concurrently with the adsorption of phosphate species, the control experiments were carried out for the adsorption of aqueous hydrogen phosphate on freshly prepared films at pH 7.

2.4.4 Adsorption isotherm using ATR-FTIR

Arsenical solutions of concentrations (0.001, 0.005, 0.01, 0.03, 0.05, 0.1, 0.15, 0.25, 0.5, 0.8, 1 and 2 mM) were prepared by dissolving the respective compound in 0.01 M NaCl background solution and all the solutions were adjusted to pH 7 using dilute and concentrated NaOH and HCl solution. No buffer was used to maintain the pH around 7. Instead, a pH meter was constantly collecting values, which did not vary much during the course of the experiment. Arsenicals used in this study include iAs(V), MMA(V) and DMA(V). For each isotherm experiment, arsenical solutions from lower to higher concentrations were flowed across the freshly prepared 6 mg Fe-(oxyhydr)oxide film for 15 min for each concentration. Single beam ATR-FTIR spectra were collected at 8 cm^{-1} resolution with 100 averaged scans all through the experiment. The acquisition time for the collection of 100 averaged scans was 50 s. At the beginning of every experiment, 0.01

M NaCl at pH 7 was flowed first for 90 min to record background spectra and then arsenical solutions were flowed one after another over the same film. Flow rates for all the solutions were maintained at 2 mL/min during their run over the hematite film. Each single beam spectrum collected at the end of passing every arsenical solution at a given concentration was referenced to the last one recorded for the background solution (0.01 M NaCl) to obtain the absorbance spectra reported herein. All the experiments were repeated at least twice in the same experimental conditions to determine the precisions of the experiments.

Isotherm experiments for each arsenical were carried out at five temperatures; 5, 15, 25, 35, and 50 °C. The temperature for each experiment was maintained by circulating water of various temperatures from an Endocal Refrigerated Circulating Bath (Neslab, RTE-5DD) through the flow channel constructed inside the cover of the ATR flow cell. A thermocouple probe (6", Chromega-Alomega, Omega Engineering) was attached using a thermocouple adhesive pad (Omega Engineering) to the top of the ATR flow cell to monitor the temperature throughout the experiment using a temperature reader (ATC-024-1, Harric Scientific Products, Inc.).

2.4.5 Adsorption pH(D) edge using ATR-FTIR

pH(D) edge experiments were carried out for iAs(V), MMA(V) and PhAs of concentration 0.5 mM prepared in 0.01 M NaCl/KCl background solution. At the beginning of each experiment, the 0.01 M NaCl/KCl solution at pH 7 was flowed first over the freshly prepared hematite film (6 mg) for 90 min to record the background spectra. The background solution was passed for 30 min at pD 7 to equilibrate the surface with D₂O. The flow rate for all the solutions was maintained at 1 mL/min during their run

over the hematite film. Then the arsenic solution was started flowing from pH(D) 10 to 4 at room temperature on the same hematite film. The flow time for the arsenicals was maintained 15 and 10 min at each pH(D) for pH and pD edge experiments, respectively. For the pH edge experiments, single beam spectra for the adsorption of arsenicals were collected by lowering the pH 0.5 in each step. The spectra were also collected at four pD values of 10, 8.5, 5.5 and 4 in the D₂O system. pH edge experiments were performed in ordinary open condition but for pD edge experiments some special measures were taken into account during the course of the experiments. These are:

- (1) The glass electrode was cleaned and filled with a 3 M KCl solution prepared in D₂O. The pD meter was calibrated using buffer solutions of pD = 4.00, 7.00 and 10.00 (Micro Micro Essential Laboratory (USA), pHydrion Tri-Chek Buffer Capsule Set) and prepared in D₂O.
- (2) Arsenic solutions were prepared using a 0.01 M KCl background solution previously prepared in D₂O as the solvent and the pD adjustments were done using a dilute and concentrated solutions of DCl and NaOD.
- (3) All the above steps were completed inside a glove box at 0% relative humidity and the prepared solutions (pD adjusted) were covered with parafilm to prevent any exchange of hydrogen isotope with deuterium from atmospheric moisture. During the flow of solutions, a very small hole was made on the parafilm cover just to allow one end of Tygon tube for pumping the solution towards the ATR flow cell.

Absorbance spectra were obtained by referencing the single beam spectra collected for arsenicals to the last one recorded for the background solution (0.01 M KCl/NaCl).

3 Results and Discussion

3.1.1 ATR-FTIR spectra for inorganic and organic arsenicals in the aqueous phase

ATR-FTIR is a demonstrated technique for studying the surface interaction of arsenic compounds on a number of metal oxides. Such surface interactions are affected by a number of factors; the protonation state of the arsenicals, the presence of organic substituent/s in arsenicals, and the nature of the oxide surfaces (Cowen et al., 2008). For the interpretation of surface interactions of arsenicals with iron (oxyhydr)oxides, spectra for standard solutions of arsenicals were collected on a ZnSe ATR crystal as a function of concentration. The left panel in Figure 3.1 shows the bulk liquid phase ATR-FTIR absorbance spectra for iAs(V), MMA(V), PhAs and DMA(V). Spectra were collected on clean dry ZnSe ATR crystal (no hematite film) as a function of concentration in flow mode (2 mL/min) at pH 7 and 0.01 M KCl/NaCl.

The most intense peak, at 875 cm^{-1} , arises in the bulk phase spectra (Figures: 3.1a, 3.1c and 3.1e) collected for iAs(V), MMA(V) and PhAs whereas that for DMA(V) is at 840 cm^{-1} (Figure 3.1g). These spectral features were assigned to the As-O stretching vibration of the AsO_x moiety of the dominant arsenic species at pH 7. The speciation of arsenicals; iAs(V), MMA(V), PhAs and DMA(V), in the aqueous phase is shown in Figure 1.4 as a function of pH, which also highlights the pK_a values of these acids. Due to the structural differences that influence molar absorptivity, the detection limits of the ZnSe ATR accessory for various arsenicals differ depending on the species present in the aqueous phase at pH 7. The detection limits of the ATR accessory were observed to be 1, 10, 8 and 8 mM for iAs(V), MMA(V), PhAs and DMA(V), respectively.

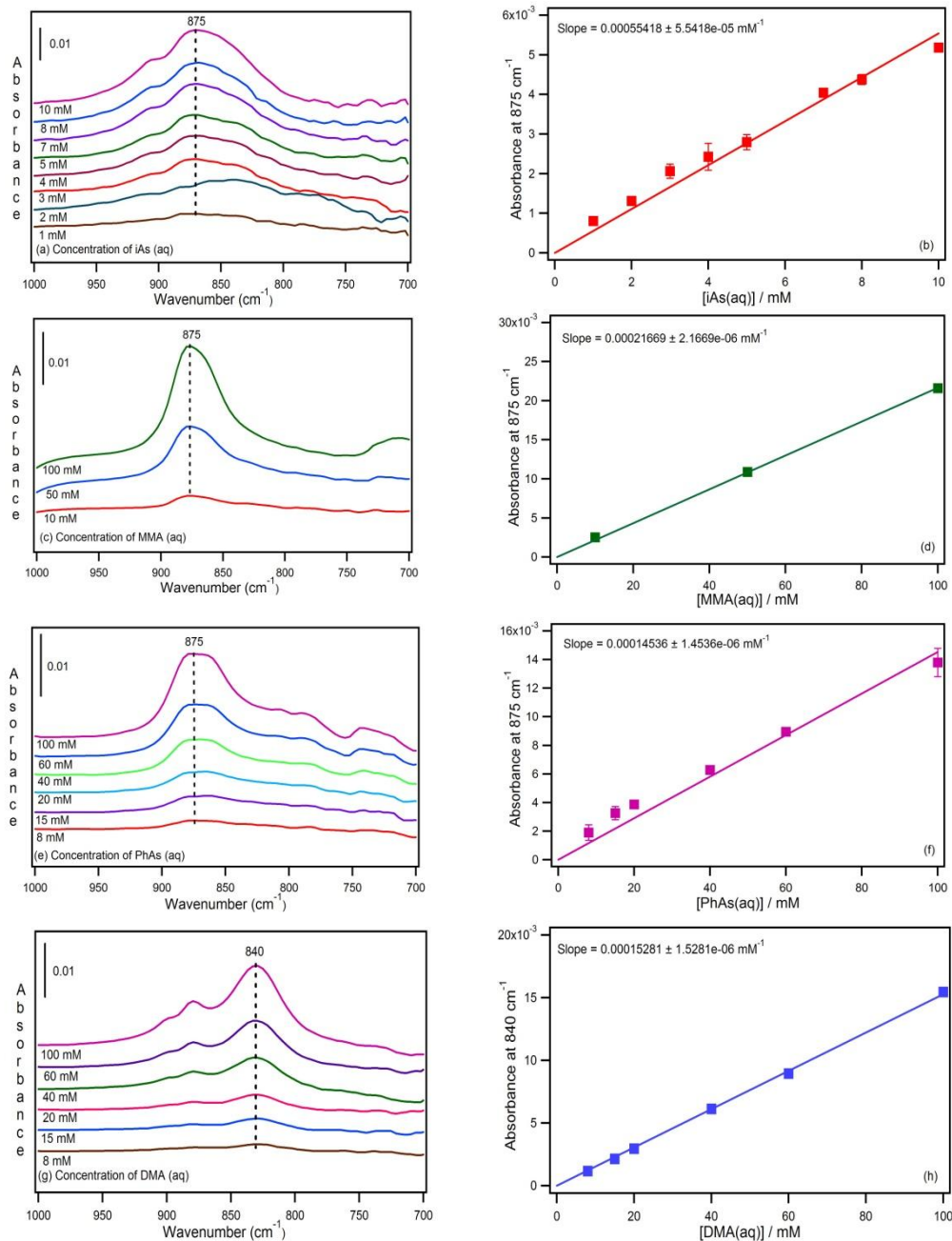


Figure 3.1. Bulk phase ATR-FTIR spectra collected for (a) iAs (1, 2, 3, 4, 5, 7, 8 and 10 mM), (c) MMA (10, 50 and 100 mM), (e) PhAs (8, 15, 20, 40, 60 and 100 mM), and (g) DMA (8, 15, 20, 40, 60 and 100 mM) as a function of concentration at room temperature pH=7, I=0.01 M NaCl at room temperature. The right panels show the corresponding calibration curves. Two trials were averaged for the preparation of each calibration curve.

3.1.2 Calibration curves

An individual calibration curve for each arsenic compound has been constructed from the baseline corrected absorbance of the most intense feature assigned to $\nu(\text{As-O})$ as a function of concentration in aqueous phase. According to the Beer–Lambert law, the slope of each line in the calibration curves represents the molar absorption coefficient (ϵ) multiplied by the effective path length of the respective arsenic compound. Table 3 lists values of the molar absorption coefficient (ϵ) for each arsenical, which gives information about how strongly a chemical species absorbs light at a specific wavelength. A sample calculation on how ϵ is calculated is provided in Appendix B. The coefficient is useful in converting the baseline absorbance, assigned to surface species, to surface coverage in units of molecule/cm². The main assumption for the determination of surface coverage is that; the molar absorption coefficient for a given arsenic compound and its surface complex are equal.

Table 3. List of ϵ values for each arsenical at pH 7

As compound	Structure at pH 7 (mostly)	Most intense $\nu(\text{As-O})$	ϵ (cm ² molecules ⁻¹)
iAs(V)		875	3.19×10^{-18}
MMA(V)		875	1.25×10^{-18}
PhAs		875	8.38×10^{-19}
DMA(V)		840	8.46×10^{-19}

3.2 Adsorption kinetics

3.2.1 Spectra for the adsorption of arsenicals on hematite

The adsorption experiments of these arsenicals have been conducted on hematite film (spread over ZnSe crystal) at concentrations below the detection limits of the ATR crystal in the aqueous phase. Adsorption kinetic experiments were also carried out as a function of concentration from 0.1 to 1 mM for iAs(V) and from 0.25 to 0.85 mM for each of MMA(V), pAsA and PhAs, respectively. Figure 3.2 shows representative adsorption spectra for the experiments done using 0.5 mM concentration of each. The IR signature for the adsorbed arsenate has been studied extensively at equilibrium on a number of metal-(oxyhydr)oxides that include hematite and goethite. These studies coupled with results from x-ray absorption studies reported that arsenate forms predominantly inner-sphere bidentate binuclear complexes which gives rise to $\nu(\text{As-OFe})$ in the range 824 to 800 cm^{-1} (Catalano et al., 2008; Goldberg and Johnston, 2001; Myneni et al., 1998; Roddick-Lanzilotta, 2001). The IR signals for $\nu(\text{As-O})$ in these complexes within 860-780 cm^{-1} have been assigned to singly protonated monodentate complexes around neutral pH (Loring et al., 2009). A broad absorption in the range 800 to 900 cm^{-1} is composed of a number of overlapping bands. This feature contains absorptions assigned to $\nu(\text{As-OFe})$, uncomplexed $\nu(\text{As-O})$ with a bond order of 1.5 due to resonance, or $\nu(\text{As-O})$ weakly H-bonded to neighboring $-\text{FeOH}$ sites. Based on the above discussion, mono- and bidentate inner-sphere protonated complexes can contribute mostly to the spectral feature 787 cm^{-1} to $\nu(\text{As-O})$. In addition, the peak arising at 875 cm^{-1} (Figure 3.2a) can be interpreted as evidence for the presence of outer-sphere surface complexes suggested by Roddick-Lanzilotta et al. (2001). The spectral features at 840

and 793 cm^{-1} for MMA(ads) appear to be due to surface species (Figure 3.2b) which were clearly absent from the bulk phase spectra (Figure 3.1c). The assignment of the spectral components at 837 and 793 cm^{-1} for the surface species formed by pAsA(ads) and PhAs(ads) on hematite have been published from this thesis (Arts et al., 2013). The components at 793 cm^{-1} were assigned to inner-sphere complexes with an uncomplexed As-O bond and the most intense spectral feature arising at 837 cm^{-1} was assigned to $\nu(\text{As}=\text{O})$ which suggests the formation of a monodentate surface complex with two As $=\text{O}$ bonds in resonance. The nature of the MMA-hematite surface complexes formed by means of spectral features will be discussed afterward in detail on the basis of their adsorption/desorption behavior.

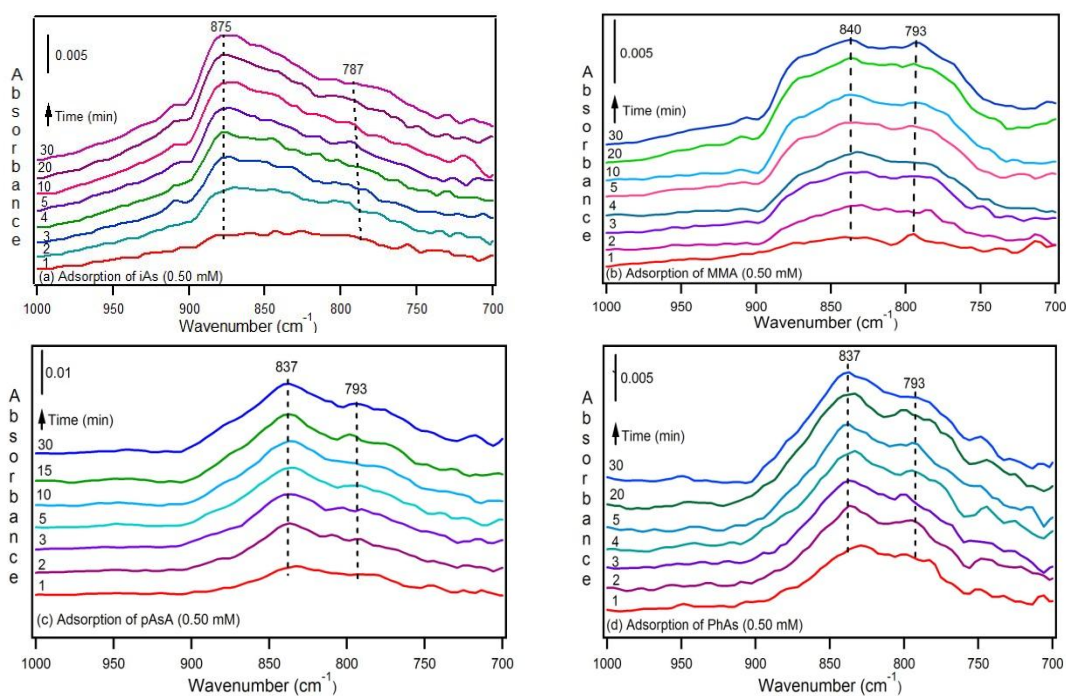
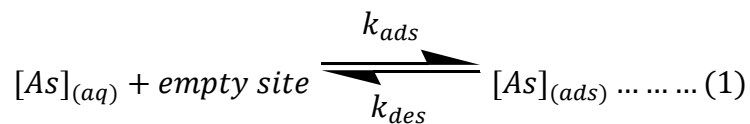


Figure 3.2. ATR-FTIR adsorption spectra collected during the adsorption of (a) iAs; (b) MMA; (c) pAsA; and (d) PhAs on hematite at pH=7, $I=0.01\text{ M NaCl}$, and 2 mL/min flow rate at room temperature as a function of time.

3.2.2 Mathematical models used in describing adsorption kinetics

To extract adsorption and desorption kinetics of surface species from ATR absorbances, a relatively accurate peak analysis method is required to estimate surface coverage from spectral data. Spectra collected as a function of time were used to generate kinetic curves by plotting the time dependence of the baseline-corrected ATR absorbance [i.e., peak height at a given wavenumber, $A(\tilde{\nu})$] of spectral features assigned to surface complexes. The advantages of considering peak heights instead of integrated peak areas for the construction of kinetic curves has been addressed earlier (Lazar-Tofan and Al-Abadleh, 2012b). Using the height tool in the OMNIC software that runs the FTIR spectrometer and a custom-written macro, values of $A(\tilde{\nu})$ were generated relative to the absorbance at 2000 cm^{-1} , which has no absorptions from any of the species used in our studies. The main assumption in this analysis method is that the uncertainty from intensity contributions of neighbouring peaks is lower than that estimated from averaging multiple experiments under the same conditions.

For the adsorption kinetic experiment, the simple Langmuir adsorption kinetic model has been used (equation 2) for reaction (1):



$$\theta(t) = b(1 - e^{-r_{obs} \cdot t}) \dots \dots \dots (2)$$

where $\theta(t)$ is the relative surface coverage of the surface species formed after adsorption which is equivalent to $A(\tilde{\nu})/A_{max}(\tilde{\nu})$, b is a collection of constants and is equal to

$k_{ads}[As]_{(aq)}/r_{obs}$ and $r_{obs} = k_{ads}[As]_{(aq)} + k_{des}$. Now, in terms of absorbance equation (2) can be rewritten as follows:

$$A(\bar{v})/A_{max}(\bar{v}) = b(1 - e^{-r_{obs} \cdot t})$$

$$\text{then, } A(\bar{v}) = b'(1 - e^{-r_{obs} \cdot t}) \dots \dots \dots (3)$$

$$\text{where, } b' = A_{max}(\bar{v}) \cdot b$$

b' can be taken by averaging the absorbance values collected in the plateau region. For the extraction of the observed initial rate of adsorption, equation (3) has been linearized according to the following equation:

$$\ln\left(1 - \frac{A(\bar{v})}{b'}\right) = -r_{obs} \cdot t \dots \dots \dots (4)$$

where r_{obs} is the observed rate of adsorption which is equal to the slope of the least-squares fit when $\ln\left(1 - \frac{A(\bar{v})}{b'}\right)$ is plotted with adsorption time. The Langmuir model predicts that r_{obs} can be expressed mathematically by equation (5), which can be used to extract values of the pseudo first order adsorption and desorption rate constants.

$$r_{obs} = k_{ads}[As]_{(aq)} + k_{des} \dots \dots \dots (5)$$

where k_{ads} and k_{des} are the adsorption and desorption rate constants.

3.2.3 Adsorption kinetic curves

The kinetic curves for the adsorption of the arsenicals on hematite nanoparticles were constructed for the peaks labeled in Figure 3.2 for the surface species. The kinetic curves for iAs(ads) was generated from the baseline corrected ATR absorbance extracted from the most intense peak at 875 cm^{-1} (Figure 3.3a) and for the peak at 787 cm^{-1} . For MMA, the spectral components for surface species taken into account were 840 and 793 cm^{-1} . The same curves for pAsA and PhAs were constructed considering the absorbances

at both 837 and 793 cm^{-1} . The kinetics curves for the adsorption of MMA (Figure 3.3b), pAsA (Figure 3.3c) and PhAs (Figure 3.3d), as a function of concentration, are shown below based only on the most intense spectral component arising within 837-840 cm^{-1} .

For the extraction of rates of adsorption from these kinetic curves, the experimental data were linearized according to equation (4). Figure 3.4 shows plots of linearized absorbances (at 875 cm^{-1} for iAs and 837/840 cm^{-1} for MMA, pAsA and PhAs) versus adsorption time. The figures for the kinetic curves and linearized absorbances at 787/793 cm^{-1} as a function of time are not shown here. The figures have been analyzed for the extraction of r_{obs} and are plotted in Figure 3.5 for the extraction of adsorption rate constant.

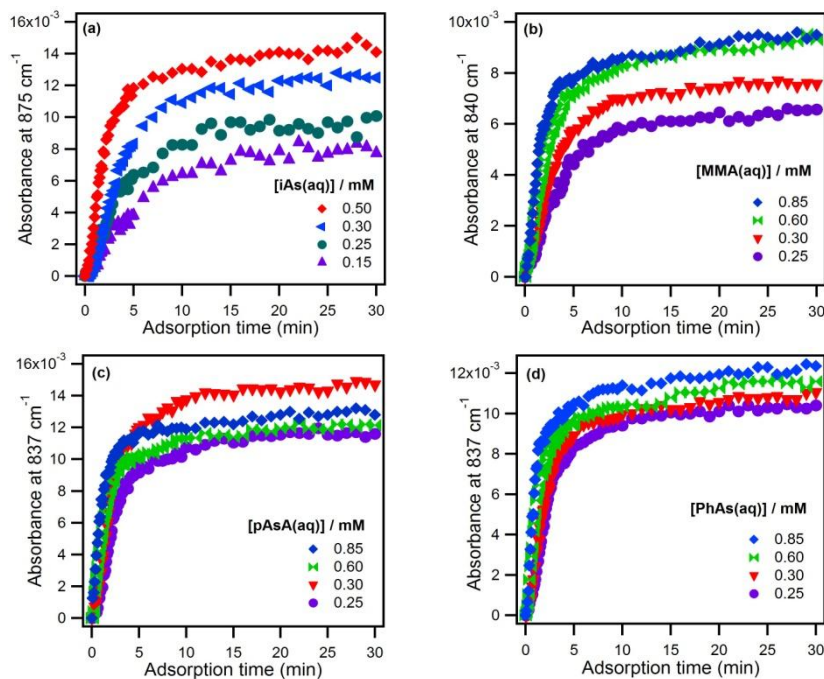


Figure 3.3. Kinetic curve generated for the adsorption of (a) iAs(aq), (b) MMA(aq), (c) pAsA(aq) and (d) PhAs(aq) on hematite at pH=7, $I=0.01$ M NaCl, and 2 mL/min flow rate at room temperature as a function of time. Not all the concentrations are shown in the kinetic curves. Data points represent the average of two to four experiments and error bars were removed for clarity. The uncertainty in the measurements is 5% ($\pm\sigma$).

From the kinetic curves, it appears that equilibrium is established after ~ 15 min of adsorption. Therefore, for chapter 3.4 and 3.5, adsorption spectra were collected after 15 min to make sure that surface species are in equilibrium mode. Our objective is to extract rates of adsorption from the experimental data within the first 1-3 min of surface interaction as we chose to show our data within this short time. The start and end points for the linear least-squares regression analysis were chosen at time zero and the time at which the initial data deviates from linearity, respectively, determined from visual inspection of the data. The slope of the least-squares fits (Figures 3.4a-d) in each represents the observed rate of adsorption (r_{obs}) during the initial stage. The start time for data in Figure 3.4 (c) and (d) is slightly higher than zero for the low concentrations.

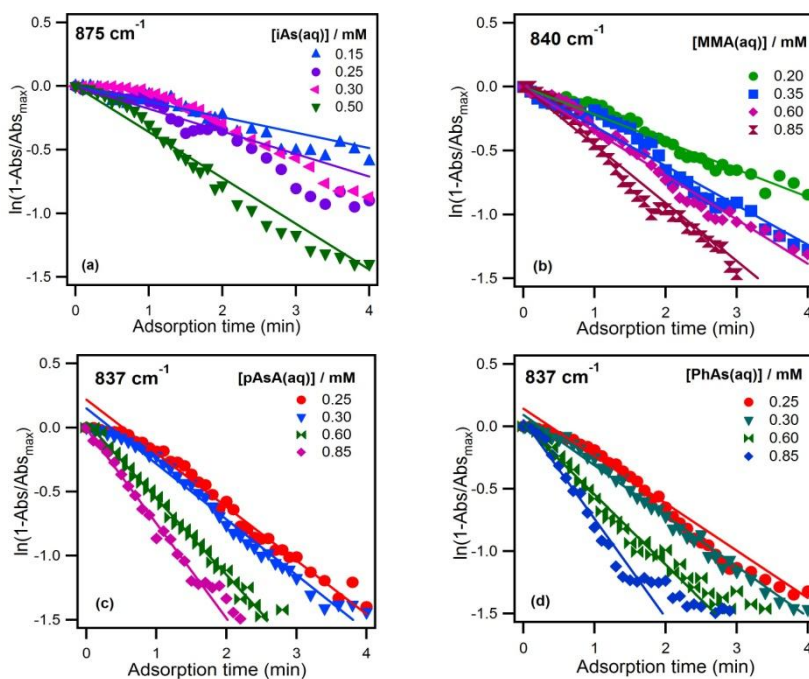


Figure 3.4. Linearized absorbances for the adsorption of (a) iAs(aq), (b) MMA(aq), (c) pAsA(aq) and (d) PhAs(aq) on hematite at $\text{pH}=7$, $I=0.01 \text{ M NaCl}$, and 2 mL/min flow rate at room temperature as a function of time. Data for each concentration represent the average of two experiments.

The simplified form of the Langmuir adsorption model, equation (5), predicts a linear relationship between the observed rate of adsorption (r_{obs}) and the concentration of arsenic compounds in aqueous phase. The following Figures 3.5a-d show the dependency of r_{obs} for iAs(V), MMA(aq), pAsA(aq) and PhAs(aq) on their bulk concentrations as a function of spectral components.

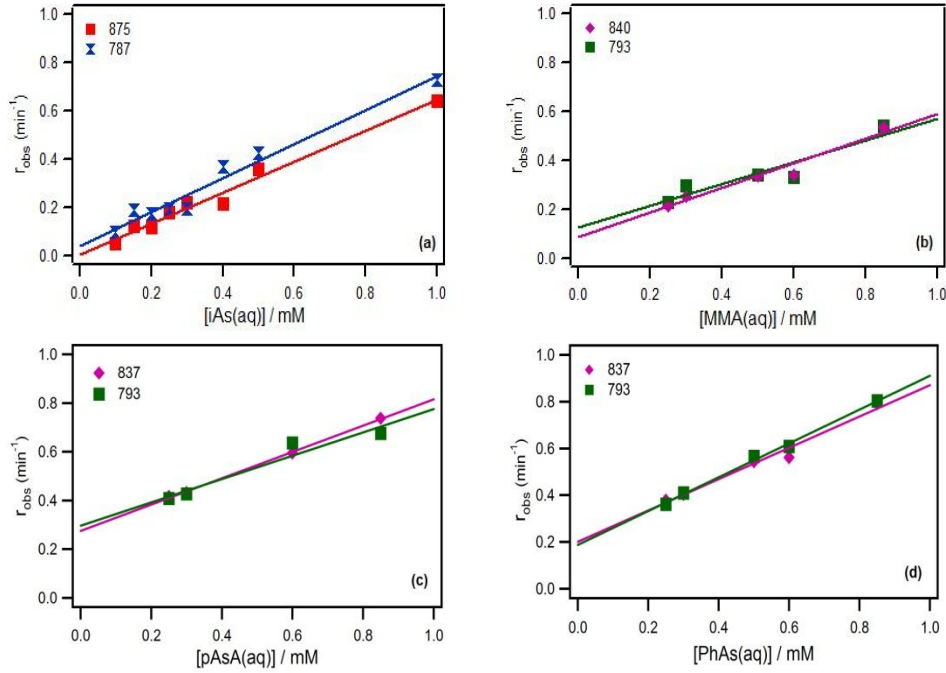


Figure 3.5. Dependency of r_{obs} with the bulk concentration of arsenicals at pH=7, $I=0.01$ M NaCl/KCl, and 2 mL/min flow rate at room temperature, 6 mg hematite.

From Figure 3.5, it is apparent that the two spectral components give almost the same trend for individual arsenic species at all concentrations. This suggests that they arise from the same type of surface complexes during the initial time of adsorption. Table 4 shows the least-squares estimates of the linear regression parameters for the adsorption of these arsenicals on hematite.

The formation of surface complexes is driven by ligand exchange reaction of these species with mostly positive surface sites. At pH 7, arsenate exists as H_2AsO_4^- or

HAsO₄²⁻ (50%-50%), and for MMA(aq), pAsA(aq) and PhAs(aq), more than 90% of the species are singly deprotonated (MeHAsO₃⁻/pAsAO₃⁻/PhHAsO₃⁻). Hence, the presence of the two negatively charged species (singly and doubly deprotonated) for iAs(V) should be responsible for larger electrostatic attraction to the surface. From the values of k_{ads} (Table 4), it can be inferred that the rates of adsorption of arsenate and monosubstituted organoarsenicals are almost similar. This suggests that the addition of methyl or aromatic group does not affect the rate of adsorption much relative to arsenate.

Table 4. Least-squares estimates of the linear regression parameters fitted to the experimental data of r_{obs} versus [As(aq)] shown in Figures 3.5a-d

As compounds	Peak	Slope (k_{ads})/min ⁻¹ mM ⁻¹	Intercept (k_{des})/min ⁻¹	R ²
iAs	875	0.64 (0.096)	0.006	0.9898
	793	0.70 (0.105)	0.043	0.9849
MMA(V)	840	0.50 (0.075)	0.086	0.9746
	793	0.44 (0.067)	0.126	0.9322
pAsA	837	0.54 (0.081)	0.276	0.9992
	793	0.48 (0.072)	0.298	0.9662
PhAs	837	0.64 (0.096)	0.201	0.9892
	793	0.66 (0.099)	0.189	0.9980

The y-intercept values which represent k_{des} (desorption rate constant during adsorption) are higher for pAsA(ads) and PhAs(ads) than iAs(ads) and MMA(ads). This reveals that there was more loosely bonded outer-sphere or monodentate surface species formed by the aromatic organoarsenicals than iAs(ads) and MMA(ads) due to the large size of the molecules. Figure 3.6 shows the probable surface complexes formed by MMA(ads) on hematite surface.

experiments have been carried out to investigate the role of phosphate in the release mechanism of arsenicals at the sediment water interface (Arts et al., 2013; Tofan-Lazar and Al-Abadleh, 2012b). In the present research, aqueous hydrogen phosphate (HPO_4^{2-}) with concentrations ranging from 0.1 to 2 mM at pH 7 and 2 mL/min flow rate were used to study the desorption kinetics of the arsenicals; iAs(ads), MMA(ads), pAsA(ads) and PhAs(ads) from surface hematite by the ATR-FTIR technique. Representative desorption spectra for these arsenicals are shown in Figure 3.7.

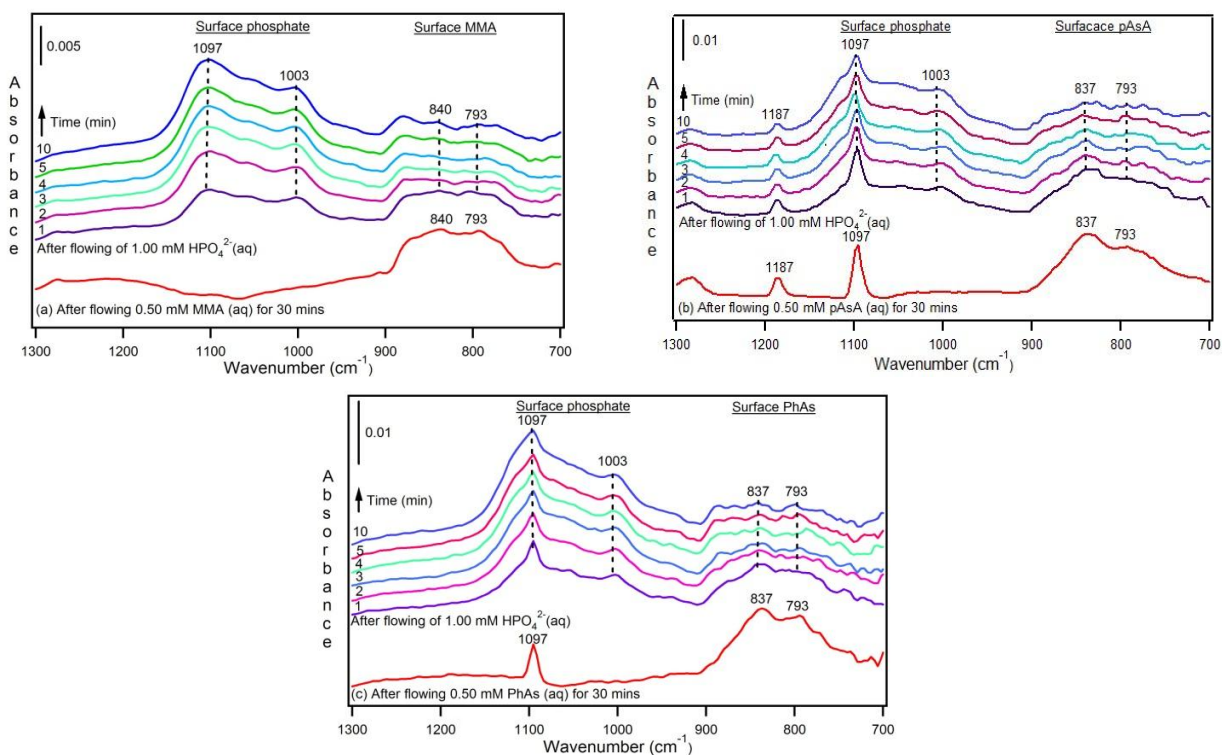


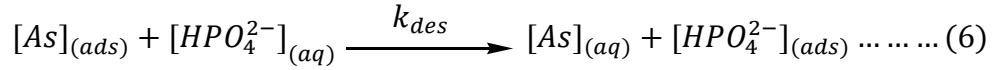
Figure 3.7. Spectra for the desorption of surface- (a) MMA; (b) pAsA; and (c) PhAs by aqueous hydrogen phosphate (not shown here for iAs(ads)). The experiment carried out at pH 7, $I=0.01$ M NaCl and 2 mL/min flow rate at room temperature.

After flowing each of the arsenicals (0.50 mM) on 6.0 mg hematite film for 30 min, the surface becomes nearly saturated, as shown by the plateau region observed in the

adsorption kinetic curves of these arsenicals (Figures 3.3a-d). Then desorption experiments were carried out using aqueous phosphate of various concentrations.

3.3.2 Mathematical models used in describing desorption

Equation (7) represents the simple Langmuir desorption model of reaction (6):



$$\theta(t) = \theta_0 \cdot e^{-k'_{des} \cdot t} \dots \dots \dots (7)$$

where, HPO_4^{2-} is the desorbing agent, $\theta(t) = A(\bar{v})/A_{max}(\bar{v})$, $\theta_0 = A_0(\bar{v})/A_{max}(\bar{v})$, and $k'_{des} = k_{des}[HPO_4^{2-}]_{(aq)}$. The linearized form of equation (7) can be written as follows:

$$\ln [A(\bar{v})/A_0(\bar{v})] = -k'_{des} \cdot t \dots \dots \dots (8)$$

where $A(\bar{v})$ is the absorbance at time t and $A_0(\bar{v})$ is the maximum absorbance before desorption starts. k'_{des} is the initial observed desorption rate which is equal to $k_{des} \cdot [HPO_4^{2-}(aq)]^n$ and n is the order of desorption.

$$k'_{des} = k_{des} \cdot [HPO_4^{2-}(aq)]^n \dots \dots \dots (9)$$

Equation (9) is the linear form of equation (8)

$$\ln k'_{des} = \ln k_{des} + n \cdot \ln [HPO_4^{2-}(aq)] \dots \dots \dots (10)$$

By plotting $\ln k'_{des}$ on the y-axis with $\ln [HPO_4^{2-}(aq)]$ on the x-axis, k_{des} can be extracted from the y intercept and slope (n) of the line represents the desorption order.

3.3.3 Desorption kinetic curves

Kinetics of the exchange process between $HPO_4^{2-}(aq)$ and surface arsenicals can be examined from trends in the pseudo desorption rate constants, k_{des} , of adsorbed

species. The desorption behavior of DMA(ads) due to chloride and flowing hydrogen phosphate was reported earlier from ATR-FTIR studies (Tofan-Lazar and Al-Abadleh, 2012b). Using the same technique with hydrogen phosphate as a desorbing agent, a study of the desorption of pAsA(ads) and PhAs(ads) has already been published from this thesis (Arts et al., 2013). Upon flowing HPO_4^{2-} (aq), a reduction of overall intensity of the spectral components assigned to the arsenicals-surface species is observed (Figure 3.7). Kinetic curves for the desorption of iAs(ads), MMA(ads), pAsA(ads) and PhAs(ads) were constructed (Figure 3.8) by measuring the peak height of features in the spectral range $700\text{-}950\text{ cm}^{-1}$ assigned to surface species as a function of desorption time.

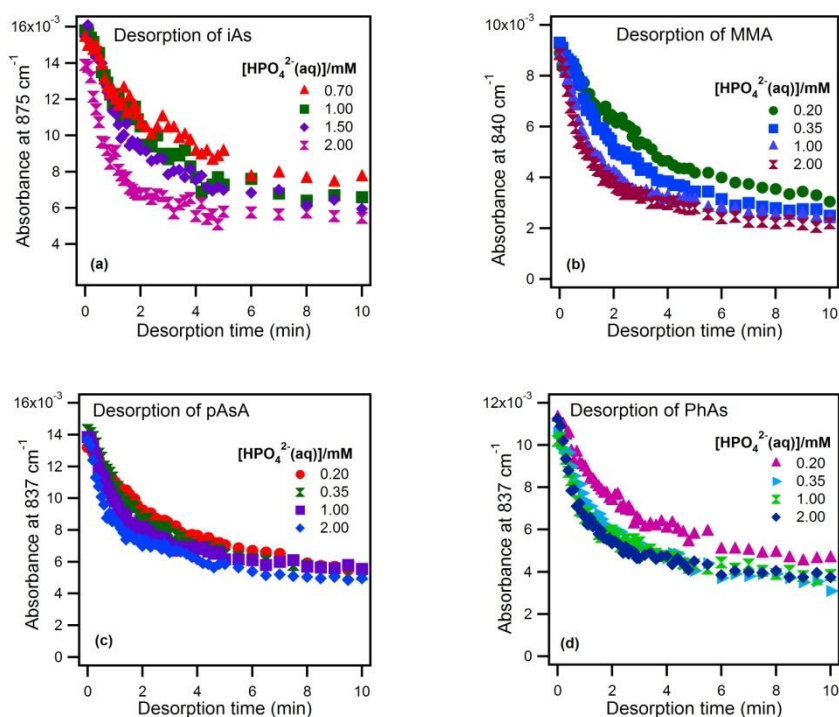


Figure 3.8. Desorption kinetics of (a) iAs(V), (b) MMA, (c) pAsA and (d) PhAs from hematite surface by various concentrations of phosphate (at pH=7) with 2 mL/min flow rate and at room temperature. Data points represent the average of two to four experiments and error bars were removed for clarity. The uncertainty in the measurements is 5% ($\pm\sigma$).

For the extraction of the observed desorption rate (k'_{des}), absorbances obtained during the desorption of iAs(ads), MMA(ads), pAsA(ads) and PhAs(ads) from hematite were linearized according to the equation (8). The linearized absorbances were plotted against desorption time (Figure 3.9) where the slope of each regression line corresponds to k'_{des} . As desorption of surface arsenicals takes place mostly within the first 1-3 min as a result of flowing aqueous phosphate, the start and end points for the linear least-squares regression analysis were considered between time zero ($t = 0$) and the time up to which the data remains linear.

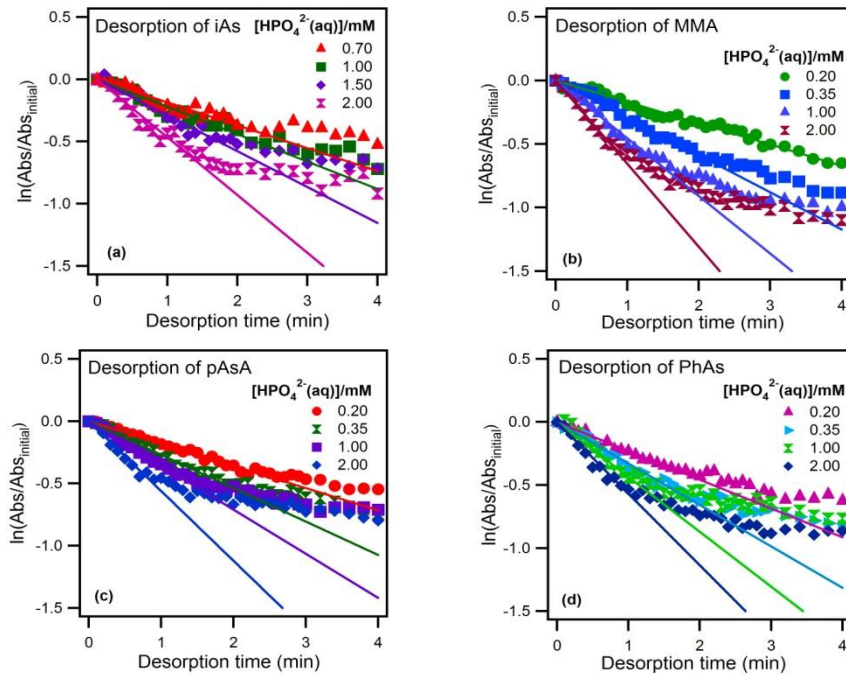


Figure 3.9. Linearized absorbances for the desorption of (a) iAs(ads), (b) MMA(ads), (c) pAsA(ads) and (d) PhAs(ads) from the hematite surface by using different concentrations of aqueous phosphate (pH=7) at flow rate 2 mL/min and room temperature.

The dependency of k'_{des} on $[\text{HPO}_4^{2-}(\text{aq})]$ is shown in Figure 3.10 for the desorption of iAs(ads), MMA(ads), pAsA(ads) and PhAs(ads). The spectral component considered for iAs(V) is 875 cm^{-1} and for MMA(V), pAsA and PhAs, they are 840/837

cm^{-1} . The results show that the order of desorption (n), 0.60, 0.59, 0.46 and 0.37 (dotted lines) produce better fit than $n=1$ (solid lines) for iAs(ads), MMA(ads), pAsA(ads) and PhAs(ads), respectively.

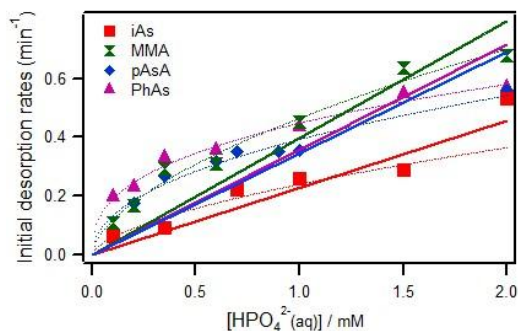


Figure 3.10. Dependency of the initial desorption rate constants, k'_{des} , on the concentration of $[\text{HPO}_4^{2-}(\text{aq})]$ from studies conducted using hematite films (6 mg) at pH 7 and 2 mL/min flow rate. Adsorbed arsenicals were introduced by flowing 0.5 mM of aqueous solutions at pH 7 and $I = 0.01$ M KCl/NaCl. Solid lines through the data represent least-squares linear fits. Dashed lines represent the non-unity overall order ($n \neq 1$).

To avoid the complexity of fitting with two lines (solid and dotted) in Figure 3.10, the equation (10) linear form of equation (9) was used for the extraction of the pseudo desorption rate constant (k_{des}) and the order of desorption (n).

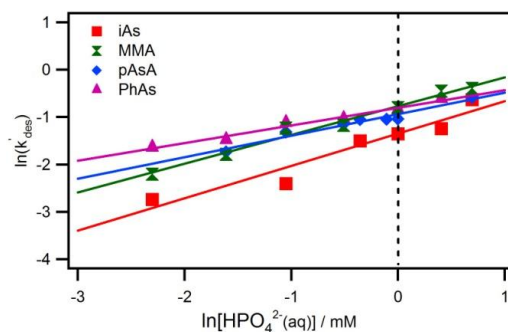


Figure 3.11. Dependency of the initial desorption rate constants, k'_{des} , obtained from the linear least-squares fitting to the experimental data shown in Figures 3.9a-d for the desorption of arsenicals as a function of $[\text{HPO}_4^{2-}(\text{aq})]$ at pH 7 and 2 mL/min flow rate. The data are plotted in the natural log form, and least-squares estimates are listed in table 5.

When plotted as a function of concentration of the desorption agent, the y-intercept of the best fit lines provides the pseudo desorption rate constant, k_{des} , for the arsenicals from the hematite surface according to equation (10). Data for $\ln k'_{des}$ vs $\ln[Phosphate(aq)]$ have been plotted for the desorption of arsenicals in Figure 3.11 where the slope, n, represents the desorption order.

Table 5. Least-squares estimates of the linear regression parameters fitted to the experimental data of $\ln k'_{des}$ vs $\ln[Phosphate(aq)]$ shown in Figure 3.11

Arsenicals	Peak ($\tilde{\nu}$)	k_{des} $\text{min}^{-1}\text{mM}^{-1}$ (n=1)	Slope (n)	y-intercept $\ln k_{des}$	k_{des} $\text{min}^{-1}\text{mM}^{-n}$	R^2
iAs(V)	875	0.23	0.68	-1.35	0.26	0.9594
MMA(V)	840	0.40	0.61	-0.77	0.46	0.9907
pAsA	837	0.35	0.45	-0.94	0.39	0.9775
PhAs	837	0.36	0.37	-0.80	0.45	0.9862

The values of k_{des} extracted from the y-intercept are listed in Table 5. For a desorption order of 1, values of the pseudo-desorption rate constants (k_{des}), show that desorption kinetics of MMA, pAsA and PhAs are almost identical and around 1.5 to 2 times higher than that of iAs(V). Furthermore, the order of desorption for MMA(ads) with one methyl group and iAs(ads) with no substituents attached to the AsO_x moiety are very similar. Monosubstituted aromatic organoarsenicals; pAsA and PhAs desorb from the hematite surface with a similar order. One can use the values of k_{des} in unit of $\text{min}^{-1}\text{M}^{-n}$ to calculate the value of k_{des} for a given phosphate concentration. For example, for a 0.5 mM phosphate concentration, k_{des} values for iAs(V), MMA(V), pAsA and PhAs are 0.16, 0.3, 0.29 and 0.35 min^{-1} , respectively.

3.3.4 Adsorption kinetics of phosphate concurrent with arsenicals desorption

Adsorption of phosphate on hematite films; both fresh and previously exposed to iAs(V), MMA(V), pAsA, and PhAs, have been studied in this thesis. During the desorption of arsenicals from hematite, phosphate molecules adsorb concurrently on the surface. Analysis of spectral features assigned to surface phosphate is used to extract values of the pseudo-adsorption rate constants (k_{ads}) which provide insight into the kinetics of ligand exchange of aqueous hydrogen phosphate with different surface groups. Figure 3.7 shows ATR-FTIR absorption spectra collected as a function of time for the desorption of arsenicals from hematite samples and concurrent adsorption of hydrogen phosphate at pH 7 and 2 mL/min flow rate. The detailed assignment of the spectral features of the adsorbed phosphate on hematite film previously exposed to iAs(ads) and DMA(ads) were discussed by Tofan-Lazar and Al-Abadleh (2012b). The bottom spectrum in Figure 3.7, shows features appearing due to surface species formed by MMA(ads), PhAs(ads) and pAsA(ads) at saturation after 30 min of adsorption. The assignment of spectral features to surface arsenic was provided in the previous section. The upper sets of spectra (Figures 3.7a-c), were collected during the first 10 min of flowing hydrogen phosphate solution. The spectral features arising at 1097 and 1003 cm^{-1} have been assigned to surface phosphate. The features at 1097 cm^{-1} have a narrow bandwidth, $\sim 11 \text{ cm}^{-1}$ at half height, and have minimal contribution to the feature at 1003 cm^{-1} which increases in intensity with time as more phosphate adsorbs on the surface. This ligand exchange process can be inferred from the temporal changes in the spectral components assigned to surface species formed by phosphate and arsenicals, respectively.

In the case of PhAs(ads) and pAsA(ads), the spectral feature at 1097 cm^{-1} appears due to the presence of the As-C bond which is absent in MMA(ads). This suggests that the carbon atom in the As-C bond could be a part of aromatic ring. The feature at 1187 cm^{-1} (Figure 3.7b) which appears for pAsA(ads) and is assigned to in-plane bending of aromatic C-H groups. The intensity of this spectral feature is too low to be observed for PhAs(ads) in Figure 3.7c. The same feature is observed for the spectrum of aqueous aniline (Arts et al., 2013). This suggests that in-plane bending of aromatic C-H groups together with the contribution from aromatic amino groups results in a more pronounced peak at 1187 cm^{-1} for pAsA(ads).

The kinetic curves were generated for the adsorption of phosphate (figures not shown here) from the baseline corrected peak height at 1003 cm^{-1} as a function of hydrogen phosphate concentration on hematite films in the presence and absence of surface arsenicals. To extract values of r_{obs} for phosphate on these surfaces, the first-order Langmuir adsorption model described before for arsenicals (section 3.2.2) was used.

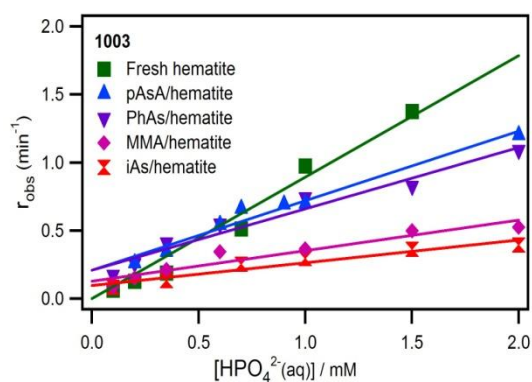


Figure 3.12. The rate of phosphate adsorption in presence and absence of surface arsenic from analyzing the spectral component 1003 cm^{-1} . Lines through the data represent linear least-squares fits and slopes of linear fits represent pseudo k_{ads} .

Experimental data were plotted in the linear form of this model and linear least-squares fittings were used to obtain values for r_{obs} , which are plotted as a function of hydrogen phosphate concentration (0.1 to 2 mM at pH 7) in Figure 3.12. The lines through the data shown in Figure 3.12 represent linear-least-squares fits and the slopes of these lines represent the pseudo adsorption rate constant (k_{ads}) as listed in Table 6. The trend for the k_{ads} values for phosphate adsorption in the presence and absence of surface arsenic follows the order: Fresh film > pAsA/hematite \geq PhAs/hematite > MMA/hematite \geq iAs(V)/hematite. The uncertainties in the values of k_{ads} were propagated from the uncertainties in the values of r_{obs} (ca. 15%). The highest values of k_{ads} (and hence the fastest phosphate adsorption kinetics) were observed on freshly prepared hematite films, followed by those with aromatic arsenicals, pAsA(ads) and PhAs(ads). The lowest values of k_{ads} (and hence slowest phosphate adsorption kinetics) are observed on hematite films with iAs(ads) and MMA(ads) (Table 6). From the above discussion, it is clear that the amount of weakly bonded pAsA(ads) and PhAs(ads) surface species are larger than those for MMA(ads) and iAs(ads) at neutral pH.

Table 6. Least-squares estimates of the linear regression parameters fitted to the experimental data of r_{obs} versus $[\text{HPO}_4^{2-}(\text{aq})]$ (date and figures are not shown here) for the adsorption of phosphate as a function of spectral components 1003 cm^{-1} in the presence and absence of surface arsenic

Films	Slope (k_{ads})/ $\text{min}^{-1}\text{mM}^{-1}$	Intercept (k_{des})/ min^{-1}	R^2
Fresh hematite	0.89 (0.134)	0	0.9921
iAs(V)/hematite	0.17 (0.026)	0.097	0.9641
MMA/hematite	0.23 (0.035)	0.127	0.9532
pAsA/hematite	0.51 (0.077)	0.210	0.9858
PhAs/hematite	0.45 (0.068)	0.209	0.9801

In summary, results from the adsorption/desorption kinetic studies strongly suggest that arsenate forms much stronger surface complexes than monosubstituted organoarsenicals. The adsorption of arsenate is very likely to be dominated by bidentate complexes. Also, the nature of the organic functional group affects the most dominant type of surface complex. The results suggest that MMA(ads) forms stronger surface complexes on hematite than pAsA(ads) and PhAs(ads), most likely more bidentate and that aromatic organoarsenicals form mostly monodentate. For the adsorption of phosphate on hematite films in the presence of arsenic, the films were exposed to arsenicals (0.5 mM) for 30 min. Within this time, MMA(ads) with a smaller methyl group, probably adsorb on the surface in a bidentate fashion like arsenate.

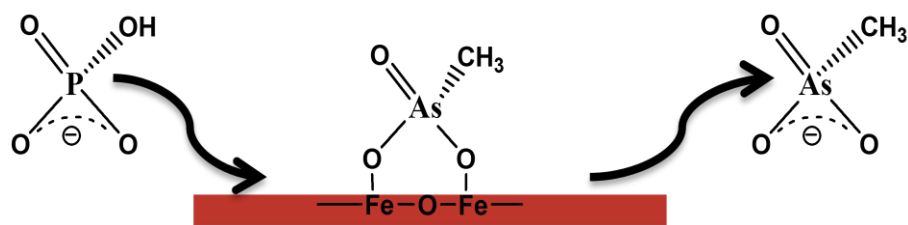


Figure 3.13. Ligand exchange process between incoming phosphate and surface MMA.

The reaction scheme in Figure 13 represents the adsorption of phosphate on the hematite with surface MMA(ads). This stronger bidentate surface species reasonably makes difficult the adsorption of phosphate molecules on the surface through the ligand exchange process.

3.4 Temperature-dependent adsorption isotherm of arsenicals

3.4.1 Spectra for the adsorption isotherm as a function of temperature and concentration

The isotherm experiments for the adsorption of iAs(V), MMA(V) and DMA(V) on hematite surface were conducted as a function of concentration and temperature (5 to 50 °C). The main objective of these experiments was to extract thermodynamic functions for the interaction of these arsenicals with iron (oxyhydr)oxides. Figure 3.14 shows the representative spectra for the adsorption of iAs(V) on hematite as a function of concentration.

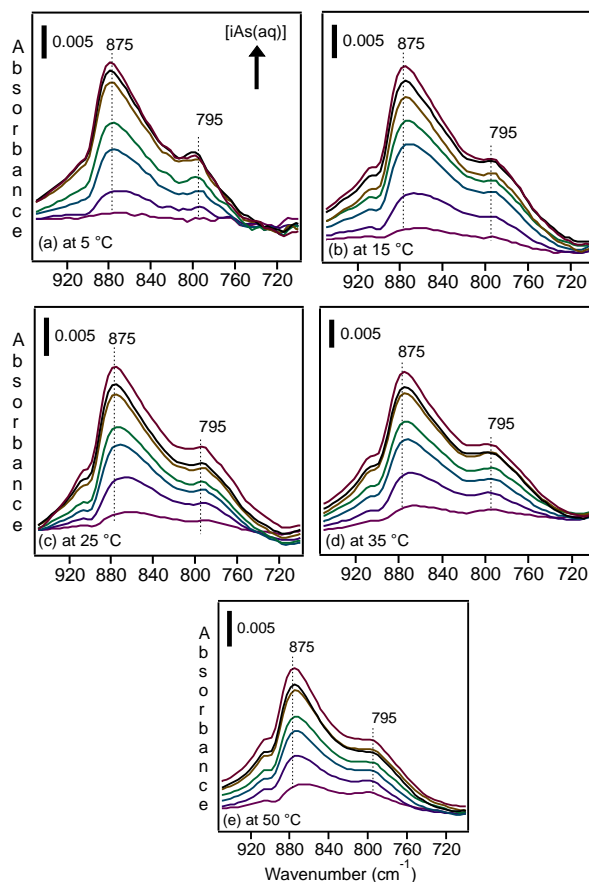


Figure 3.14. Representative ATR-FTIR absorbance spectra of iAs(ads) on hematite nanoparticles as a function of increasing temperature and concentration (from bottom): 0.005, 0.01, 0.03, 0.05, 0.25, 0.5 and 1 mM at pH 7, I = 0.01 M NaCl and 1 mL/min flow rate.

The spectral features at 875 and 795 cm^{-1} arising for the surface species exist within the experimental temperature range. For adsorbed arsenate, there is no effect of temperature on the spectral features at 875 cm^{-1} while the peak at 795 cm^{-1} gradually loses its intensity at high temperatures.

From the spectra in Figure 3.15, three infrared bands; around 872, 840 and 795 cm^{-1} have been assigned to the surface species formed by MMA(ads) on hematite. There is a remarkable loss of band intensity at 795 cm^{-1} at 50 $^{\circ}\text{C}$ as observed for iAs(ads). Other spectral features seem not to be affected by temperature.

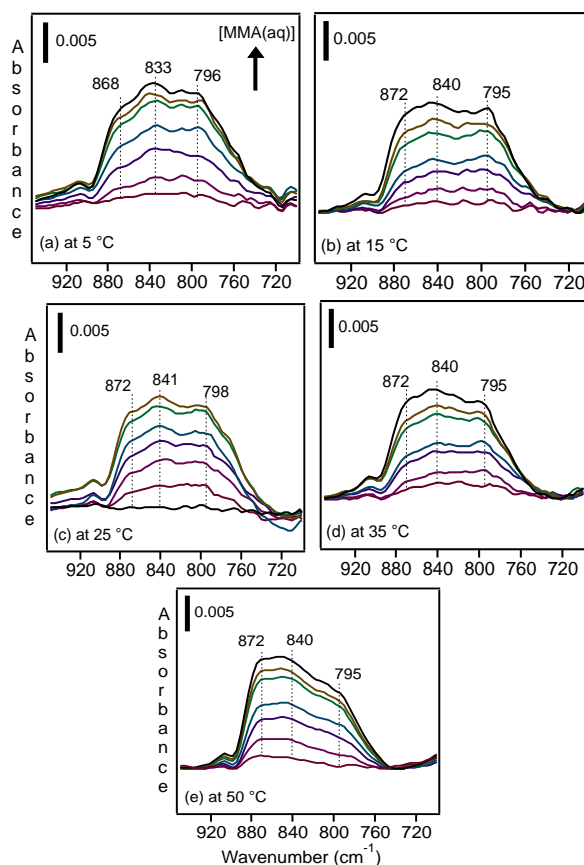


Figure 3.15. Representative ATR-FTIR absorbance spectra of MMA(ads) on hematite nanoparticles as a function of increasing temperature and concentration (from bottom): 0.005, 0.01, 0.03, 0.05, 0.25, 0.5 and 1 mM at pH 7, I = 0.01 M NaCl and 1 mL/min flow rate.

Adsorption of DMA(V) is observed to be more temperature dependent. The spectral feature observed at 798 cm^{-1} starts losing its intensity at $35\text{ }^{\circ}\text{C}$ and eventually disappears at $50\text{ }^{\circ}\text{C}$. In addition, the most intense spectral feature at 837 cm^{-1} loses its sharpness at the highest experimental temperature (Figure 3.16).

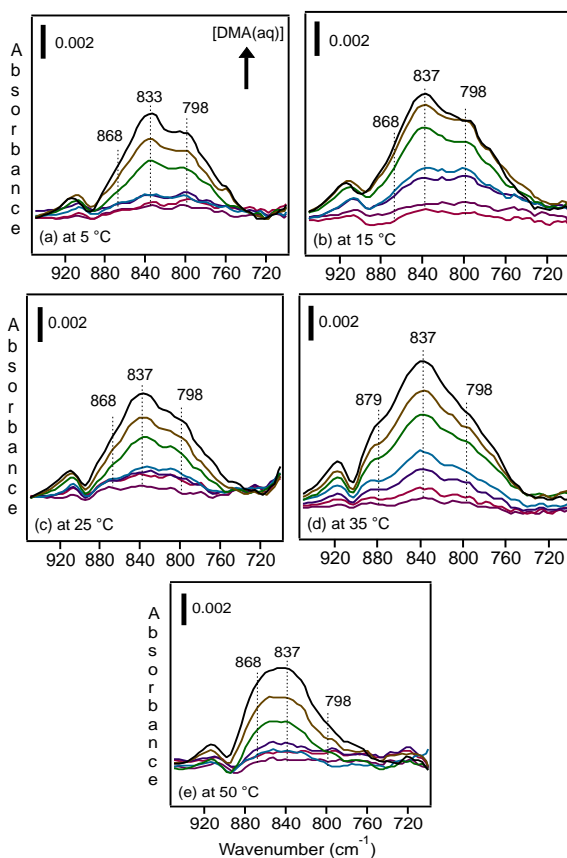


Figure 3.16. Representative ATR-FTIR absorbance spectra of DMA(ads) on hematite nanoparticles as a function of increasing temperature and concentration (from bottom): 0.005, 0.01, 0.03, 0.05, 0.25, 0.5 and 1 mM at pH 7, I = 0.01 M NaCl and 1 mL/min flow rate.

3.4.2 Mathematical models used in describing adsorption isotherm

According to the Langmuir adsorption model, a dynamic equilibrium can be expected between the adsorbed complexes and aqueous phase species. At saturation, the adsorbed arsenicals will form a molecular monolayer on the adsorbent surface (hematite

used herein) and, theoretically, no electrostatic and covalent interactions are expected among the adsorbed species. According to the simple Langmuir adsorption model, K_{eq} can be expressed as follows (equation 11) for reaction (1):

$$K_{eq} = \frac{\theta}{[As](1-\theta)} \dots \dots \dots (11)$$

where, K_{eq} is the equilibrium constant for the adsorption of arsenicals on hematite, θ is the number of surface sites covered by the adsorbate molecules, and $(1 - \theta)$ is the fraction of available unoccupied sites at equilibrium.

Equation (11) can be rearranged as follows:

$$\theta = \frac{K_{eq}[As]}{1 + K_{eq}[As]}$$

$$or, \quad \frac{A}{A_{max}} = \frac{K_{eq}[As]}{1 + K_{eq}[As]}$$

$$or, \quad A = \frac{A_{max}K_{eq}[As]}{1 + K_{eq}[As]}$$

$$or, \quad \frac{1}{A} = \frac{1 + K_{eq}[As]}{A_{max}K_{eq}[As]}$$

$$or, \quad \frac{1}{A} = \frac{1}{A_{max}K_{eq}} \cdot \frac{1}{[As]} + \frac{1}{A_{max}}$$

$$or, \quad y = mx + b \dots \dots \dots (12)$$

A plot of $\frac{1}{A}$ vs $\frac{1}{[As]}$ gives a straight line, with intercept, $b = \frac{1}{A_{max}}$ and slope, $m = \frac{1}{A_{max}K_{eq}}$. After extracting the value of A_{max} from the intercept, K_{eq} can easily be calculated from the slope.

3.4.3 Results from the temperature-dependent adsorption isotherm experiments

The isotherms for the adsorption of iAs(V), MMA(V) and DMA(V) as a function of concentration and temperature are shown in Figure 3.17. The experiments were conducted at five temperatures; 5, 15, 25, 35 and 50 °C using the concentrations; 0.001, 0.005, 0.01, 0.03, 0.05, 0.1, 0.15, 0.25, 0.5, 0.8, 1 and 2 mM for each at pH 7 and I = 0.01 M NaCl.

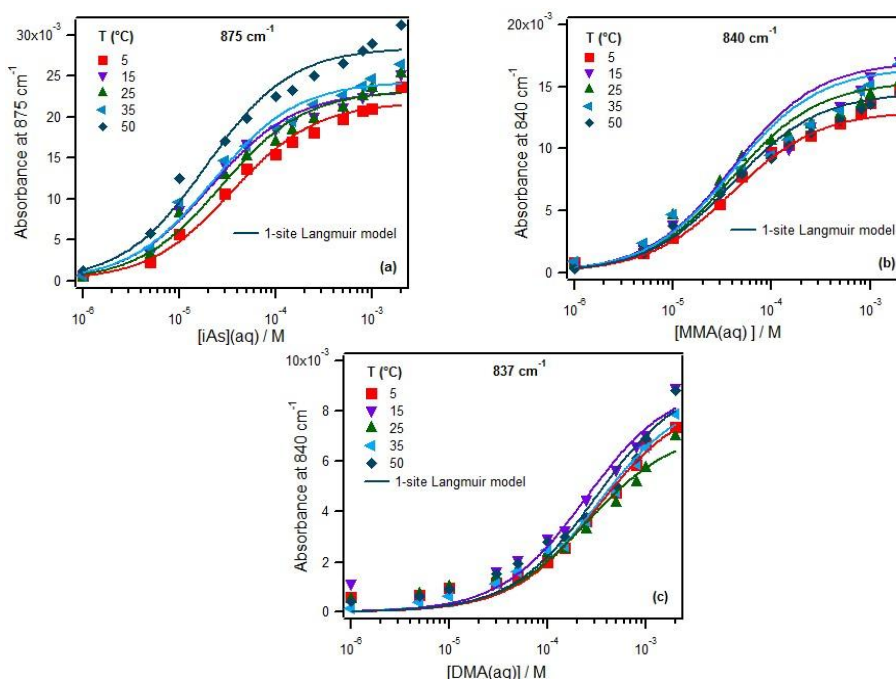


Figure 3.17. Adsorption isotherms of iAs (upper left), MMA (upper right) and DMA (bottom) on hematite nanoparticles as a function of temperature (filled markers) at pH 7 and 0.01 M NaCl. The solid line represents the least-squares fitting of the 1-site Langmuir adsorption model. Data points represent the average of two to four experiments and error bars were removed for clarity. The uncertainty in the measurements is 5% ($\pm\sigma$).

The adsorption isotherms on hematite have been constructed from the baseline corrected ATR absorbances [i.e., peak height at a given wavenumber, $A(\tilde{\nu})$] of spectral features assigned to surface complexes for each arsenical. Figure 3.17 shows the simple Langmuir adsorption isotherm from analyzing the most intense spectral feature; 875 cm^{-1}

for iAs(ads). The peaks analyzed for both MMA(ads) and DMA(ads) are 840 and 837 cm^{-1} , respectively.

For the extraction of equilibrium constant, K_{eq} , experimental data presented in Figure 3.17 were linearized according to the equation (12) and are shown as a function of temperature in Figure 3.18.

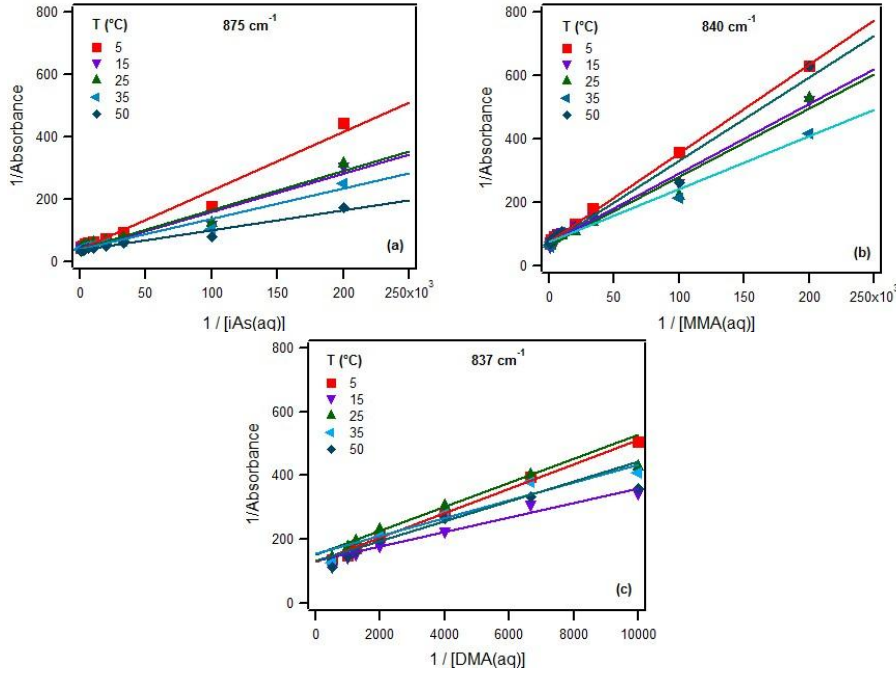


Figure 3.18. Linearized absorbances for the adsorption of iAs (upper left), MMA (upper right) and DMA (bottom) on hematite nanoparticles as a function of temperature and concentration at pH 7 and 0.01 M NaCl. Data points represent the average of two to four experiments and error bars were removed for clarity.

According to equation (12), the intercept of the fitting line represents the $1/A_{max}$ value which can be used to calculate equilibrium constants for the adsorption, K_{eq} , from the slope. The equilibrium constants have been multiplied by the molar concentration of water, 55.5 M, to eliminate mM unit. For the extraction of enthalpy for adsorption (ΔH_{ads}^0) and the entropy of adsorption (ΔS_{ads}^0), the van't Hoff equation (13) can be used:

$$\ln(55.5K_{eq}) = -\frac{\Delta H_{ads}^0}{R} \cdot \frac{1}{T} + \frac{\Delta S_{ads}^0}{R} \dots \dots \dots (13)$$

Plots of $\ln(55.5K_{eq})$ versus $1/T$ give straight lines where ΔH_{ads}^0 and ΔS_{ads}^0 can be calculated from the slope and intercept, respectively. Figure 3.19 shows the van't Hoff plots for the adsorption of iAs(ads), MMA(ads) and DMA(ads) on hematite at pH 7.

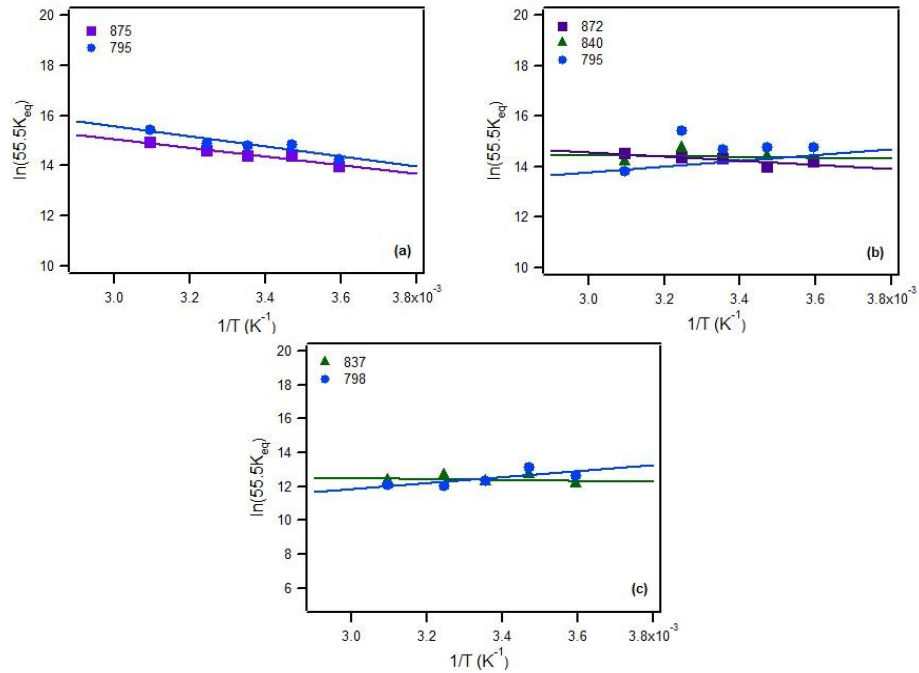


Figure 3.19. Temperature-dependence of the Langmuir equilibrium constants, K_{eq} , plotted according to van't Hoff equation (filled markers). Values of K_{eq} were extracted from least-squares Langmuir fits to adsorption isotherms obtained from the baseline-corrected absorbance at 875 and 795 cm^{-1} for iAs(ads); 872, 840 and 795 cm^{-1} for MMA(ads); and 837 and 798 cm^{-1} for DMA(ads). The solid line is the linear least-squares fitting with a slope corresponding to $-\Delta H_{ads}^0/R$.

Table 7 lists the thermodynamic functions extracted from the van't Hoff plots (Figures 3.19a-c) for the adsorption of iAs(ads), MMA(ads) and DMA(ads) as a function of the spectral components. Another thermodynamic function, the Gibbs free energy of

adsorption (ΔG_{ads}^0), can be obtained for each value of K_{eq} at a given experimental condition using equation (14):

$$\Delta G_{ads}^0 = -RT \ln(55.5K_{eq}) \dots \dots \dots (14)$$

Figure 3.20 shows the relation between ΔG_{ads}^0 and temperature (K) for arsenate, MMA and DMA adsorption on hematite. A plot of ΔG_{ads}^0 as a function of temperature (K) gives a straight line and the entropy of adsorption (ΔS_{ads}^0) can be extracted from the slope according to equation (15).

$$\Delta G_{ads}^0 = \Delta H_{ads}^0 - T\Delta S_{ads}^0 \dots \dots \dots (15)$$

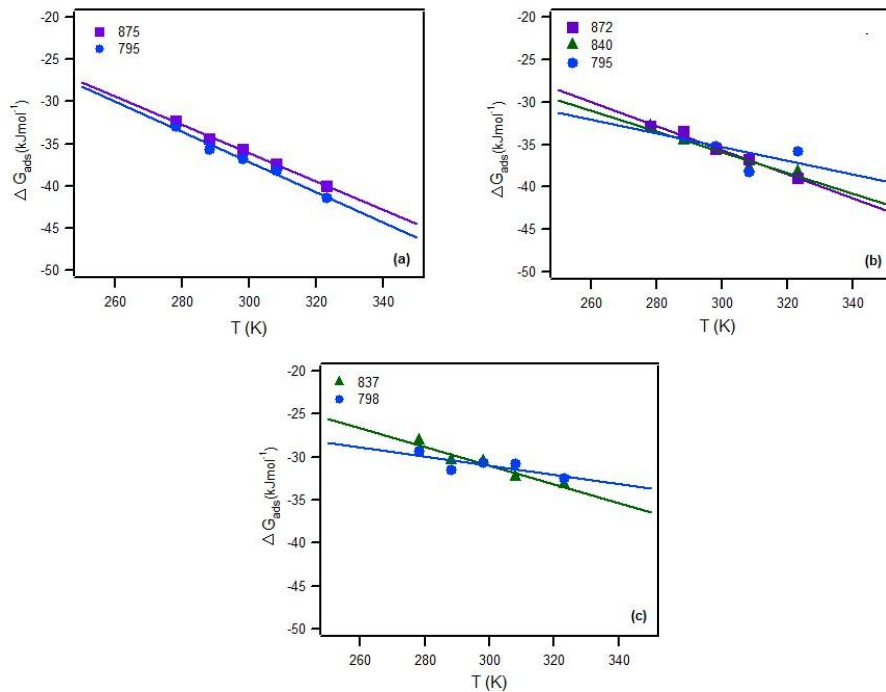


Figure 3.20. Temperature-dependence of the Gibbs free energy, ΔG_{ads}^0 , for the adsorption of (a) iAs(ads), (b) MMA(ads) and (c) DMA(ads) which were obtained using: $\Delta G_{ads}^0 = -RT \ln(55.5K_{eq})$ (filled markers). The solid line represents the linear least-squares fitting and the slope, which corresponds to $-\Delta S_{ads}^0$.

Table 7. Least-squares estimates of the linear regression parameters fitted to the experimental data of $\ln(55.5K_{eq})$ versus $1/T$ (K^{-1}) shown in Figure 3.19 from the peak height measurements

Arsenicals	Peak ($\tilde{\nu}$)	ΔH_{ads}^0 (kJ/mol)	ΔS_{ads}^0 ($kJmol^{-1}K^{-1}$)
iAs(V)	875	14.35	0.17
	795	16.59	0.18
MMA(V)	872	6.75	0.14
	840	1.50	0.12
	795	-9.54	0.09
DMA(V)	837	2.34	0.11
	798	-14.81	0.05

* For comparison thermal energy in the temperature range from 5 to 50 °C is 2.3 to 2.7 kJ/mol

The values of ΔH_{ads}^0 and ΔS_{ads}^0 obtained using equation (15) from the least-square estimates of the linear regression parameters fitted to the experimental data shown in Figure 3.20 coincide with those presented in Table 7 and hence are not shown here separately.

3.4.4 Discussion on the results obtained from the temperature-dependent isotherm experiments

The Gibbs free energy for adsorption, ΔG_{ads}^0 , depends on the change of enthalpy (ΔH_{ads}^0) and on the change of entropy (ΔS_{ads}^0) during the adsorption process, as well as on the absolute temperature (K). For heterogeneous systems where species in the reaction are in different phases and can be separated mechanically, a negative ΔG_{ads}^0 value describes a spontaneous process in the forward direction. A zero value of ΔG_{ads}^0 describes a system at equilibrium. The values of ΔG_{ads}^0 reported herein (-32 to -41 kJ/mol^{-1} for iAs(ads); -33 to -39 kJ/mol^{-1} for MMA(ads); and -28 to -33 kJ/mol^{-1} for DMA(ads)) are

negative for the adsorption of all arsenicals undertaken in this study. The negative ΔG_{ads}^0 values indicate that the adsorption processes are spontaneous.

The positive enthalpy of adsorption (ΔH_{ads}^0) obtained from both the spectral components (875 and 795 cm^{-1}) for iAs(ads) are almost identical (+14.35 and +16.59 kJ/mol) and indicate that the process is endothermic. For MMA(ads) and DMA(ads), with the ΔH_{ads}^0 values, it is tricky to understand from the peak height measurements whether the process is endothermic or exothermic. Based on two (more intense) of the three spectral features, 872 and 840 cm^{-1} for the adsorption of MMA(ads), the process seems endothermic. However, both the endothermic and exothermic process can be supposed (Table 7) for the adsorption of DMA(ads). From the relative values of ΔH_{ads}^0 for DMA(ads), it could be inferred that the process is more likely exothermic. To further investigate, the spectral data was reanalyzed for band area instead of peak height discussed in the next section. Also, the positive change of entropy (ΔS_{ads}^0) observed for all arsenicals suggest that the reaction is entropy-driven in most cases where ΔH_{ads}^0 is positive as shown in Table 7. It is very likely that the increase in the degrees of freedom in surface arsenic species compared to surface water or hydroxyl groups is responsible for the net increase the entropy of adsorption.

3.4.5 Discussion on the results obtained from the temperature-dependent isotherm experiments considering integrated peak area as analysis method

Measurement of integrated peak areas was also employed for studying the binding thermodynamics of iAs(ads), MMA(ads) and DMA(ads) with iron-(oxyhydr)oxide.

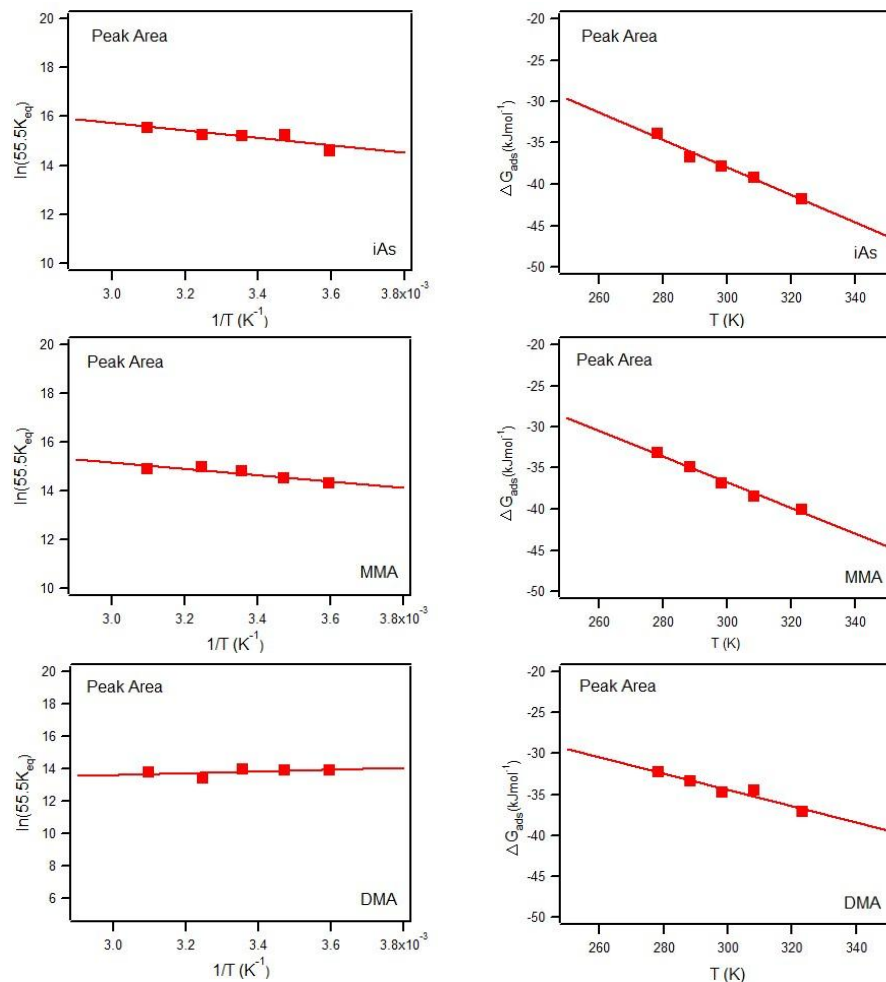


Figure 3.21. Temperature-dependence of the Langmuir equilibrium constants, K_{eq} , plotted according to van't Hoff equation (filled markers). Values of K_{eq} were extracted from least-squares Langmuir fits to adsorption isotherms obtained from the integrated peak area for iAs(ads), MMA(ads) and DMA(ads). The solid line is the linear least squares fitting and the slope, which corresponds to $-\Delta H_{ads}^0/R$. The right panel shows the temperature-dependence of the Gibbs free energy of adsorption, ΔG_{ads}^0 , which were obtained using: $\Delta G_{ads}^0 = -RT \ln(55.5K_{eq})$ (filled markers). The solid line represents the linear least-square fitting and the slope, which corresponds to $-\Delta S_{ads}^0$.

Langmuir adsorption isotherms for the arsenicals were constructed (not shown here) with the integrated peak areas assigned to the surface species within the spectral range $700-950\text{ cm}^{-1}$. According to equation (12), $1/(\text{peak area})$ vs $1/[As]$ were plotted (not shown here) for these arsenicals and K_{eq} values were extracted from the slope of the

least-squares linear fits. ΔG_{ads}^0 can be calculated for temperature-dependent adsorption using equation (13). Figure 3.21 show $\ln(55.5K_{eq})$ and ΔG_{ads}^0 plotted as a function of $\frac{1}{T}$ (K^{-1}) and T (K), respectively. Least-squares estimates are listed in Table 8 for ΔH_{ads}^0 and ΔS_{ads}^0 .

The values of $\ln(55.5K_{eq})$ and ΔG_{ads}^0 obtained from integrated peak areas assigned to the surface species as an analysis method for the arsenicals are in agreement with the values obtained from the peak height analysis. In addition, results obtained for the enthalpy and entropy of adsorption for iAs(ads) and MMA(ads) from both the analytical methods are comparable. The value of ΔH_{ads}^0 for the adsorption of DMA(ads) on iron-(oxyhydr)oxide is negative (-4.49 kJ/mol) from the integrated peak area measurements which supports the prediction made from the peak height analysis.

Table 8. Least-squares estimates of the linear regression parameters fitted to the experimental data of $\ln(55.5K_{eq})$ versus $1/T$ (K^{-1}) shown in Figure 3.21 based on the integrated peak area

Arsenicals	ΔH_{ads}^0 (kJ/mol)	ΔS_{ads}^0 ($\text{kJmol}^{-1}\text{K}^{-1}$)
iAs(V)	12.41	0.17
MMA(V)	10.57	0.16
DMA(V)	-4.49	0.10

* For comparison thermal energy in the temperature range from 5 to 50 °C is 2.3 to 2.7 kJ/mol

Overall, the thermodynamic functions analyzed using the Langmuir model suggest that ligand exchange of arsenicals on hematite is entropy driven at pH 7. As mentioned in the future work section, extracting values of K_{eq} using a surface complexation model will provide future insights into the driving force of the ligand exchange process.

3.5 Adsorption of monosubstituted arsenicals as a function of pH(D)

pH(D) edge experiments were carried out for the adsorption of iAs(V) and the monosubstituted organoarsenicals, MMA(V) and PhAs at room temperature using 0.5 mM concentration of the arsenicals on hematite nanoparticles. The adsorption experiments were conducted within the pH range from 10 to 4 changing 0.5 unit in each subsequent step. When D₂O was used as solvent, the pD considered for the experiments were 10, 8.5, 5.5 and 4. The absorbance spectra were obtained (as described in the previous sections) by referencing the single beam ATR spectra collected for each pH(D) dependent adsorption to the last one recorded for the background solution flowing over the time. Figure 3.22 shows the results of the pH edge experiments for the arsenicals undertaken in this study.

In the pH edge experiments, for the all the arsenicals, the most intense spectral features for the surface species formed by iAs(ads), MMA(ads) and PhAs(ads) arise around 875, 840 and 837 cm⁻¹ at pH 7. However, these features shift from lower to higher wavenumber with increasing hydrogen ion concentration of the system. This means that in an acidic environment, surface arsenicals are likely to become more protonated giving rise to less resonance and stronger As=O bonds. Also, absorbance from the baseline corrected ATR spectra for the surface arsenicals are found to increase with decreasing pH suggesting an increase in the surface coverage.

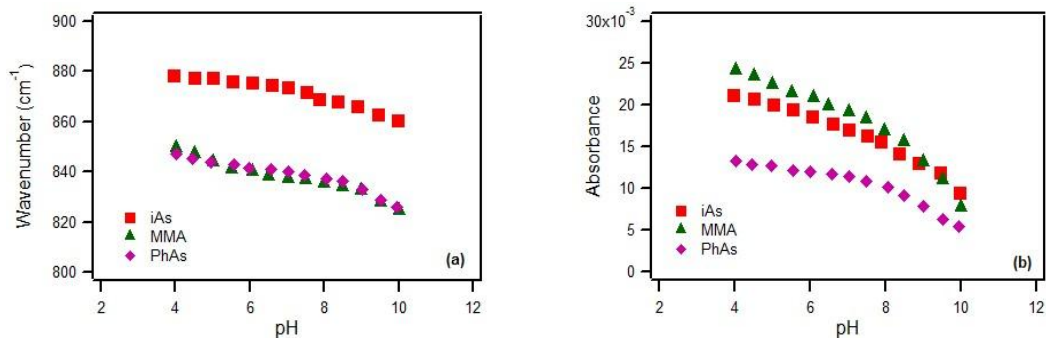


Figure 3.22. pH edges of iAs(V), MMA(V) and PhAs on (a) effect of pH on the wavenumber of the most intense spectral feature; and (b) pH edge at room temperature, $I=0.01$ M NaCl and 1 mL/min flow rate. Data points represent the average of two to four experiments and error bars were removed for clarity.

For the adsorption of PhAs, the absorbance starts leveling off at approximately pH 6 and does completely by pH 4 due to the effective interaction between the dominant species, $\equiv\text{FeOH}_2^+$ with PhHAsO_3^- . Another PhAs(aq) species, PhH_2AsO_3 , could be expected in the system (Figure 1.4c) with little chance of interacting with the surface. The absorbance for the iAs(ads) and MMA(ads) surface species do not reach a plateau even at pH 4 unlike PhAs(ads). In acidic pH (6 to 4), H_2AsO_4^- is the dominant aqueous iAs(V) species whereas $\text{CH}_3\text{HAsO}_3^-$ and $\text{CH}_3\text{H}_2\text{AsO}_3$ are for MMA(V). The adsorption behavior of the monosubstituted organoarsenicals, MMA and PhAs should apparently be the same on the iron (oxyhydr)oxide surface. In fact, the arisen discrepancy for the adsorption of MMA and PhAs could be explained by the attached organic substituents; $-\text{CH}_3$ and $-\text{Ph}$, respectively. The methyl group, in MMA, exhibits less influence than the phenyl group and hence behave more similarly to iAs(V) adsorption.

Within the spectral range $700\text{-}900\text{ cm}^{-1}$, water molecules adsorb IR radiation and hence interfere with $\nu(\text{AsO}_x)$ (Cowen et al., 2008). Thus, pD edge experiments were conducted for a detailed understanding the spectral features formed by the surface species. Another reason for using D_2O instead of H_2O was addressed by Carabante et al.

(2009) for reducing the signal to noise ratio in the region where the As-O bonds appear for the surface species.

The Figures in 3.23 show the ATR-FTIR spectra recorded for aqueous phase iAs(V) and MMA(V) using the concentration 0.02 M as a function of pD. Solutions of iAs(V) and MMA(V) were prepared in KCl (0.01M) background solution which previously was prepared in D₂O. For individual arsenic compounds, the spectra collected using the same solution and pD were adjusted to the desired point separately before the start of each experiment.

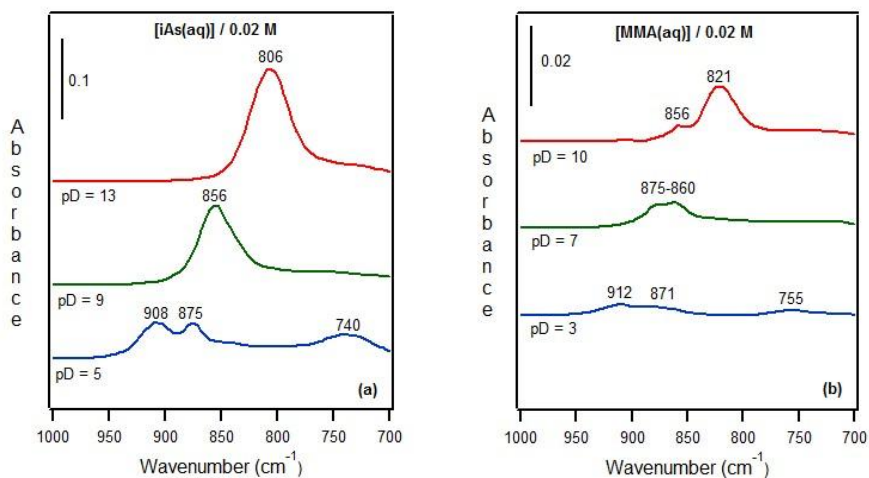


Figure 3.23. Spectra recorded as a function of pD and at I=0.01 M KCl for (a) aqueous iAs(V) on Ge crystal, and (b) aqueous MMA(V) on ZnSe crystal.

The spectra for aqueous iAs(V) were recorded on germanium (Ge) crystal as ZnSe is very sensitive over a broad acid-base range. Since iAs(V) has three different pK_a values, absorption bands can originate from different solution species depending on the pD (Figure 3.23a). In acidic pD, the bands appearing at 908, 875 and 740 cm⁻¹ originate from H₂AsO₄⁻ in D₂O. The spectrum recorded at higher pD ≥ 9 show only one IR band in the As-O stretching region. The spectral shoulders 856 cm⁻¹ at pD 9 and 806 cm⁻¹ at pD 13 have been assigned to the As-O stretching vibration from HAsO₄²⁻ and AsO₄³⁻ entity,

respectively. Carabante et al. (2009) reported almost the same spectral features for iAs(V) in D₂O solution on ZnSe ATR crystal.

MMA(V) has two pK_a (3.6 and 8.2) values and hence the species CH₃H₂AsO₃, CH₃HAsO₃⁻ and CH₃AsO₃²⁻ can exist depending on the pH(D) (Figure 1.4b). At pD 3, three peaks; 912, 871 and 855 cm⁻¹ were observed mainly from CH₃H₂AsO₃ with a little contribution from CH₃HAsO₃⁻ (Figure 3.23b). The peak for As-O stretching vibration for aqueous MMA(V) gives a wider band within 875-860 cm⁻¹ at pD 7 which could arise due to the combined effects of CH₃HAsO₃⁻ and CH₃AsO₃²⁻ in D₂O. Besides these, the feature at 821 cm⁻¹ originating at pD 10 can be assigned to CH₃AsO₃²⁻.

For pH(D) edge experiments, spectra were collected on hematite coated ZnSe crystal. Before the start of each adsorption experiment, 0.01 M KCl solution at pD 7 (prepared in H₂O/D₂O) was flowed across the hematite film for 30 min to equilibrate the hematite surface with H₂O/D₂O. Single beam spectra collected for background solution on the film were referenced to each other to ensure the surface was stable. The PZC for D⁺ on the hematite surface has not been measured and, considering it close to the PZC for H⁺ charge, the dominating surface sites can be presented as ≡FeOD₂⁺, ≡FeOD and ≡FeO⁻ in acidic, neutral and basic pD, respectively. The ATR-FTIR absorbance spectra for the pH(D) edge experiments of iAs(ads) are shown in the left panel of Figure 3.24. The peaks for iAs(V) adsorption are more pronounced when D₂O is used as solvent as expected. The more pronounced spectral components for iAs(ads) arises around 860 cm⁻¹ at pH 10 whereas at pD 10 in D₂O solvent, it appears at 844 cm⁻¹. In relatively acidic pH(D) for both the solvents (H₂O/D₂O), the characteristic infrared spectroscopic signature follows a similar trend and appears at 879 cm⁻¹ at pH(D) 4.

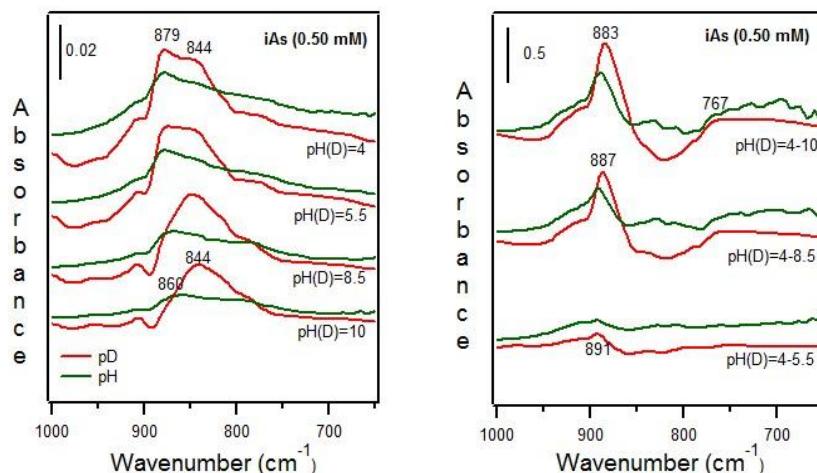


Figure 3.24. ATR-FTIR adsorption spectra for 0.5 mM iAs(ads) on hematite (6.0 mg) as a function of pH(D) at equilibrium with 1 mL/min flow rate and $I=0.01$ M KCl (Left panel). The right panel shows the differences between normalized absorbance spectra shown in the left panel. Spectra are offset for clarity.

At pD 4, for iAs(V) adsorption, the spectra exhibit broad and intense absorption band with an additional peak at 844 cm^{-1} observed at pD 10 when D_2O is used as solvent. The absorbance spectra in the left panel of Figure 3.24 clearly suggest that the two intense bands at 879 and 844 cm^{-1} originate from the surface species formed by iAs(V) with iron (oxyhydr)oxide. The shoulder at 844 cm^{-1} can be assigned to the strongly bonded inner-sphere (most likely bidentate) surface complexes as it originates even in a low electrostatic attraction setting at pD 10. The gradual appearance of the spectral feature at 879 cm^{-1} at relatively lower pD could be assigned to the formation of protonated complexes as a result of the strong electrostatic attraction between iAs(V) and surface hematite. In order to extract the new spectral features appearing with lowering of pH(D), each single beam spectrum collected for pH(D) 4 was referenced to the single beam spectra collected at pH(D)>4; such as 10, 8.5 and 5.5. This resultant normalized difference spectra show that the band at 767 cm^{-1} arises slowly which is distinct in D_2O

solvent and seems undetectable in the absorbance spectra (left side). The peak 767 cm^{-1} has been assigned to the As-OFe bond.

pH(D) edge experiments for MMA(ads), a singly methyl substituted arsenical, were carried out. The left panel of Figure 3.25 shows the ATR-FTIR spectra of MMA(ads) on iron (oxyhydr)oxide as a function of pH(D). The spectra in the right panel (Figure 3.25) represent the difference between the normalized absorbance spectra for the adsorption of MMA(ads) within the same pH(D) range as done for iAs(ads).

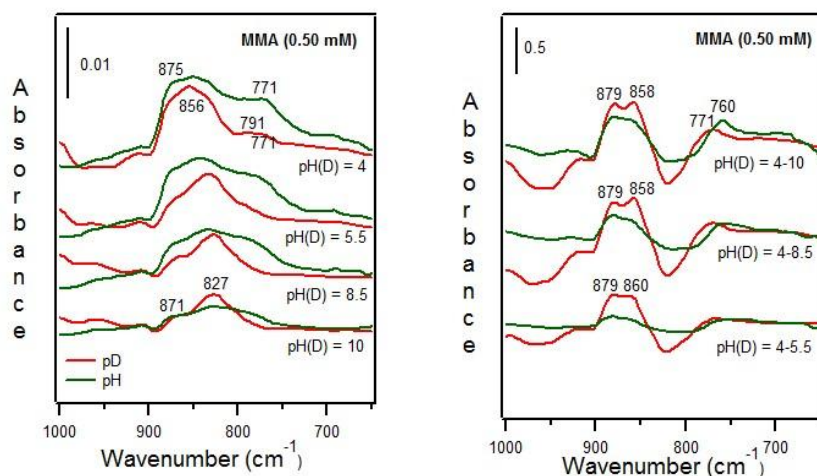


Figure 3.25. ATR-FTIR adsorption spectra for MMA(ads) on hematite (6.0 mg) as a function of pH(D) at equilibrium with 1 mL/min flow rate and $I=0.01\text{ M KCl}$ (left panel). The right panel shows the differences between normalized absorbance spectra shown in the left panel. Spectra are offset for clarity.

Spectral components for the MMA(ads) surface species arise at 871 and 827 cm^{-1} at pH(D) 10 and the feature at 827 cm^{-1} is more pronounced in D_2O solvent. At pH(D) 4, the pronounced feature shifts from 827 to 856 cm^{-1} and the other feature shifts from 871 to 875 cm^{-1} . In addition, the features at 791 cm^{-1} (in D_2O) and 771 (in $\text{D}_2\text{O}/\text{H}_2\text{O}$) cm^{-1} becomes visible when the adsorption takes place in acidic conditions and are assigned to the outer-sphere or inner-sphere monodentate surface complexes. In the normalized

difference spectra (right panel of Figure 3.25), peaks at 760 and 771 cm^{-1} appear gradually in lower pH and pD, respectively and could be assigned to the As-OFe surface species as observed in the case of iAs(ads) adsorption.

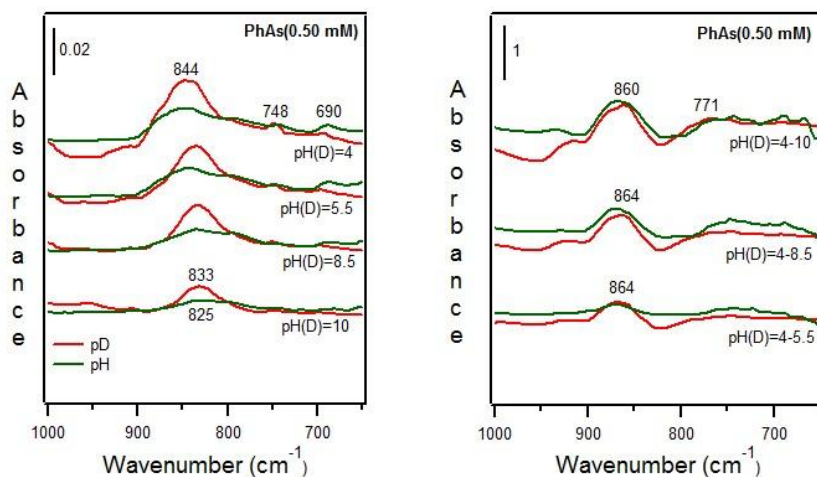


Figure 3.26. ATR-FTIR adsorption spectra for PhAs(ads) on hematite (6.0 mg) as a function of pH(D) at equilibrium with 1 mL/min flow rate and $I=0.01$ M KCl (left panel). The right panel shows the differences between normalized absorbance spectra shown in the left panel. Spectra are offset for clarity.

Similar to iAs(ads) and MMA(ads), the peaks for PhAs adsorption are more intense in D_2O solvent. The more pronounced spectral components for PhAs(ads) arise around 825 cm^{-1} at pH 10 and 833 cm^{-1} at pD 10. In relatively acidic pH(D), both the signals shift to higher wavenumbers and appear at 844 cm^{-1} at pH(D) 4. In addition, from the analysis of the normalized difference spectra, the adsorption of PhAs in acidic p(D) leads to the development of the spectral feature at 771 cm^{-1} which is more pronounced in the D_2O solvent. The gradual growth of this spectral feature is observed with decreasing system p(D) (right panel, Figure 3.26) and is assigned to the As-OFe complex. The features emerging in the more acidic conditions may be due to the strong electrostatic attraction could arise from the contribution of outer-sphere complexes.

4 Conclusions and future work

The chemical literature is flooded with papers that looked at how strong and how quickly arsenic compounds interact with soil components. These studies, however, can only theorize on the mechanisms controlling the behavior of arsenic. Using the ATR-FTIR technique, the experiments completed in this thesis provide new data on how strong and how fast arsenicals bind to reactive iron-containing materials commonly found in geosorbents and arsenic removal technologies. Thermodynamic and kinetic parameters were extracted from these molecular level experiments and provided trends that were not observed before from published bulk experiments.

Results reported herein are the first to analyze in detail the comparative rapid kinetics of monosubstituted organoarsenicals; MMA(V), PhAs, and pAsA adsorption and desorption by hydrogen phosphate on hematite nanoparticles under neutral conditions. Initial adsorption kinetics were compared with those of arsenate under the same conditions, and insights into the ligand exchange mechanism were gleaned from analyzing the trend in phosphate adsorption kinetics in the absence and presence of surface arsenic. Monosubstituted organoarsenicals adsorb with similar rate and the addition of methyl or aromatic group does not affect the rate of adsorption relative to arsenate. The desorption of the monosubstituted organoarsenicals takes place more rapidly from the iron (oxyhydr)oxide surface than the iAs(ads) does. The non-unity overall order for the desorption of these arsenicals suggests the existence of more than one type of surface complex. The presence of these arsenical surface complexes lowered the initial adsorption rate for hydrogen phosphate relative to fresh iron oxides.

The isotherm experiments, as a function of concentration and temperature, suggest that adsorption of iAs(ads) and MMA(ads) is endothermic whereas that of DMA(ads) is likely exothermic. Thermodynamic functions analyzed using the Langmuir model indicate that ligand exchange of arsenicals on hematite is entropy driven at pH 7. pH(D) edge experiments for iAs(ads), MMA(ads) and PhAs(ads) provide information in assigning detailed spectral features for the surface species. In relatively acidic pH(D), the IR signal shifts to higher wavenumber which describes stronger adsorptions due to the formation of inner-sphere complexes.

This research provides a molecular level understanding for the interaction of arsenicals with iron minerals. The outcome of this research could be reflected in understanding mechanistic details for the mobilization of arsenic in geochemical environment. The research is also significant in improving existing cleanup measures against arsenic pollution. Most of the conventional arsenic removal technologies are adsorption-based where iAs(V) is considered the major arsenic species in contaminated water. Recently, the presence of various forms of organoarsenic compounds along with the dominant arsenate species in aquatic environments have been reported. In this research, it has become possible to establish how organoarsenicals behave in different ways on the surface of iron (oxyhydr)oxides, one of the widely used arsenic removal material.

Since conditions in geochemical environments are highly variable, more experiments should be carried out to understand the mechanisms of arsenic adsorption and mobilization. Future research should focus on temperature dependent adsorption kinetic studies for these arsenicals to extract activation energy of adsorption.

Furthermore, competitive adsorption of arsenic compounds with other ions, e.g., phosphate, carbonate, sulfate etc., which are involved in the release mechanism of arsenic, could be investigated using synthetic arsenic rich groundwater.

Appendix A

Collection of ATR-FTIR spectra

After opening up the OMNIC software, there is an “edit” option in the left side of the main menu. In scrolling down, using the “option” option, specific folder can be chosen for the spectra, will be recorded. The same folder is chosen for both “initial spectra” and “initial autosave” under “file” menu (Figure A1). Some settings needs to be done under the “collect” manu as well (Figure A2).

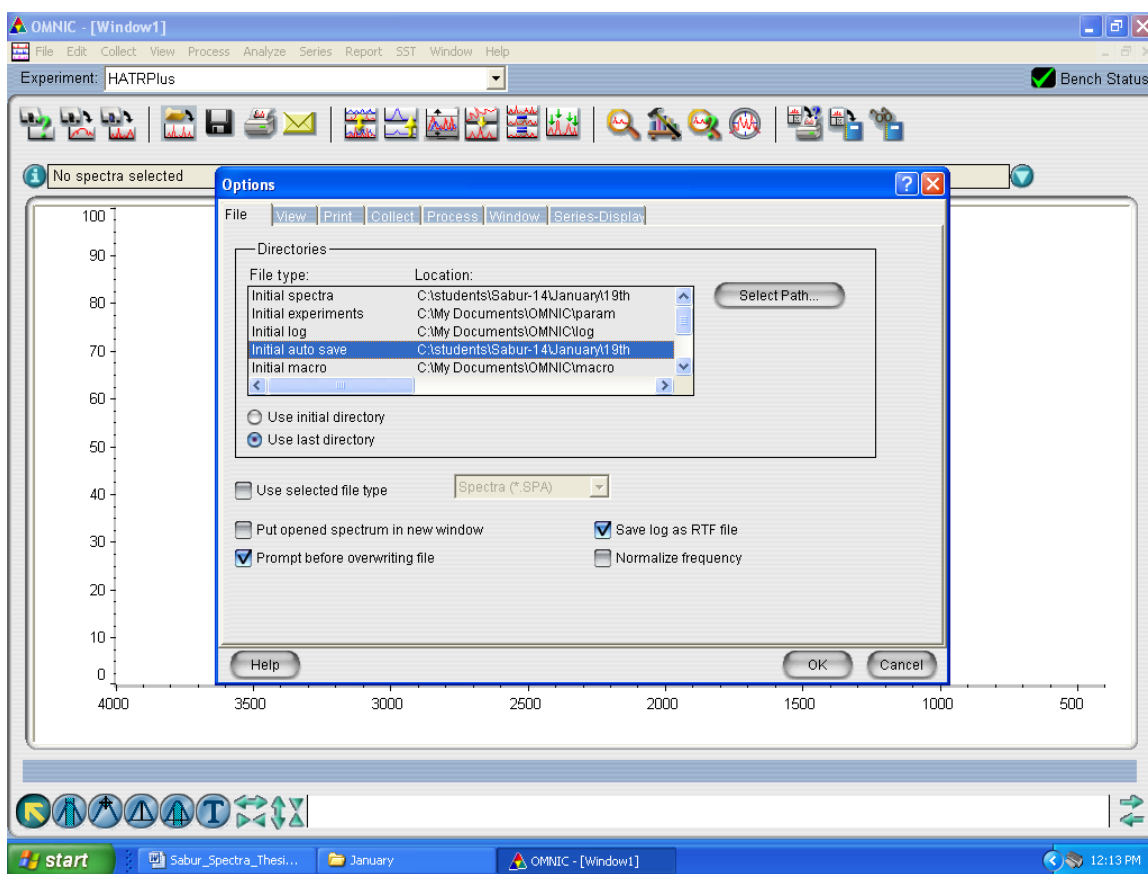


Figure A1. “File” menu in “Options” window in OMNIC.

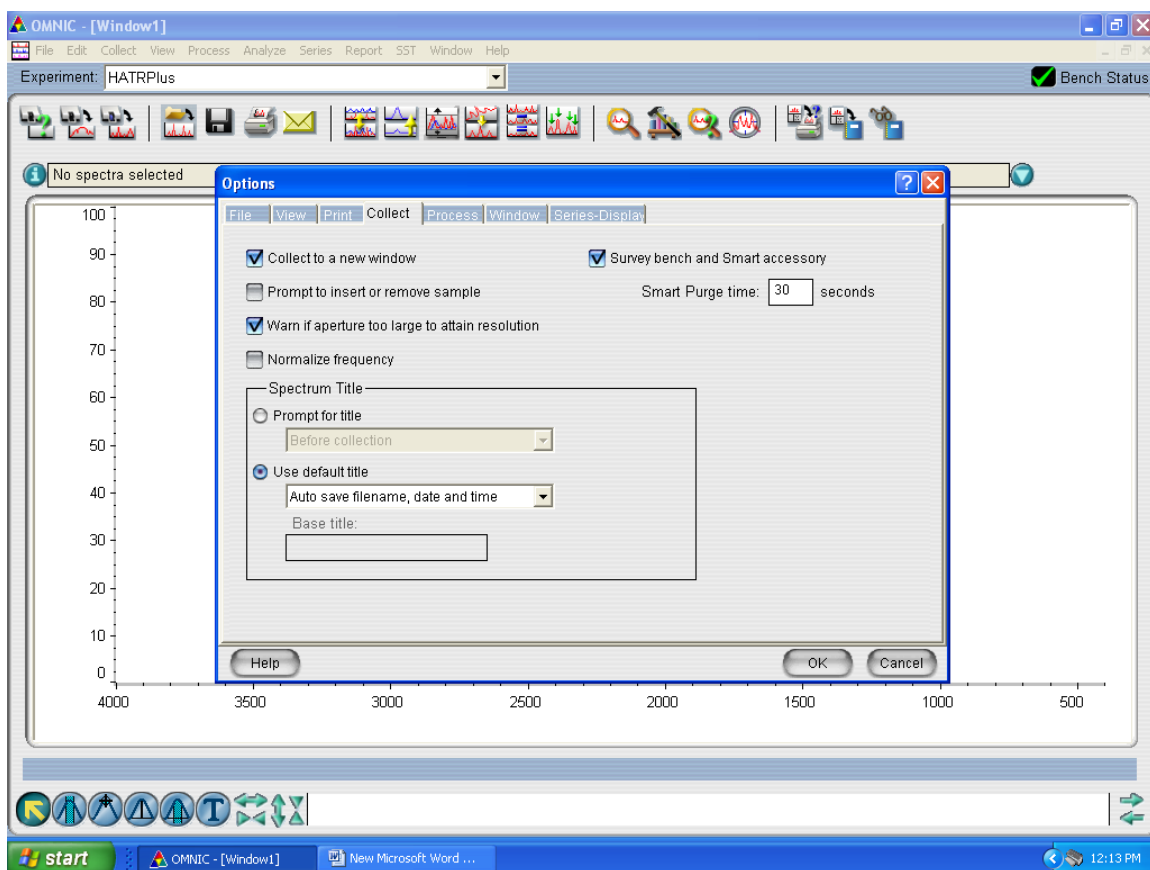


Figure A2. “Collect” menu in “Options” window in OMNIC.

Before starting the collection of single beam spectra, some additional settings such as number of scans, resolution, base name etc. are completed as desired under “collect” menu (Figure A3) in “experimental setup” window which comes from “collect” main menu. The base name can be set as MMDDYY with the full name MMDDYYXXXX where XXXX ranges from 0001 to the total number of collected spectra. Using the “Bench” (Figure A4) option under the same “Experimental Setup” window, some other things can be fixed depending on the experimental requirements.

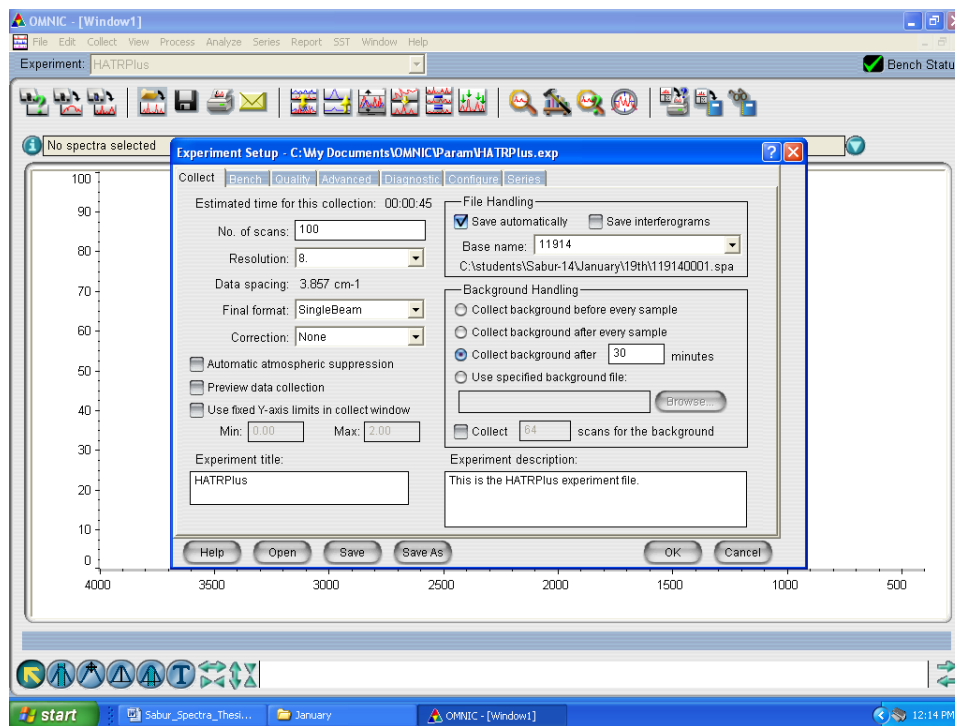


Figure A3. Collect menu in “Experimental Setup” window in OMNIC.

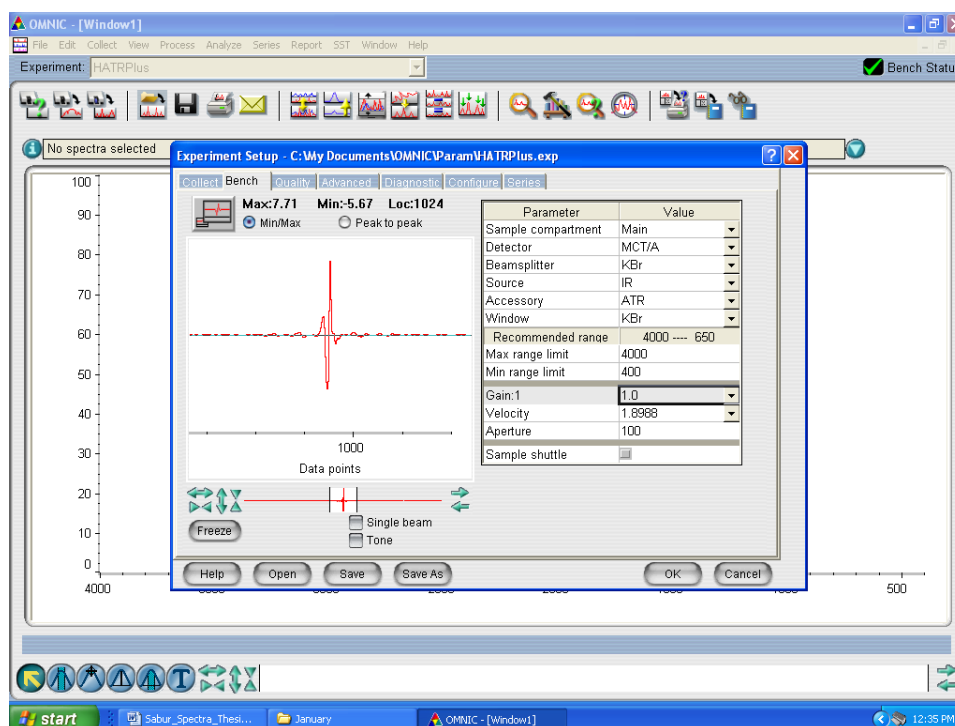


Figure A4. Bench menu in “Experimental Setup” window in OMNIC.

Single beam ATR-FTIR spectrum is then collected as follows (Figure A5).

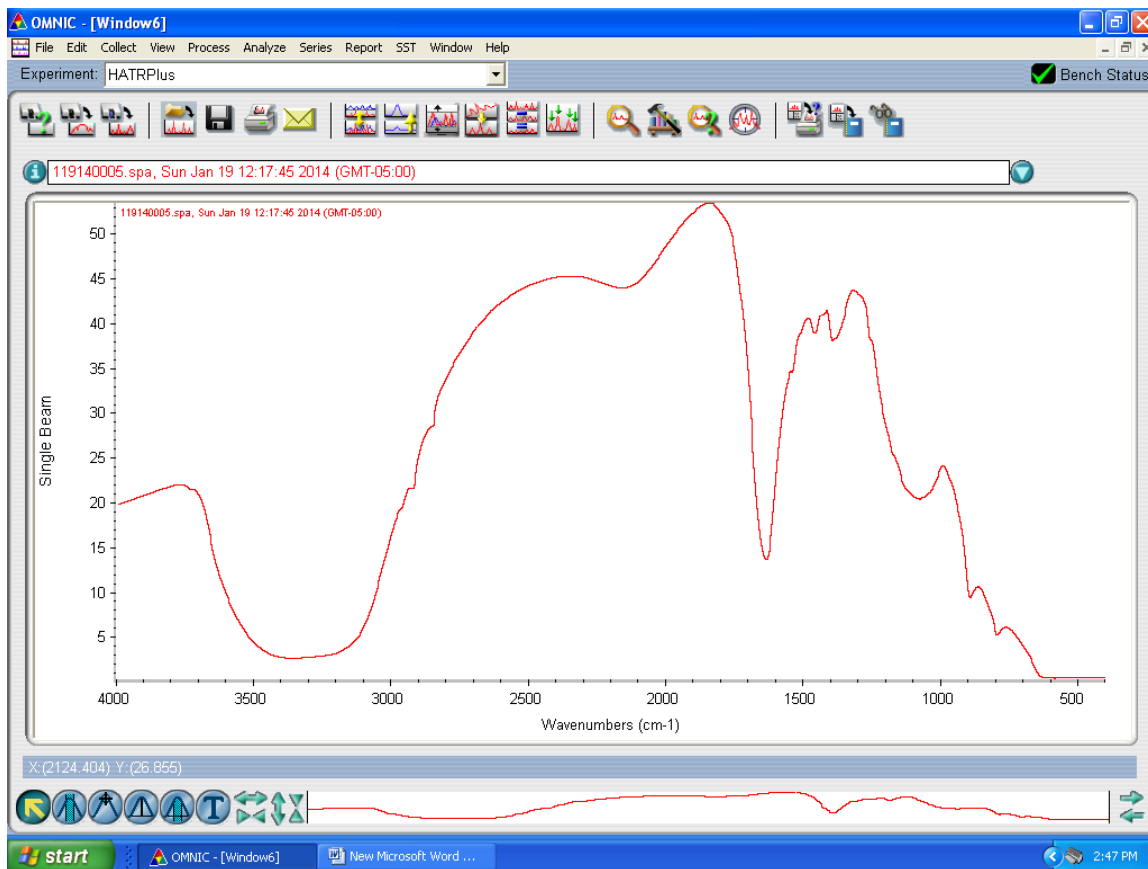


Figure A5. Single beam ATR-FTIR spectrum in OMNIC.

Reprocessing single beam spectra to absorbance spectra

In order to obtain absorbance spectra, single beam spectra collected for a sample can be reprocessed by referencing those to the last single beam spectrum collected for the background same (NaCl/KCl solutions in my experiments). A “Reprocess” option is found in the main menu “Process”. On clicking “Reprocess” a small window appears on the ONMIC main window containing the spectrum to be reprocessed (Figure A6).

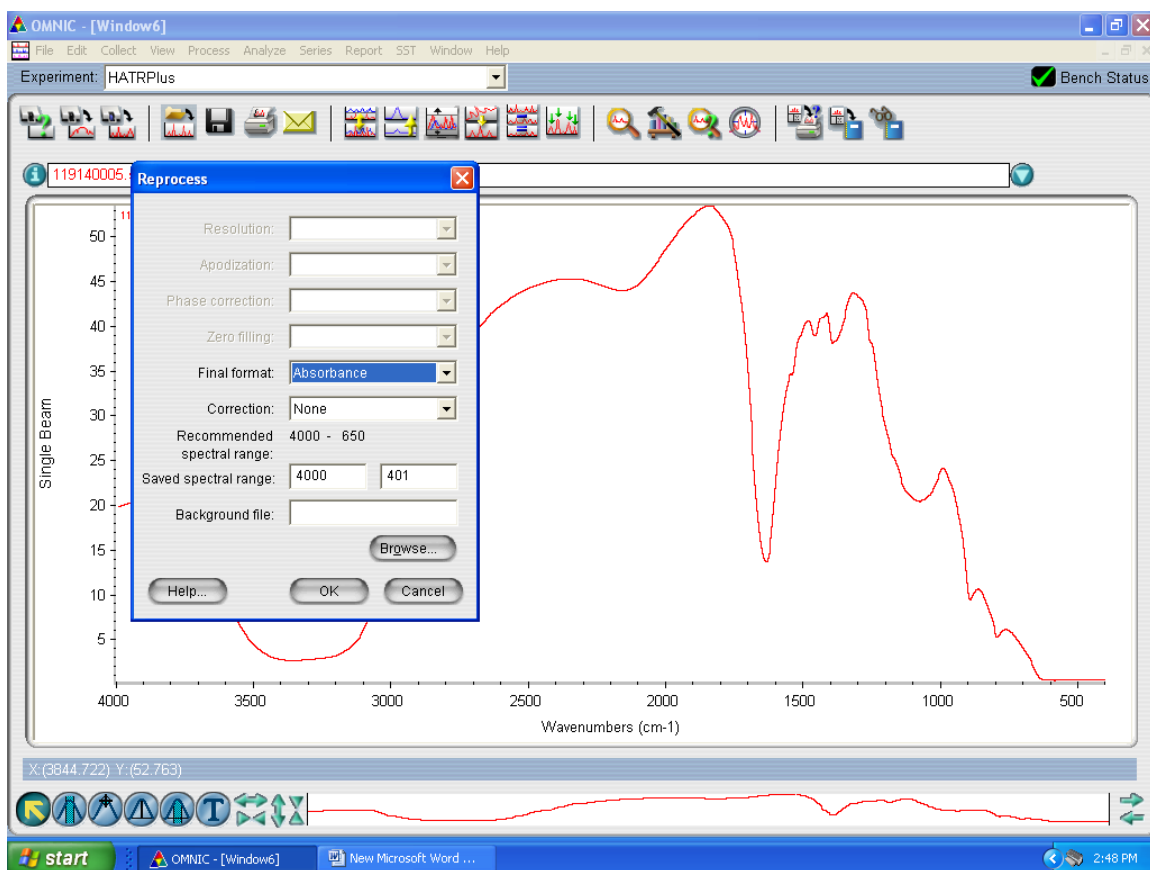


Figure A6. Reprocessing single beam spectrum to absorbance spectrum.

Using the “Browse” option on the small “Reprocess” window, the background spectrum can be chosen. A sample absorbance spectrum is shown in Figure A7. Absorbance/peak height for a specific spectral component is measured with respect to the absorbance/peak height around 2000-1800 cm^{-1} (as no species absorb IR radiation within this region in my experimental system) using the Peak Height tool in the bottom left corner of the OMNIC window. The value for the peak height appears on the bottom left corner of ONMIC window just above some operational tools.

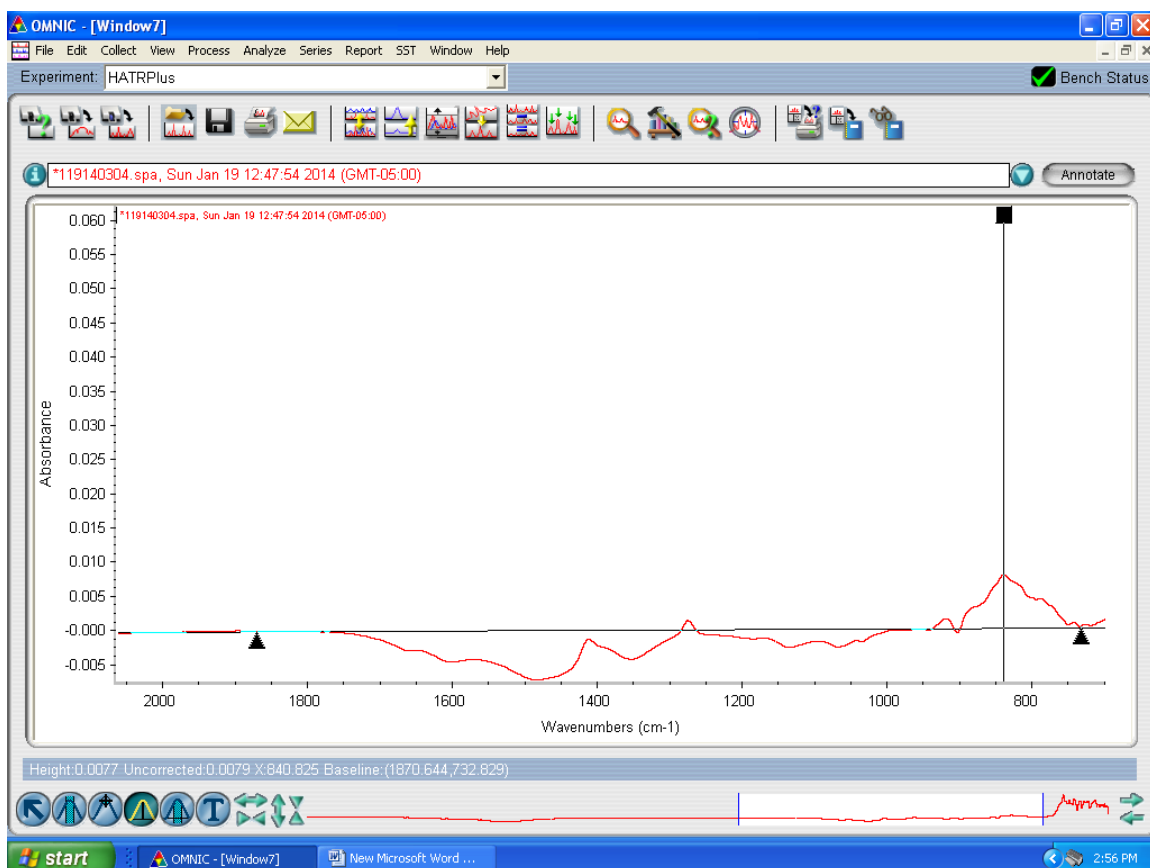


Figure A7. Absorbance spectrum in ONMIC.

Collection of ATR spectra using Macros Basic

For the adsorption/desorption kinetic part of the experiments, single beam ATR spectra were collected for 30 min with 5 average scans. The collection acquisition time for each spectrum is very low (5 s) and really much difficult or almost impossible to record manually. Collection of spectra was automated using a custom-written macro in OMNIC run on a PC computer which attached to the spectrophotometer.

In this regard, OMNIC and MACRO windows are kept at the same time. Spectracollect Macros Basic file should be opened through the MACRO window and the number of expected spectra can be fixed using the “start of loop” command (Figure A8).

The number of spectra to be collected is possible to calculate from the desired experimental time, number of average scans and collection acquisition time for each spectrum. For example, 30 min experimental time with 5 average scans for each spectrum will give rise to 300 spectra. Practically, for the collection of 300 spectra with 5 average scans for each, it takes 30 min plus few seconds more, usually within 5 to 25 s.

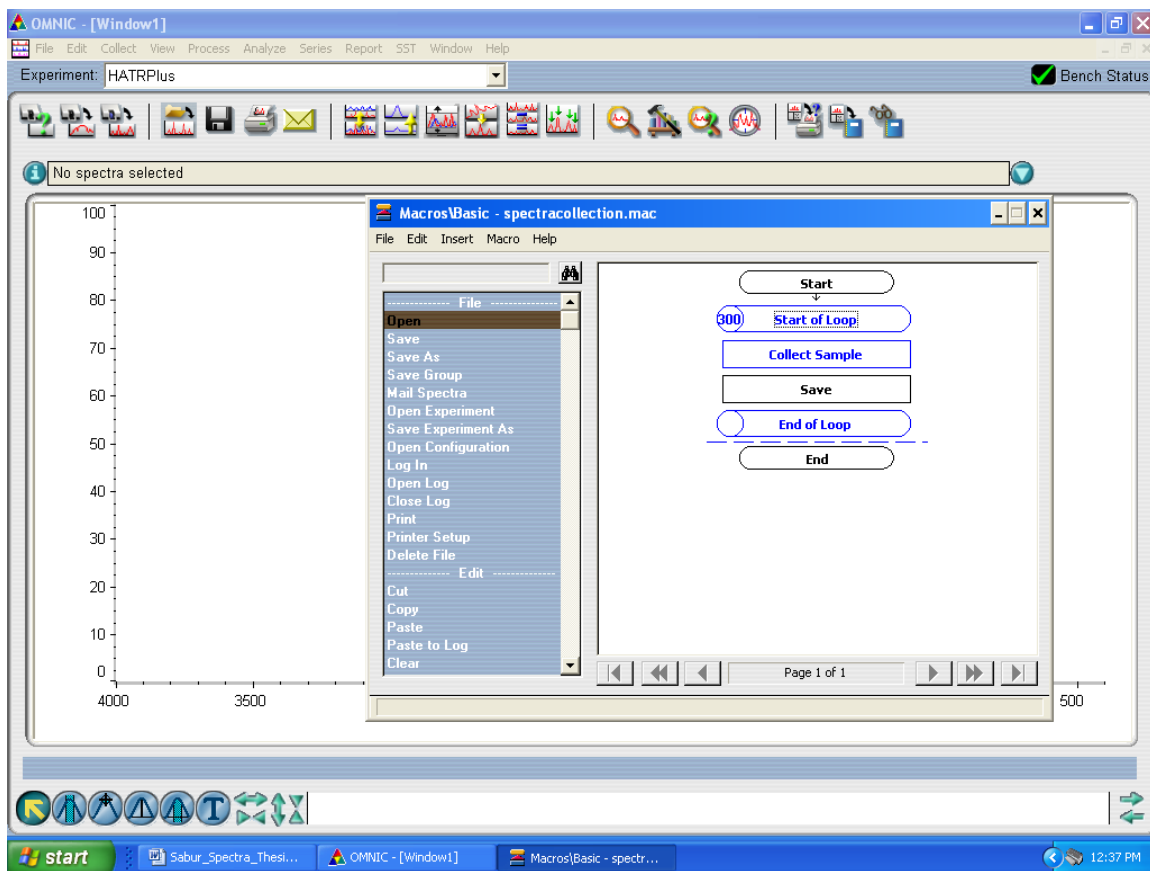


Figure A8. Spectracollect Macro Basic file used to collect multiple spectra consecutively.

When all the settings in both OMNIC and macro are completed then collection of spectra can be started by the “run” option (Figure A9) obtained by scrolling down the “file” options in macro window. In clicking the “run” option, it will ask the software for

automated spectra collection. Collection of spectra is started by double clicking the Spectracollect Macros Basic file which is same as shown in Figure A8.

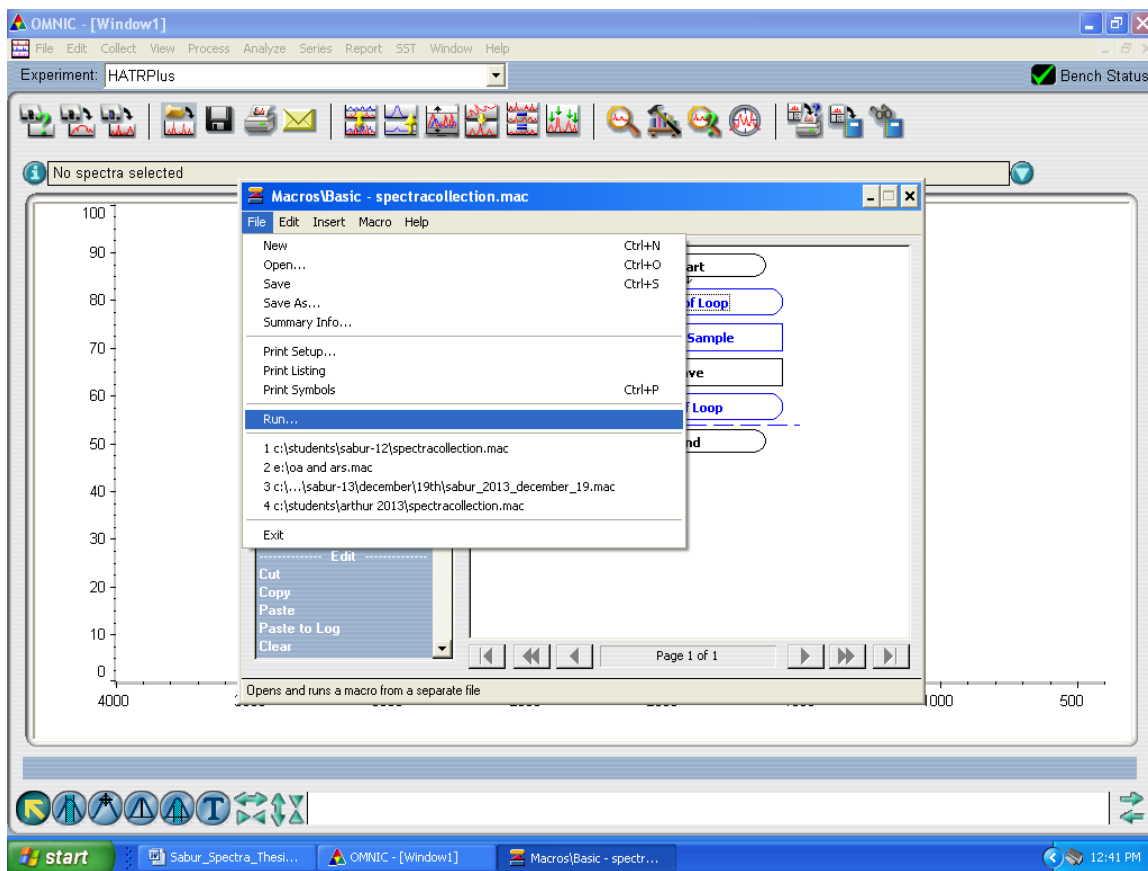


Figure A9. Collection of spectra with the help of macro.

Obtaining absorbance spectra using macro

In 30 min adsorptio/desorption time, with 5 average scans, 300 spectra are collected. Adsorptio/desorption kinetic curves are constructed with the baseline corrected peak height (assigned to the surface species) as a function of time. Reprocessing and measuring the baseline corrected peak height in all 300 spectra is a matter of few hours.

With the help of macro, it is possible be benefitted with these two facilities in only a quarter of an hour. Detailed operations are provided here.

ONMIC and macro, both should be opened first. Wavenumber in OMNIC should be zoomed in within the shortest range containing the expected feature to get more accuracy in measuring the peak heights. Before running macro for reprocessing, the ONMIN should be in full scale. Spectra reprocessing software (different than the collection spectra) is then opened in MACROS Basic window (Figure A10). The Macros window now contains three pages.

In the first page, the first two commands, “Select” and “Clear” are used to clear any active window with any spectra in OMNIC. Three Request commands after “Clear” are actually for three questions, such as the identity of the initial single beam spectra, number of spectra to be reprocessed and the basename of the spectra, to the user in order to obtain certain variables. The file containing the single beam spectra to be reprocessed can be directed by clicking the “Open”. By clicking “Reprocesses”, the single beam background spectrum can be chosen and the “Save as” refers to the folder which the reprocessed absorbance spectra will be saved to. In the second page (not shown here), almost the same basic operations are done as first page.

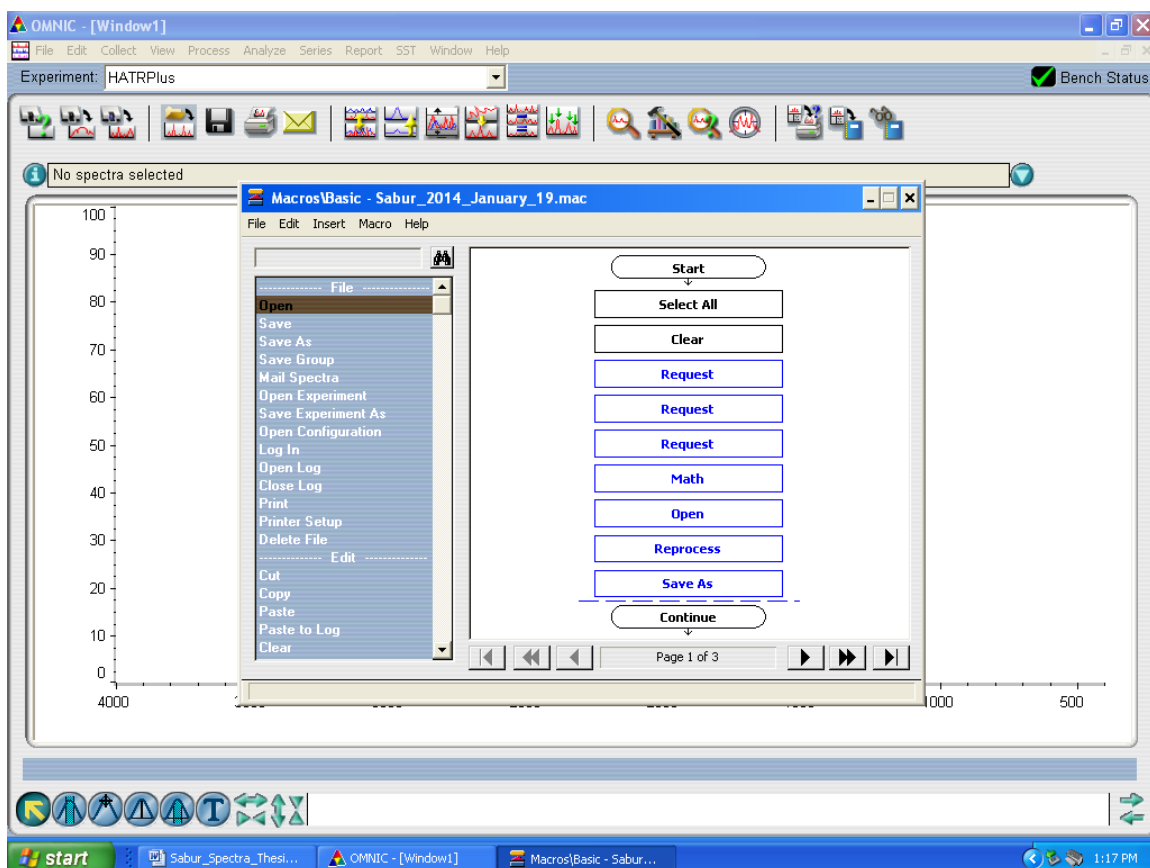


Figure A10. Macro Basic file used to reprocess collect multiple spectra consecutively

In third page (Figure A11), clicking the “Peak Height” option, it is possible to change the peak location and start and end of the wavenumber for this measurement. In the “Open log” command, there needs to be mentioned the address where the log file will be generated at the end of MACROS reprocessing.

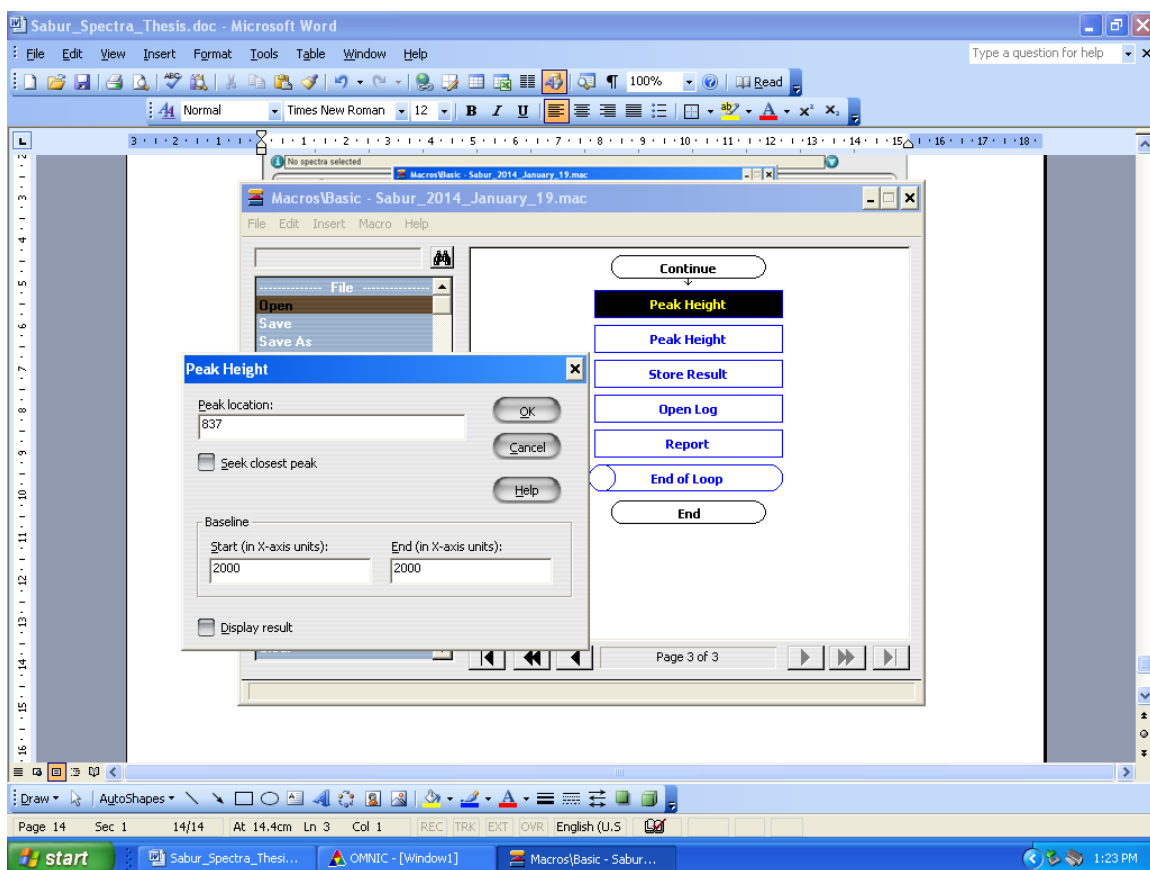


Figure A11. Macro Basic file used to reprocess collect multiple spectra (3rd page).

Then running the MACROS Basic (Figure A12) with reprocessing file, together with ONMIC, will ask the questions one after another for 3 “Request” as mentioned earlier. A sample question, “what is the number of first single beam spectra?”, is shown in the Figure A13. One after another, values for all the three questions have to be given in specific places. Then MACROS starts reprocessing the spectra.

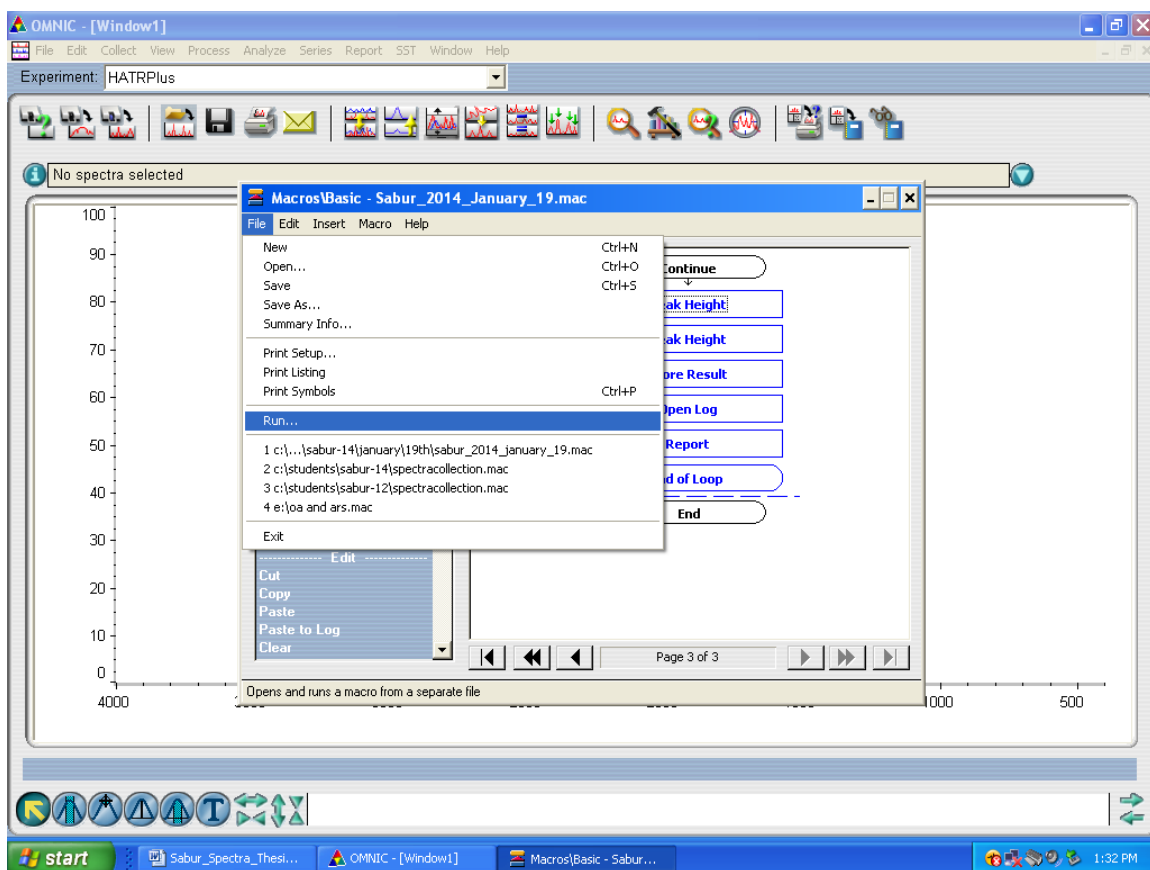


Figure A12. Running the Macro Basic together with ONMIC for reprocessing spectra.

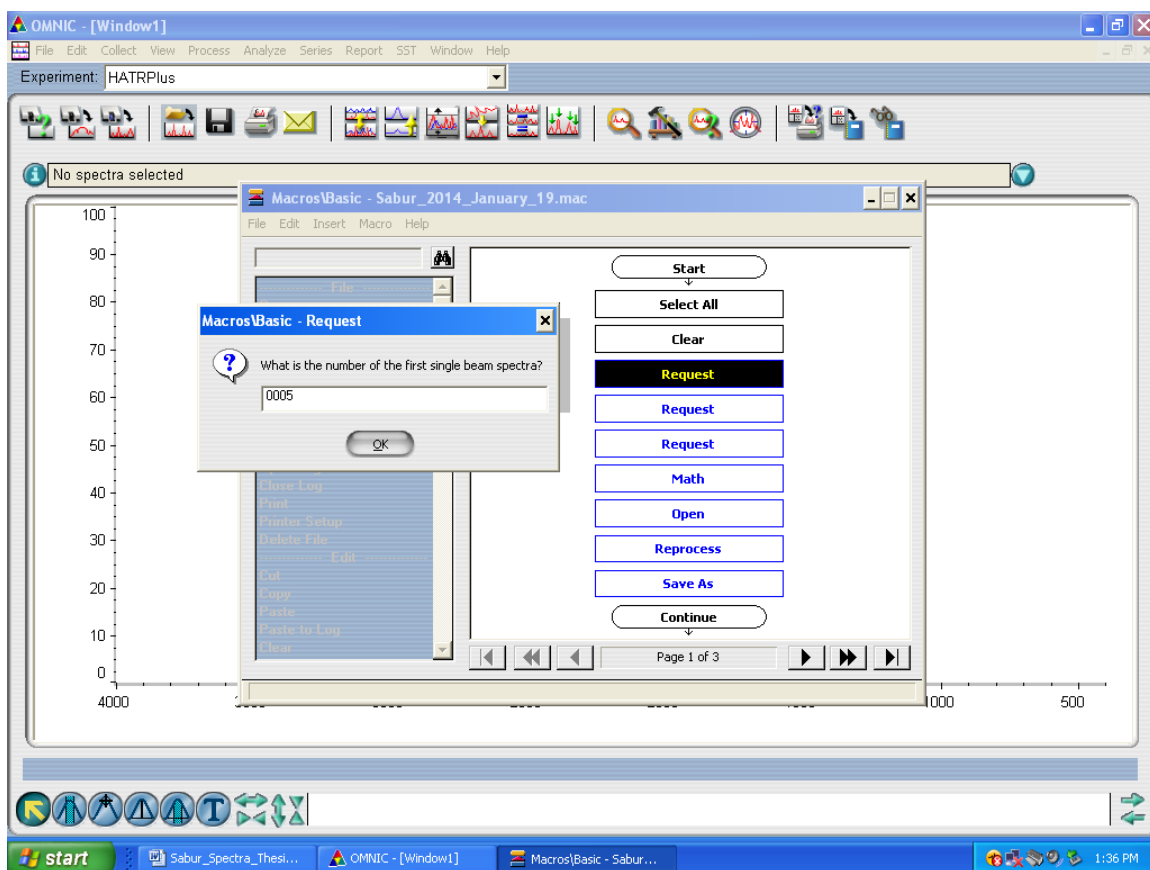


Figure A13. A sample question in the “Request” command.

At the end of the reprocessing, a LOG file is generated on OMNIC window which eventually is saved automatically to the indicated folder. The LOG file is then opened with Microsoft Excel program. On the Excel sheet, some mathematical operations are done which leads to the absorbance values at specific wavenumbers as a function of time.

Appendix B

Calculation of molar extinction coefficients

Molar extinction coefficients of the arsenic compounds (in $\text{cm}^2/\text{molecule}$) were obtained from the Beer's plot. Calibration curves were prepared with the most intense spectral features in aqueous phase at pH 7 and room temperature. A sample calculation is shown below for MMA(V) standard solutions. Beer's can be written as equation (1):

$$A = \epsilon bc \dots \dots \dots (1)$$

where, ϵ is the molar extinction coefficient, A is the absorbance at a given wavenumber, b is the effective path length for IR beam, and c is the aqueous phase concentration of MMA(V). The most intense spectral component for aqueous MMA(V) arises at 875 cm^{-1} at pH 7. The graph of absorbance vs concentration (Figure 3.1b) gives a straight line ($0.00021669 \text{ mM}^{-1}$) with an intercept zero, and ϵ can be calculated for MMA(V) using equation (2).

$$\epsilon b = \text{slope} = 0.00021669 \text{ mM}^{-1} \dots \dots \dots (2)$$

Effective path length(b), in equation (2), for the incident IR beam can be calculated as follows:

$$b = N \cdot d_p = N \cdot \frac{\lambda_{IR}}{2\pi n_1 \sqrt{\sin^2 \theta - \left(\frac{n_2}{n_1}\right)^2}} \dots \dots \dots (3)$$

N is the total number of reflections inside the IRE which is equals 3 for the ATR IRE used in my experiments. The effective angle of incidence θ is equal to 73.3° considering the optical properties of liquid water as described in the Supporting Information of reference (Depalma et. al., 2008).

d_p is the depth of penetration per reflection in cm and approximately equals to $\lambda_{IR}/2\pi n_1 \sqrt{\sin^2\theta - (\frac{n_2}{n_1})^2}$, where n_1 and n_2 are the refractive indices of IRE (2.4 for ZnSe crystal) and the sample (1.3 for water), respectively. Wavelength (λ_{IR}) can be obtained from converting wavenumber (875 cm^{-1} for MMA(V) at pH 7).

Effective path length ($b = 0.000288 \text{ cm}$) obtained using the equation (3) at wavenumber 875 cm^{-1} can be used to calculate molar extinction coefficient of iAs(V), $\varepsilon = 3.19481 \times 10^{-18} \text{ cm}^2/\text{molecules}$ (at pH 7) for MMA(V), from equation (2).

$$\varepsilon = \text{Slope}/b$$

$$\text{or, } \varepsilon = 0.00021669 \text{ mM}^{-1}/0.000288 \text{ cm}$$

$$\text{or, } \varepsilon = 0.21669000/0.000288 \text{ L}/(\text{mol. cm})$$

$$\text{or, } \varepsilon = (0.21669000 \times 1000) / (0.000288 \times 6.023 \times 10^{23}) \text{ cm}^2/\text{molecules}$$

$$\text{Therefore, } \varepsilon = 1.25 \times 10^{-18} \text{ cm}^2/\text{molecules}$$

Estimation of surface coverage

The surface coverage (S) of arsenic compounds on hematite nanoparticles can be estimated from equation (4) described in the supporting document by Arts, et. al. (2013).

$$S(\text{molecules. cm}^{-2}) = \frac{A(\lambda)}{\varepsilon \cdot N^2 \cdot d_p(\lambda) \cdot p_b \cdot (S \cdot A_{BET})} \dots \dots \dots (4)$$

Where,

$A(\lambda)$ is the baseline-corrected absorbance for the spectral feature assigned to surface species at a given λ

$\epsilon(\lambda)$ is molar extinction coefficient of the adsorbate calculated as 1.25×10^{-18} $\text{cm}^2/\text{molecules}$ for MMA(V) at pH 7 and 875 cm^{-1}

p_b is the bulk density of the deposited hematite film which is equals 2.45 g/cm^3

$S.A_{BET}$ is the specific surface area of the hematite particles (equals $1.9 \times 10^5 \text{ cm}^2/\text{g}$)

In the presence of a porous hematite film, the porosity and the presence of solvent in the pores have been taken in to account for the value of n_2 . A volume-weighted average of the refractive index of the particles (n'_2) is calculated as:

$n'_2 = F_V \cdot n_{par} + (1 - F_V) \cdot n_{H_2O}$, where $F_V = p_b(\text{gcm}^3)/p_{true}(\text{gcm}^3)$, n_{par} is the particles refractive index which is 2.9 for hematite and $n_{H_2O(l)} = 1.3$. For a 6 mg hematite film, F_V is calculated to be 4.6 using $p_{true} = 5.3 \text{ gcm}^3$. Hence the value of n'_2 is calculated to be 2.0. Using this value for the refractive index ($n'_2 = 2.0$) of the porous sample in contact with water results in the $d_p(\lambda)$ value different than that obtained for fresh ZnSe crystal with no hematite film. The calculation for $d_p(\lambda)$ for the adsorption of MMA(V) on 6 mg hematite/ZnSe film is shown below. λ_{IR} was calculated from the wavenumber, 840 cm^{-1} for the surface species formed by MMA(ads) at pH 7.

$$d_p(\lambda) = \lambda_{IR} / 2\pi n_1 \sqrt{\sin^2 \theta - \left(\frac{n'_2}{n_1}\right)^2} \dots \dots \dots (5)$$

$$\text{or, } d_p(\lambda) = (1/840) / 2\pi n_1 \sqrt{\sin^2 \theta - \left(\frac{n'_2}{n_1}\right)^2}$$

Therefore, $d_p(\lambda) = 0.000167 \text{ cm}$

Using this $d_p(\lambda)$ value, surface coverage for the adsorption of MMA can be estimated from equation (4) which is $2.28 \times 10^{13} \text{ molecules.cm}^{-2}$ at baseline-corrected absorbance, $A(\lambda)=0.02$.

5 References

Adamescu, A., Mitchell, W., Hamilton, I.P., and Al-Abadleh, H.A. (2010) Insights into the surface complexation of dimethylarsinic acid on iron (oxyhydr)oxides from ATR-FTIR studies and quantum chemical calculations. *Environ. Sci. Technol.* 44, 7802-7807.

Akkari, K.H., Frans, R.E., and Lavy, T.L. (1986) Factors affecting degradation of MSMA in soil. *Weed Sci.* 34, 781-787.

Anderson, L.C.D., and Bruland, K.W. (1991) Biogeochemistry of arsenic in natural waters: the importance of methylated species. *Environ. Sci. Technol.* 25(3), 420-427.

Arts, D., Sabur, M.A., and Al-Abadleh, H.A. (2013) Surface interactions of aromatic organoarsenical compounds with hematite nanoparticles using ATR-FTIR: studies. *J. Phys. Chem. A* 117, 2195-2204.

Bednar, A.J., Garbarino, J.R., Ranville, J.F., and Wildeman, T.R. (2002) Presence of organoarsenicals used in cotton production in agricultural water and soil of the southern United States. *J. Agric. Food Chem.* 50, 7340-7344.

Bentley, R., and Chasteen, T.G. (2002) Microbial methylation of metalloids: arsenic, antimony, and bismuth. *Microbiol. Molecular Biology Rev.* 66(2), 250-271.

Bowell, R.J. (1994) Sorption of arsenic by iron oxides and oxyhydroxides in soils. *Applied Geochem.* 9, 279-286.

Bright, D.A., Dodd, M., and Reimer, K.J. (1996) Arsenic in subarctic lakes influenced by gold mine effluent: the occurrence of organoarsenicals and 'hidden' arsenic. *The Sci. Total Environ.* 180, 165-182.

Brown, B.L., Slaughter, A.D., and Schreiber, M.E. (2005) Controls on roxarsone transport in agricultural watersheds. *Applied Geochem.* 20, 123-133.

Carabante, I., Grahn, M., Holmgren, A., Kumpiene, J., and Hedlund, J. (2009) Adsorption of arsenic(v) on iron oxide nanoparticle films studied by in situ ATR-FTIR spectroscopy. *Colloids and Surfaces A: Physiochem. Engg. Asp.* 346, 106-113.

Catalano, J.G., Park, C., Fenter, P., and Zhang, Z. (2008) Simultaneous inner- and outer-sphere arsenate adsorption on corundum and hematite. *Geochim. et Cosmochim. Acta.* 72, 1986-2004.

CCME (1997) Canadian environmental quality guidelines, Appendix XXIII-Canadian water quality guidelines: updates, arsenic, bromacil, carbaryl, chlorpyrifos, deltamethrin, and glycols. In: Canadian water quality guidelines, Canadian Council of Resource and Environment Ministers.

CCME (1991) Canadian environmental quality guidelines, Interim Canadian environmental quality criteria for contaminated sites, Winnipeg.

Challenger, F. (1945) Biological methylation. *Chem. Rev.* 36, 315-361.

Chen, C.Y., Pickhardt, P.C., Xu, M.Q., and Folt, C.L. (2008) Mercury and arsenic bioaccumulation and eutrophication in baiyangdian lake, China. *Water Air Soil Pollut.* 190, 115-127.

Cheng, H., Hu, Y., Luo, J., Xu, B., and Zhao, J. (2009) Geochemical processes controlling the fate and transport of arsenic in acid mine drainage (AMD) and natural systems. *J. Hazard. Mater.* 165, 13-26.

Clarke, T. (2001) Bangladeshis to sue over arsenic poisoning. *Nature* 413, 556.

Cohen, S.M., Arnold, L.L., Eldan, M., Lewis, A.S., and Beck, B.D. (2006) Methylated arsenicals: the implications of metabolism and carcinogenicity studies in rodents to human risk assessment. *Critical Rev. Toxicol.* 36, 99-133.

Cornell, R.M., and Schwertmann, U. (2003) The iron oxides: structure, properties, reactions, occurrences and uses. *WILEY-VCH Verlag GmbH & Co. KGaA*, Weinheim.

Cowen, S., Duggal, M., Hoang, T., and Al-Abadleh, H.A. (2008) Vibrational spectroscopic characterization of some environmentally important organoarsenicals- a guide for understanding the nature of their surface complexes. *Can. J. Chem.* 86, 942-950.

Cox, C.D., and Ghosh, M.M. (1994) Surface complexation of methylated arsenates by hydrous oxides. *Water Res.* 28(5), 1181-1188.

Cullen, W.R. (2008) Is Arsenic an Aphrodisiac? The Sociochemistry of an Element, *RBC Publishing*, Cambridge.

Depalma, S., Cowen, S., Hoang, T., and Al-Abadleh, H.A. (2008) Adsorption thermodynamics of p-arsanilic acid on iron (oxyhydr)oxides: in-situ ATR-FTIR studies. *Environ. Sci. Technol.* 42, 1922-1927.

Dzombak, D.A., and Morel, F.M.M. (1990) Surface complexation of modeling: hydrous ferric oxide, *John Wiley and Sons*.

Environment Canada (2013) Date Accessed, January 7, 2013

<http://www.ec.gc.ca/scitech/default.asp?lang=En&n=4B40916E1&xsl=privateArticles2,viewfull&po=DA247312>

Fillol, C., Dor, F., Labat, L., Boltz, P., Bouard, J.L., Mantey, K., Mannschott, C., Puskarczyk, E., Viller, F., Momas, I., and Seta, N. (2010) Urinary arsenic concentrations and speciation in residents living in an area with naturally contaminated soils. *Sci. Total Environ.* 408, 1190–1194.

Garbarino, J.R., Bednar, A.J., Rutherford, D.W., Beyer, R.S., and Wershaw, R.L. (2003) Environmental fate of roxarsone in poultry litter. I. degradation of roxarsone during composting. *Environ. Sci. Technol.* 37, 1509-1514.

Goldberg, S., and Johnston, C.T.J. (2001) Mechanisms of Arsenic Adsorption on Amorphous Oxides Evaluated Using Macroscopic Measurements, Vibrational Spectroscopy, and Surface Complexation Modeling. *Colloid Interface Sci.* 234, 204-216.

Gong, Z., Lu, X., Cullen, W.R., and Le, X.C. (2001) Unstable trivalent arsenic metabolites, monomethylarsonous acid and dimethylarsinous acid. *J. Anal. At. Spectrom.* 16, 1409-1413.

Hasegawa, H. (1997) The behaviour of trivalent and pentavalent methylarsenicals in Lake Biwa. *Applied Organometallic Chem.* 11, 305-311.

Hayakawa, T., Kobayashi, Y., Cui, X., and Hirano, S. (2005) A new metabolic pathway of arsenite: arsenic-glutathione complexes are substrates for human arsenic methyltransferase Cyt19. *Arch Toxicol.* 79, 183-191.

Health Canada (2005) Fact sheet on chromated copper arsenate (CCA) treated wood, Health Canada, Ottawa, ON.

Health Canada (2012) Guidelines for Canadian drinking water quality-summery table, Water, Air and Climate Change Bureau, Healthy Environments and Consumer Safety Branch, Health Canada, Ottawa, ON.

Jackson, B.P., Seaman, J.C., and Bertsch, P.M. (2006) Fate of arsenic compounds in poultry litter upon land application. *Chemosphere* 65, 2028-2034.

James, R.O., and Parks, G.A. (1982) Characterization of aqueous colloids by their electrical double-layer and intrinsic surface chemical properties. *Surface Coll. Sci.* 12, 119-216.

Jing, C., Meng, X., Liu, S., Baidas, S., Patraju, R., Christodoulatos, C., and Korfiatis, G.P. (2005) Surface complexation of organic arsenic on nanocrystalline titanium oxide, *J. Coll. Int. Sci.* 290, 14-21.

Jones, F.T. (2007) A broad view of arsenic. *Poultry Sci.* 86, 2-14.

Khan, M.A., Stroud, J.L., Zhu, Y., Mcgrath, S.P., and Zhao, F. (2010) Arsenic bioavailability to rice is elevated in Bangladeshi paddy soils, *Environ. Sci. Technol.* 44, 8515-8521.

Kosmulski, M. (2009) pH-dependent surface charging and points of zero charge. IV. Update and new approach. *J. Coll. Int. Sci.* 337, 439-448.

Lafferty, B.J., and Loeppert, R.H. (2005) Methyl arsenic adsorption and desorption behavior on iron oxides. *Environ. Sci. Technol.* 39, 2120-2127.

Li, Y., Low, G.K.C., Scott, J.A., and Amal, R. (2010) Arsenic speciation in municipal landfill leachate. *Chemosphere* 79, 794-801.

Li, Y., Low, G.K.C. Scott, J.A., and Amal, R. (2011) Microbial transformation of arsenic species in municipal landfill leachate. *J. Hazard. Mater.* 188, 140-147.

Loring, J.S., Sandstrom, M.H., Noren, K., and Persson, P. (2009) Rethinking arsenate coordination at the surface of goethite. *Chem. Eur. J.* 15, 5063-5072.

Mandal, B.K., and Suzuki, K.T. (2002) Arsenic round the world: a review. *Talanta* 58, 201-235.

Mcknight-Whitford, A., Chen, B., Naranmandura, H., Zhu, C., and Lee, X.C. (2010) New method and detection of high concentrations of monomethylarsonous acid detected in contaminated groundwater. *Environ. Sci. Technol.* 44, 5875-5880.

Mudhoo, A., Sharma, S.K., Garg, V.K., and Tseng, C. (2011) Arsenic: an overview of applications, health, and environmental concerns and removal processes. *Crit. Rev. Env. Sci. Technol.* 41, 435-519.

- Myneni, S.C.B., Traina, S.J., Waychunas, G.A., and Logan, T.J. (1998) Experimental and theoretical vibrational spectroscopic evaluation of arsenate coordination in aqueous solutions, solids, and at mineral-water interfaces. *Geochim. Cosmochim. Acta* 62, 3285-3300.
- Nickson, R.T., McArthur, J.M., Shrestha, B., Kyaw-Myint, T.O., and Lowry, D. (2005) Arsenic and other drinking water quality issues, Muzaffargarh district, Pakistan. *Applied Geochem.* 20, 55-68.
- Nuallain, C.O., and Cinneide, S.O. (1973) Thermodynamic ionization constants of aromatic arsonic acids. *J. Inorg. Nucl. Chem.* 35, 2871-2881.
- Qi, Y., and Donahoe, R.J. (2008) The environmental fate of arsenic in surface soil contaminated by historical herbicide application. *Sci. Total Environ.* 405, 246-254.
- Qiang, Z., and Adams, C. (2004) Potentiometric determination of acid dissociation constants (pK_a) for human and veterinary antibiotics, *Water Res.* 38, 2874-2890.
- Roddick-Lanzilotta, A.J., McQuillan, A.J., and Craw, D. (2002) Infrared spectroscopic characterisation of arsenic (V) ion adsorption from mine waters. Macreas mine, New Zealand. *Appl. Geochem.* 17, 445-454.
- Safiullah, S., Mahamud-Ul-Hoque, M., Sabur, M.A., and Haque, M.E. (2013) Arsenic in coconut water: a case study. *Asian J Water Env. Poll.* 10(3), 23-28.
- Sanchez-Rodas, D., Gomez-Ariza, J.L., Giraldez, I., Velasco, A., and Morales, E. (2005) Arsenic speciation in river and estuarine waters from southwest Spain. *Sci. Total Environ.* 345, 207-217.
- Shimizu, M., Ginder-Vogel, M., Parikh, S.J., and Sparks, D.L. (2010) Molecular scale assessment of methylarsenic sorption on aluminum oxide. *Environ. Sci. Technol.* 44, 612-617.
- Shimizu, M., Arai, Y., and Sparks, D.L. (2011a) Multiscale assessment of methylarsenic reactivity in soil. 2. distribution and speciation in soil. *Environ. Sci. Technol.* 45, 4300-4306.
- Shimizu, M., Arai, Y., and Sparks, D.L. (2011b) Multiscale assessment of methylarsenic reactivity in soil. 1. sorption and desorption on soils. *Environ. Sci. Technol.* 45, 4293-4299.

Sierra-Alvarez, R., Yenal, U., Field, J.A., Kopplin, M., Gandolfi, A.J., and Garbarino, J.R. (2006) Anaerobic biotransformation of organoarsenical pesticides monomethylarsonic acid and dimethylarsinic acid. *J. Agric. Food Chem.* 54, 3959-3966.

Smedley, P.L., and Kinniburgh, D.G. (2002) A review of the source, behaviour and distribution of arsenic in natural waters. *Applied Geochem.* 17, 517-568.

Smith, S. (2007) Solution of simultaneous chemical equilibria in heterogeneous systems: implementation in MATLAB, Wilfrid Laurier University. Date accesses, January 11, 2014

http://www.wlu.ca/documents/24984/matlab_speciation_calculation.pdf

Styblo, M., Razo, L.M.D., Vega, L., Germolec, D.R., LeCluyse, E.L., Hamilton, G.A., Reed, W., Wang, C., Cullen, W.R., and Thomas, D.J. (2000) Comparative toxicity of trivalent and pentavalent inorganic and methylated arsenicals in rat and human cells. *Arch Toxicol.* 74, 289-299.

Tchounwou, P.B., Patlolla, A.K., and Centeno, J.A. (2003) Carcinogenic and systemic health effects associated with arsenic exposure - a critical review, *Toxicologic Pathol.* 31, 575-588.

The Environmental Conservation Rules (1997) Ministry of Forest and Environment, The Peoples Republic of Bangladesh.

Tofan-Lazar, J., and Al-Abadleh, H.A. (2012a) ATR-FTIR studies on the adsorption/desorption kinetics of dimethylarsinic acid on iron-(oxyhydr)oxides. *J. Phys. Chem. A* 116, 1596-1604.

Tofan-Lazar, J., and Al-Abadleh, H.A. (2012b) Kinetic ATR-FTIR studies on phosphate adsorption on iron (oxyhydr)oxides in the absence and presence of surface arsenic: molecular-level insights into the ligand exchange mechanism. *J. Phys. Chem. A* 116, 10143-10149.

US EPA (2012) 2012 edition of the drinking water standards and health advisories, Washington, DC, Spring 2012.

Vahter, M. (2002) Mechanisms of arsenic biotransformation. *Toxicology* 181-182, 211-217.

Wang, S., and Mulligan, C.N. (2006) Occurrence of arsenic contamination in Canada: sources, behavior and distribution, *Sci. Total Environ.* 366, 701-721.

WHO (World Health Organization) (2004) Guidelines for drinking-water quality, Volume 1 (Recommendations), 3rd edition, Geneva.

Wu, J., and Ho, P.C. (2004) Speciation of inorganic and methylated arsenic compounds by capillary zone electrophoresis with indirect UV detection application to the analysis of alkali extracts of As₂S₂ (realgar) and As₂S₃ (orpiment). *J. of Chromatography A* 1026, 261-270.

Xu, H., Allard, B., and Grimvall, A. (1991) Effects of acidification and natural organic materials on the mobility of arsenic in the environment. *Water, Air and Soil Poll.* 57-58, 269-278.

Xu, T., Cai, Y., and O'Shea, K.E. (2007) Adsorption and photocatalyzed oxidation of methylated arsenic species in TiO₂ suspensions. *Environ. Sci. Technol.* 41, 5471-5477.

Zheng, M., Cai, C., Hu, Y., Sun, G., Williams, P.N., Cui, H., Li, G., Zhao, F., and Zhu, Y. (2011) Spatial distribution of arsenic and temporal variation of its concentration in rice. *New Phytologist* 189, 200-209.